RATIONAL DESIGN OF TARGETED DRUG DELIVERY DEVICES FOR ENHANCING THERAPEUTIC POTENTIAL OF ANTICANCER AGENTS THROUGH BIOORTHOGONAL REACTIONS.

By

MANISH S. HUDLIKAR

(Under the Direction of Geert-Jan Boons)

ABSTRACT

Although Paul Ehrlich has envisioned the concept of targeted delivery of a cytotoxic agent to cancer cells back to 1913, the clinical efficacy of anticancer agents has been limited due to poor solubility, lack of selectivity, unmanageable off-target toxicities, and the emergence of multidrug resistance. Combination of active tumor targeting and covalent attachment of drug molecules to carriers such as proteins, peptides, carbohydrates, polymers, and nanoparticles has shown great potential in enhancing solubility, selectivity, and therapeutic index. However, producing homogeneous drug products has been difficult due to a lack of orthogonal conjugation chemistries that combines covalent drug attachment with targeted delivery on a single platform.

To address these limitations, in first approach we describe a multifunctional gold nanoparticle decorated with hydrazine, amine, or dibenzocyclooctynol for sequential conjugation of doxorubicin through an acid-labile hydrazone linkage, an imaging agent through an amide bond, and a glycan-based ligand for the cell surface receptor CD22 of B-cells using SPAAC showing excellent conjugation efficiencies. In the second approach, an orthogonal glycoengineering strategy that allows sequential site-specific conjugation of dual-drug to anti-

CD22 antibody was described. This method relies on an observation that sialyltransferase (ST6Gal1) has a preference for the α1,3-Man-β1,2-GlcNAc-β1,4-Gal bottom arm of the glycan of IgG over top arm. This unique feature has enabled the sequential introduction of reactive functional groups that in turn can undergo SPAAC with FDA approved anticancer agent such as paclitaxel and zosuquidar, potent P-glycoprotein modulator currently under phase-III clinical trials for the treatment of acute myeloid leukemia. The resulting anti-CD22 antibody showed superior anti-cancer activities and can bypass multidrug resistance in lymphoma cancer cells.

Payloads that overcome multidrug resistance are highly desired for ADCs. A novel paclitaxel scaffold with 2-methylpropenyl at C3' and (*E*)-6-((*tert*-butoxycarbonyl)amino) hexenoic acid modification at C3'-N-acyl position has been synthesized. The dual modification furnished highly potent analogs against multidrug-resistance cancer cells and has enabled flexibility of introducing various clickable groups or stable yet cleavable linkers.

INDEX WORDS: Antibody-Drug Conjugates, B-cell Lymphoma, CD22, Chemotherapy, Drug Delivery, Doxorubicin, Esterase, Hydrazone linkage, Glutathione, Multidrug Resistance, N-glycan, Nanoparticles, Paclitaxel, P-Glycoprotein, Sialyltransferase, & Zosuquidar

RATIONAL DESIGN OF TARGETED DRUG DELIVERY DEVICES FOR ENHANCING THERAPEUTIC POTENTIAL OF ANTICANCER AGENTS THROUGH BIOORTHOGONAL REACTIONS.

by

MANISH S. HUDLIKAR

B.S., Pune University, India, 2008

M.S., Pune University, India, 2010

A Dissertation Submitted to the Graduate Faculty of The University of Georgia in Partial Fulfillment of the Requirements for the Degree

DOCTOR OF PHILOSOPHY

ATHENS, GEORGIA,

2017

RATIONAL DESIGN OF TARGETED DRUG DELIVERY DEVICES FOR ENHANCING THERAPEUTIC POTENTIAL OF ANTICANCER AGENTS THROUGH BIOORTHOGONAL REACTIONS.

by

MANISH S. HUDLIKAR

Major Professor:	Geert-Jan Boons
Committee:	Richard Steet
	Robert Phillips

Electronic Version Approved:

Suzanne Barbour
Dean of the Graduate School
The University of Georgia
December 2017

DEDICATION

I would like to dedicate this work to my parents Satish Hudlikar, Pratibha Hudlikar, and my younger sister Harshada Hudlikar for their unconditional support, love, and encouragement.

"Be less curious about people and more curious about ideas"

Dr. Marie Curie, Noble Laureate in Physics and Chemistry

ACKNOWLEDGEMENTS

There are many personalities who have influenced and played a vital role in my success as a graduate student. First and foremost, Prof. Dr. Geert-Jan Boons for allowing me to work in his lab and giving all the freedom to explore projects that I found interesting. I would like to acknowledge and thank you for your mentorship, advice, and your desire to always push me out of my comfort zone has inspired me to think critically, creatively, and excited me to participate in innovative research. Without your guidance and persistent help, this dissertation would not have been possible. Dr. Steet and Dr. Phillips provided excellent feedback and encouragement throughout my Ph.D. studies as committee members.

There have been numerous people in Boons' group who have assisted me in different areas of research. A very special thank to Dr. Petr Ledin and Dr. Nagesh Kolishetti for teaching me synthetic and polymer chemistry skillsets to undertake drug delivery project and providing excellent guidance. Dr. Andre Venot was the real hero that held the lab together and always showed an interest in my project. My special thanks to Ivan Gagarinov, Drs. Xiuru Li, and Tiantian Sun for fruitful collaboration on the nanoparticle, ADC project and for being extremely helpful and supportive during my Ph.D. Drs. Margreet Wolfert and Eric Ngalle Mbua helped with manuscript preparation, taught me cell culture techniques, and was a constant resource for any biology-based questions I had. I would like thanking current and past lab mates Robert Chapman, Apoorva Joshi, Nitin Supekar, Anthony Prudden, Omkar Dhamale, Chengli Zong, Pradeep Chopra, and Anju Sirohiwal for their suggestions and advice throughout my study. I would like to thank Dr. John Glushka for all the help associated with NMR experiments. Finally,

I would like to thank my entire family and all my friends in UGA for their support and unconditional encouragement.

TABLE OF CONTENTS

Page

LIST OF TABLES

Page

LIST OF FIGURES

Page

LIST OF SCHEMES

Page

LIST OF ABBREVIATIONS

BSA	Bovine serum albumin
CH_2Cl_2	Dichloromethane
CMP	Cytidine monophosphate
COSY	Correlation Spectroscopy
DCC	N,N-Dicyclohexylcarbodiimide
DHB	2,5-dihydroxy-benzoic acid
DIPEA	N,N-Diisopropylethylamine
DMAP	4-Dimethylaminopyridine
DMF	N,N-Dimethylformamide
DMSO	Dimethyl sulfoxide
Et_3N	Triethylamine
FT-IR	Fourier-transform infrared spectroscopy
h	hours
HATU	1-[Bis(dimethylamino)methylene]-1H-1,2,3-triazolo[4,5-b]pyridinium 3-oxid hexafluorophosphate
$HAuCl_4$	Chloroauric acid
HMBC	Heteronuclear Multiple Bond Correlation
HPAEC	High-pH anion-exchange chromatography
HPLC	High-performance liquid chromatography
HSQC	Heteronuclear Single Quantum Coherence Spectroscopy

IgG	Immunoglobulin G
KCL	Potassium chloride
LacNAc	N-Acetyl-D-lactosamine
$LiBH_4$	Lithium borohydride
LiHMDS	Lithium bis(trimethylsilyl)amide
MALDI-TOF/TOF	Matrix Assisted Laser Desorption / Ionization and Time of Flight
MeCN	Acetonitrile
MeOH	Methanol
MTT	3-(4,5-dimethylthiazol-2-yl)-2,5-diphenyltetrazolium bromide
$NaBH_4$	Sodium borohydride
NaOMe	Sodium methoxide
NHS	N-Hydroxysuccinimide
NMO	N-methyl morpholine N-oxide
NMR	Nuclear Magnetic Resonance
P-gp	P-glycoprotein
PNGase F	Peptide N-glycosidase F
PPh_3	Triphenylphosphine
RT	Room temperature
TBTA	Tris(benzyltriazolylmethyl)amine
TEM	Transmission electron microscopy
TFA	Trifluoroacetic acid
TGA	Thermogravimetric analysis
THF	Tetrahydrofuran

TIPS	triisopropylsilane
TMSOTf	Trimethylsilyl trifluoromethanesulfonate
TPAP	tetrapropylamine perruthenate
UDP-Gal	Uridine 5'-diphosphate galactose

CHAPTER 1

INTRODUCTION AND LITERATURE OVERVIEW

In the past decades, the use of chemotherapy drugs for the treatment of cancer is based on the premise that these agents would preferentially kill rapidly dividing cancer cells while sparing normal cells. The first class of chemotherapeutic agents to be tested in humans was the nitrogen mustards, chlorambucil, and cyclophosphamide that exert their cytotoxic effect by alkylation of the DNA.[1] Although the success of above compounds was short-lived, the initial success spurred the development of a continuous stream of new anticancer agents with improved activity. One of the early examples was the anti-folate drug called methotrexate. The design of this drug was based on the fact that cancer cell growth is stimulated by folic acid. Methotrexate is one of the first antitumor agents. After the elucidation of the structure of the DNA, compounds that interfered with DNA synthesis and caused cell death were developed. These included nucleoside analogues such as thioguanine, 5-fluorouracil, and the anthracyclines entered the array of drugs to treat cancer. Chemotherapeutic agents targeting tubulin (e.g. the *Vinca* alkaloids from plants) also entered clinical evaluation.[2]

Although the area of anticancer drug research for the treatment of cancer has rapidly evolved due to the discovery of a variety of potent chemotherapeutic agents. Despite the fast progress in drug innovation, little clinical impact on the cancer chemotherapy has been made to date. This is mainly because of the following hurdles: (i) most of the potent drugs are hydrophobic and hence are sparingly water-soluble, making them unsuitable for clinical applications; (ii) they usually lack specificity, causing high-level of off-target toxicities to

healthy cells mainly of bone marrow and gastrointestinal tract; (iii) many of these drugs suffer from an undesirable bio-distribution following intravenous administration, that results in low therapeutic efficacy as well as significant side effects in patients; (iv) in addition, they show poor pharmacokinetic and bioavailability[3] *in vivo*; and (v) there is a very little known about tumor physiology[4], role of immune system, and cancer stem cells that are responsible for the cancer development[5]. Most of the anticancer drugs had to be used near their maximum tolerated dose (MTD) in order to achieve a clinically meaningful therapeutic effect resulting in high dosage and poor selectivity. One of the major advancement was the introduction of the concept of combination drug therapy[6]. Cancer drugs with non-overlapping toxicity profiles and different mechanism of action could often be combined at full doses with resultant additive or synergistic effect. However, with this approach systemic toxicity to the host remains a major drawback of cytotoxic drugs in cancer, and hence complete remission can be achieved only in the small group of patients[6]. The low clinical efficacy of cytotoxic drugs could be due to the insufficient therapeutic window irrespective of whether used alone or in combination. For example, it has been proposed that more than 99% of the cells in the tumor have to be killed to achieve a complete remission in the patients. To systematically improve the therapeutic index of the cancer drugs, either potency of the cytotoxic drug needs to be improved to lower the minimum effective dose (MED), or tumor selectivity had to be improved to increase the MTD. In this instance the ideal solution would be to decrease the MED and increase MTD, thus can increase the overall therapeutic index of the drug[2].

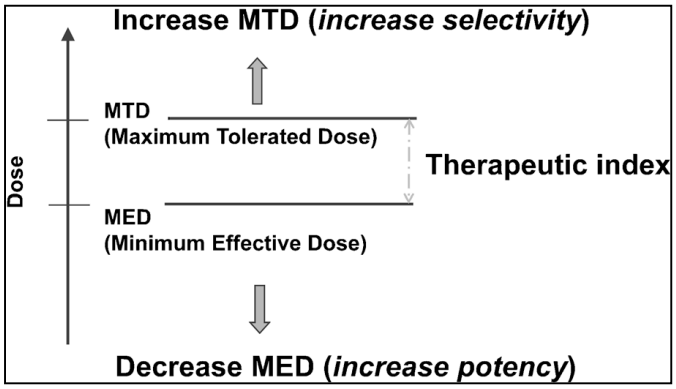

Figure 1.1 Approach to optimize the therapeutic index.

The concept of delivering a cytotoxic drug to cancer cells using an active targeting approach has been envisioned back to 1913 when Paul Ehrlich described the use of 'magic bullet', which can deliver a 'toxophore' selectively to the tumor[7]. The clinical output of cancer chemotherapy still relies upon selection of the right targets, the drug combinations, and an optimized drug delivery platform that can deliver and release the drug of interest into the specific tumor site[8]. In order to address above challenges, active and passive targeting approaches utilizing various forms of drug vehicles such as liposomes, polymeric nanoparticles, mesoporous silica nanoparticles, metallic nanoparticles (e.g. gold, iron oxide), and antibody-drug conjugates (ADCs) have been developed for the controlled drug delivery applications[2, 9]. Polymeric nanoparticles have gained most attention as they usually contain an intrinsically stealthy surface, possess enhance in vivo stability, and furthermore can be synthesized with diverse polymer structures, molecular weights, compositions, and functions to fulfill the requirements of a specific drug and application associated with it. In contrast to silica and metallic nanoparticles, polymeric nanoparticles made on several synthetic and natural polymers such as biodegradable aliphatic polyesters, polypeptides, poly(ethylene glycol) (PEG), hyaluronic acid (HA), and dextran have demonstrated excellent safety and are approved by the authorities for various biomedical applications. Depending upon the purpose, polymeric nanoparticles can be fabricated into various distinct nanostructures ranging from macromolecular prodrugs, micelles, nanogels, vesicles, and varying particle sizes from 4-250 nm[10]. Many *in vivo* studies interestingly have

shown that polymeric nanoparticles are able to circulate for a prolonged time and preferentially accumulate in the tumor site via the enhanced permeability and retention (EPR)[11] effect and also called as "passive tumor targeting." Interestingly, a few polymer-based nanomedicines such as Genexol-PM[12], NK 911[13], NK 105[14], and NC 6004[15] have been translated to the clinic or are into different phases of clinical trials. Overall, these clinical trials have demonstrated clear benefits such as improved patient compliance, better drug tolerance, and decreased side effects over current chemotherapy treatment.

However, the therapeutic efficacy of passive tumor-targeting drug delivery is still far away from the optimal. One of the major drawbacks is poor tumor cell uptake resulting from their stealth surface that is required for prolonged circulation[15]. It appears that EPR effect by which polymeric nanoparticles accumulate in tumor site is not universal and varies across different human tumor types[16]. It is important to note that the same nanoparticle characteristic that facilitates the EPR effect for tumors can also lead to accumulation of nanoparticles in liver and spleen, so it is highly unlikely that EPR alone can achieve full selectivity[17]. The surface decoration of polymeric nanoparticles with a specific tumor-homing ligand such as antibody, antibody fragment, peptide, aptamer, polysaccharide, saccharide, folic acid, and so on can largely increase the nanoparticle uptake/accumulation in tumor vasculature and facilitate selective internalization by target tumor cells, which is defined as "active tumor-targeting" (Scheme 1.1)[18]. Many studies have demonstrated that the ligand-directed active targeting nanoformulations have shown improved, through to varying degrees, therapeutic performances as compared to their passive targeting counterparts[19]. It is very important to note that besides targeting tumor-specific antigen, tumor neovasculature represents other interesting targets for

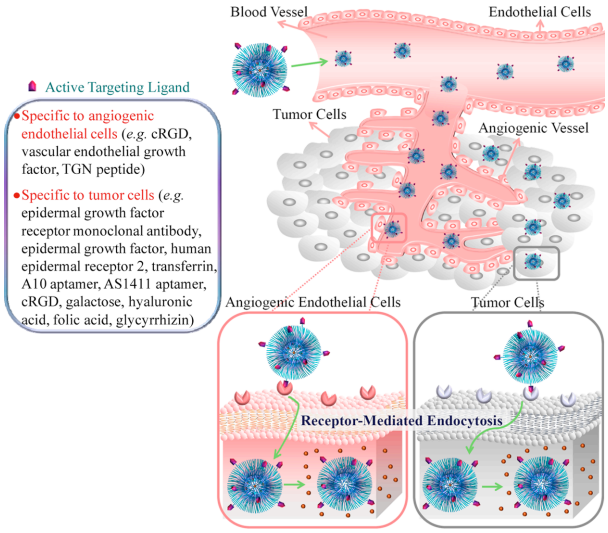

Scheme 1.1 Tumor targeting achieved through two strategies: (i) nanoparticle surface modification by tumor specific ligands and (ii) targeting to angiogenic endothelial cells using EPR effect of nanoparticles. Adapted with prior permissions from American Chemical Society.

targeted drug delivery, as tumor angiogenesis is known of critical importance to the growth and metastasis of solid tumors[19b, 20].

Broad ranges of targeting ligands have been used for the modification of various nanoparticles. This has been described in detail elsewhere[21] but mainly includes folic acid (FA), cyclic RGD (cRGD), hyaluronic acid, galactosamine, selectin, human epidermal receptor 2 (Her2), glycyrrhizin, bisphosphonates, (*S,S*-2-(3-(5-amino-1-carboxypentyl)-ureido)-pentanedioic acid) (ACUPA), and many genetically engineered monoclonal antibodies[2] (e.g. anti-Her2, anti-CD33, anti-CD22 etc.) have been employed for targeted drug delivery. It is important to notice that the type of targeting ligands, the size, shape, charge, and the stability of nanoparticle, as well as the ligand density, and affinity of targeting ligand plays a crucial role in the successful design of targeted cancer therapy[22]. Unfortunately, out of many targeted nanomedicines developed worldwide very few candidates have advanced to clinical trials illustrating the fact that the area of nanomedicines still remains at the early stage in the development.

Targeted drug delivery of polymeric nanoparticles

Polymeric nanoparticles have attracted significant attention as a versatile class of drug delivery vehicles. They can be generally classified into (Table 1)[21] macromolecular prodrugs, stealth nanoparticles, micelles, nanogels, nanocapsules, and vesicles. A wide variety of

nanoparticles have been fabricated that can be composed of unique shapes and different kind of materials including lipids, polymers, inorganic, hybrid materials etc. resulting in delivery systems that can provide desirable physicochemical properties. These properties can be tailored to suit for the delivery of a diverse group of drugs and applications. In general, drug delivery applications rely upon either encapsulation of hydrophobic drugs or covalent attachment of the chemotherapeutic drug to the water-soluble polymer backbone through stable yet cleavable linkage. These two forms represent the simplest versions of polymeric nanoparticle-based drug delivery system. It is important to note that for non-degradable polymer carrier, polymer molecular weight above 40 kDa is not suitable for its excretion from the body[23].

Stealth nanoparticles are in general composed of, for example, poly(D,L-lactide) (PLA) and poly(D,L-lactide-co-glycolide) (PLGA) polymers that are coated with water-soluble polymers such as PEG, dextran, and poly(acrylic acid) (PAA). To achieve prolonged circulation times, nanoparticles are often coated with above polymers that impart stealth character. Nano-precipitation, emulsification-solvent evaporation, and spray-drying are some of the methods used in the preparation of stealth nanoparticles utilizing a wide variety of drugs, either hydrophilic (e.g., cisplatin, peptides, and proteins) or hydrophobic (e.g., paclitaxel (PTX) and doxorubicin (DOX)), can be encapsulated. The stealth nanoparticles prepared by using above methods usually generates nanoparticles having mean diameters of 100-350 nm[24]. Polymeric micelles are generated through self-assembly of amphiphilic block or graft copolymers. They possess characteristic core-shell structure and average diameters ranging from 10-100 nm. They can significantly increase the water solubility of many lipophilic drugs and their bioavailability[25] and emerged as one of the best systems for targeted delivery of water-insoluble drugs like PTX, docetaxel (DTX), and DOX[26]. However, one of the major practical issues with polymeric

micelles is that they tend to dissociate and can cause burst release of payloads upon extensive dilution and interaction with proteins and cells in the blood circulation, which often lead to premature drug release following intravenous injection[27].

Nanosystem	Structure	Characteristics	Examples
Macromolecular prodrug	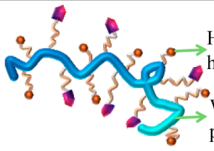	(i) Size: 4 ~ 15 nm; (ii) Drugs are chemically conjugated to water-soluble polymer backbone; (iii) Inactive during circulation while activated at the site of action; (iv) Active targeting achieved by grafting ligand to the polymer	RGDfK-HPMA-DTX; Gal-HPMA-DOX
Stealth nanoparticle	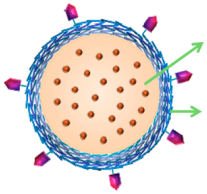	(i) Size: 100 ~ 350 nm; (ii) Able to carry hydrophobic and hydrophilic drugs; (iii) Targeting nanoparticles obtained by employing ligand-containing surfactant	Tf-PEG-HCPT; FA-PEG-DSPE/PEG-DSPE/DLPC
Micelle	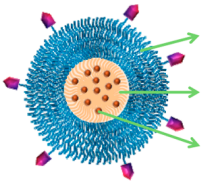	(i) Size: 10 ~ 100 nm; (ii) Core-shell architechture; (iii) Hydrophobic drug are loaded in the hydrophobic core; (iv) Targeting ligand introduced by attaching to the other terminal of the hydrophilic chain	EGF-PEG-PCL; A10-PEG-PLGA/PEG-PLGA; cRGD-PEG-P(Glu)
Nanogel	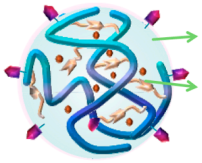	(i) Size: 20 ~ 250 nm; (ii) Hydrophilic polymer network; (iii) Drugs are loaded throughout the whole nanogel; (iv) Stable while fast responsive to environmental factors; (v) Active targeting obtained by conjugating ligand onto the outer surface	Gal-CS-g-PNIPAm
Nanocapsule	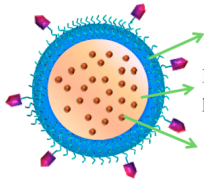	(i) Size: 100 ~ 500 nm; (ii) Consisting of an inner liquid core surrounded by a polymeric membrane; (iii) Hydrophobic drugs are loaded inside the capsule; (iv) Active targeting obtained by conjugating ligand onto the outer surface	FA-PEG/PEO-PPO-PEO
Polymersome	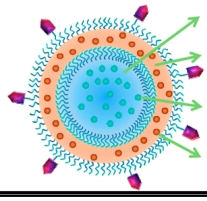	(i) Size: 10 nm ~ 10 μm; (ii) Polymeric vesicle containing a watery core; (iii) Able to carry both hydrophobic and hydrophilic drugs; (iv) Active targeting gained by installing ligand onto the other terminal of hydrophilic chains	Tf-PEG-PCL; Lf-PEG-PLA

Table 1. Structure and Characteristics of various Ligand-Directed Tumor-Targeting Polymeric Nanoparticles. Adapted with the permission of American Chemical Society.

Polymersomes are one of the popular drug delivery vehicles made up of polymeric vesicles that contain a watery core and are prepared by self-assembly of amphiphilic block copolymers in aqueous conditions. They can be made in a broad range of sizes from 10 nm to 10 μm[28]. It is interesting to note that polymersomes are highly versatile since they are not only used to deliver hydrophobic drugs but also hydrophilic drugs such as peptides, proteins, and siRNA. They possess some unique mechanical properties such as the membrane of polymersomes, owing to their higher molecular weights and existing chain entanglements is in general thicker, stronger, and tougher than liposomes[29].

Tumor-specific targeted drug delivery can be achieved by functionalizing various ligands (Table 1)[30] on the surface of polymeric nanoparticles. For example, tumor-targeting prodrugs are usually synthesized by grafting ligands to the polymer carrier backbones. Active tumor-targeting micelles and polymersomes are obtained by installing ligands onto the other terminal of hydrophilic chains of amphiphilic block copolymers. The stealth nanoparticles can be decorated with active targeting moiety by employing functional surfactants containing a specific ligand. Active targeting nanogels and nanocapsules can be obtained by conjugating ligands onto their outer surfaces by, for example, click and carbodiimide chemistry. It should be noted that installation of targeting ligands not only will enhance specific tumor cell uptake but also may further improve the retention and accumulation of nanoparticles in the tumor vasculature, which would result in the significantly improved therapeutic window and reduced systemic toxicity.

The *in vivo* performance of the targeted nanoparticle is greatly influenced by the stability of nanoparticles in the blood circulation. It is often noticed that a significant amount of drug would quickly leak out from the nanoparticles. This premature drug release is one of the major reasons for low drug accumulation in the tumor site. To circumvent the problem of premature

drug release, rational design of the linkers that plays an important role not only in carrying covalently attached drug molecule but also in providing a unique mechanism for controlled drug release has been developed and continued to grow as an active area of research. It should also be noted that tumor targetability[31] is also highly dependent upon type and position of ligands. Ligands like antibodies are highly specific, while other ligands, such as cRGD and FA, are more ubiquitous and can also target healthy cells hence there use can lead to confusing outcomes hence cannot be generalized. To illustrate the targeting effect, ligands need to be fully exposed to the outer surface of nanoparticles. Hence, the ligand density is one of the most important criteria and however, should be optimized, depending on types of ligands and nanoparticles, to attain a high level of tumor accumulation as well as efficient and selective internalization by tumor cells[32].

Other types of nanocarriers for drug delivery

Nanoscale materials can be synthesized in various shapes (Figure 1.2) such as globular particles, tubes, and rods, and can serve as modular platforms that have the potential to also provide multifunctional properties. They have found broad applications and actively investigated for the development of targeted nano-therapeutics and diagnostic devices for applications in cancer, as well as other applications such as in inflammatory, infectious, and autoimmune diseases[33]. Currently, there are many other classes of such nanocarriers such as organic/inorganic-based nanomaterials that includes dendrimer nanoparticles (NPs)[34], carbon nanotubes[35], iron oxide NPs (IONPs)[36], and gold NPs (AuNPs)[37].

Each of these types of nanoparticles is unique in its chemical and physical aspects such as synthetic methods, surface functionality and modification, core-shell architecture, size, and shape. Deep understanding of the physicochemical properties of these materials and their

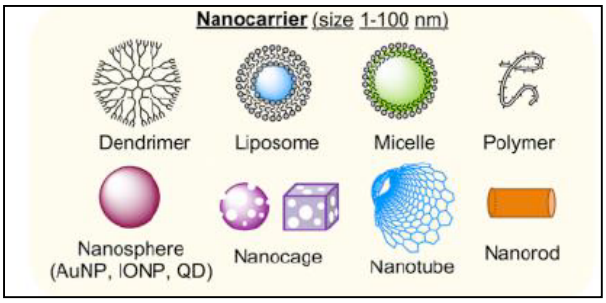

Figure 1.2 Nanocarriers fabricated in various shapes ranging from spherical to nanorods. Image adapted with prior permissions from American Chemical Society.

possible interactions with biological systems is extremely important in designing therapeutic applications, as some of these nanomaterials are known to cause unwanted effects due to their intrinsic toxicity[38] or immunogenicity[39] often caused due to suboptimal surface modification[40]. For example, cationic nanoparticles have an ability to disrupt cellular membranes and are highly cytotoxic as shown by unmodified poly(ethylene imine) (PEI) and poly(amidoamine) (PAMAM) dendrimers[41]. However, the cell-killing effect of these nanomaterials is reduced or completely eliminated by a modification of the surface with neutral or anionic groups[42]. This surface modification is an important aspect of developing certain other inorganic classes of nanoparticles that are also found to be intrinsically toxic, namely cobalt/chromium nanoparticles and multiwalled nanotubes (MWNTs). They act by damaging DNA strands[43] or suppress immune function[39], respectively. Many aspects of nanotoxicity associated with therapeutic applications have been recently reviewed thoroughly in many articles[44]. Thus, the construction and development of nanomaterials for drug delivery applications warrant a need for alternative approaches.

Mechanisms of drug release

The control drug release by triggering linker cleavage mainly revolves around a condition that is highly specific to diseased cell such as pathophysiological and subcellular properties. Triggering mechanisms in many cancer cells includes tumor hypoxia (low oxygen levels due to increased metabolic rates in tumor cells), low intracellular pH (endosomes and lysosomes where targeted nanomaterials are taken up), lowered extracellular pH for tumor cells, tumor-specific

enzymes (matrix metalloproteinase, prostate-specific membrane antigen) overexpressed on the cell membrane, and upregulation of glutathione. Above mechanisms of drug release are highly relevant to the design of cleavable yet stable linkers. Linker type chemistries to be discussed include ester, amide/peptide, disulfide, hydrazone, hypoxia-activated, and self-immolative linkages[45]. Finally, recently reported strategy that uses photochemistry or thermolysis for triggering drug release in an actively controlled manner will be discussed for its mechanism and applications. Overall, comprehensive information summarizing various aspects important to linker design and specific molecular mechanisms to achieve controlled release of therapeutic agents have been illustrated.

Ester hydrolysis

a) Biochemical mechanism for the release of ester-linked drugs

Many therapeutic agents having a functional group such as a carboxylic acid or alcohol allows the use of a conjugation strategy using ester-based drug attachment to the nanocarrier. The ester bond subsequently opens a route for drug release due to its susceptibility to hydrolysis when exposed to physiological conditions *in vivo*. The ester linker, in general, can be cleaved by the hydrolytic reactions catalyzed mainly by acids, bases, metal ions, and hydrolytic proteins such as human serum albumin and esterase's. It is an interesting case where metal ion can bring about hydrolysis of ester bonds has been reported with metal ions such as Cu^{2+} but significant rate acceleration has only been observed where metal ions are chelated proximal to the carboxylate functional group.

Alternative mechanisms that make a greater contribution to the ester cleavage relate to cellular events that occur during the uptake and processing of the drug-carrying nanoparticle or antibody-drug conjugates by a target cell. As shown in figure 1.3 after receptor-mediated

endocytosis, drug conjugates are processed first in early endosomes and then into late endosomes. Many of these vesicular compartments contain different types of acid hydrolases that can catalyze the hydrolysis of a wide set of substrates including ester or amide linked drugs. These compartments contain an abundant amount of cholesteryl ester acid hydrolase, aryl sulfatase, acid phosphatase, N-acetylglucosaminidase, and cathepsin D and display optimum enzyme activity in acidic conditions (pH 5-6) created mainly by endosomes and lysosomes. Hence, the majority of drug release from ester-based drug linkers on targeted nanoparticle is attributable to intracellular linker processing and hydrolysis by the action of acid hydrolases occupying the acidic compartments.

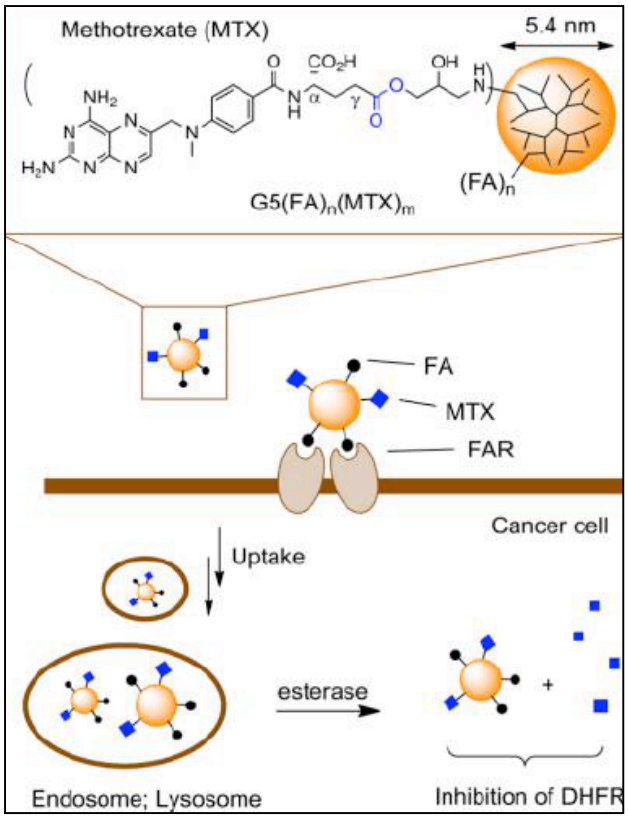

Figure 1.3 Methotrexate (MTX) conjugated to G5 PAMAM dendrimer through an ester linker and its mechanisms of antitumor action. Each MTX is attached through an ester linkage at its α- and/or γ-carboxylic acid positions. FA = folate. DHFR = dihydrofolate reductase. Images adapted with prior permission of American Chemical Society

b) Representative example of ester-linked drug: Release mechanism of methotrexate (MTX)

MTX belongs to the family of antifolate molecules widely used for the treatment of cancers and inflammatory diseases. It particularly inhibits cytosolic dihydrofolate reductase at subnanomolar concentrations. Dihydrofolate reductase catalyzes the reduction of dihydrofolate to tetrahydrofolate, a cofactor that is involved in the biosynthesis of thymidine and related DNA building blocks. MTX suffers from the narrow therapeutic index and dose-limiting systemic toxicity. In order to overcome limitations, MTX has been delivered using targeted nanoparticles.

As represented in figure 1.3 MTX[46] has two carboxylic acids displayed on the L-Glu portion of the molecules. 1-Ethyl-3-(3-dimethylaminopropyl)carbodiimide (EDC) based ester coupling method for conjugation of MTX to the fifth generation (G5) PAMAM dendrimer was employed where MTX was pre-conjugated with the folic acid receptor targeting ligand and subsequently modified with a glycidyl moiety. This folic acid targeting MTX conjugate was studied in details for their biological activity. *In vitro* studies showed selective uptake by a FA positive KB cells via a receptor-mediated endocytosis mechanism and demonstrated potent inhibition of cell proliferation. When tested *in vivo*, the conjugate showed improved therapeutic efficacy in disease models for epithelial cancers, head and neck tumors, and inflammatory arthritis. Despite well documented *in vitro* and *in vivo* studies for the conjugate, the actual mechanisms of action and release of this ester-conjugated MTX remains undetermined. So, it is unclear to what extent MTX remains conjugated to the dendrimer after cellular uptake, and whether MTX has to be released from its conjugate in order to show therapeutic activity. This uncertainty was addressed in part by a separate cell-free DHFR activity assay, which showed that the conjugated form of MTX also displayed inhibitory activity, though less potently than free MTX.

Amide hydrolysis

a) Biochemical mechanism for the release of amide-linked drugs

Drug attachment to the nanovehicle using an amide bond is broadly applicable for many molecules because many drug molecules are commonly functionalized with either a carboxylic acid or amine group. The resulting amide bond is much more stable and less susceptible to chemical hydrolysis as compared to ester bond. Unless designed with a special functional group, the amide linker has never observed to be cleaved by chemical hydrolysis under physiological conditions, since its chemical cleavage requires harsh conditions such a combination of much higher temperatures and presence of strong acid or base catalysts. Stability through amide linkage can provide certain benefits for achieving improved pharmacokinetic profiles by extending the duration of circulation in the blood. Generally, amide hydrolysis is based on enzymatic mechanisms and is carried out by hydrolytic proteases[47] such as serine proteases, cysteine proteases, and zinc-dependent endopeptidases. Each of the above enzymes is localized in one or more sites in the cell ranging from the extracellular environment, to the cellular membrane, to intracellular lysosomes, and thus their site-specific action is nothing but the site of drug release. Classical illustrations of matrix metalloproteinases (MMPs)[48] such as collagenases are zinc-dependent endopeptidases secreted primarily into the extracellular matrix (ECM) of tumor cells. MMPs are mainly involved in remodeling of the extracellular matrixes through degradation of ECM proteins. Many MMPs are overexpressed in different tumor types and are implicated in the dysregulation of angiogenesis leading to tumor growth and metastasis. This is demonstrated by the MMP-associated release of methotrexate linked to a poly(lysine) dendrimer through a peptide linker containing the MMP specific cleavage sequence, PVG↓ LIG. MTX

release upon incubation with MMP 2 or MMP 9 was shown in a time-dependent manner with ≤ 20% efficiency at 24 h.

b) A Representative example of amide-linked drug:

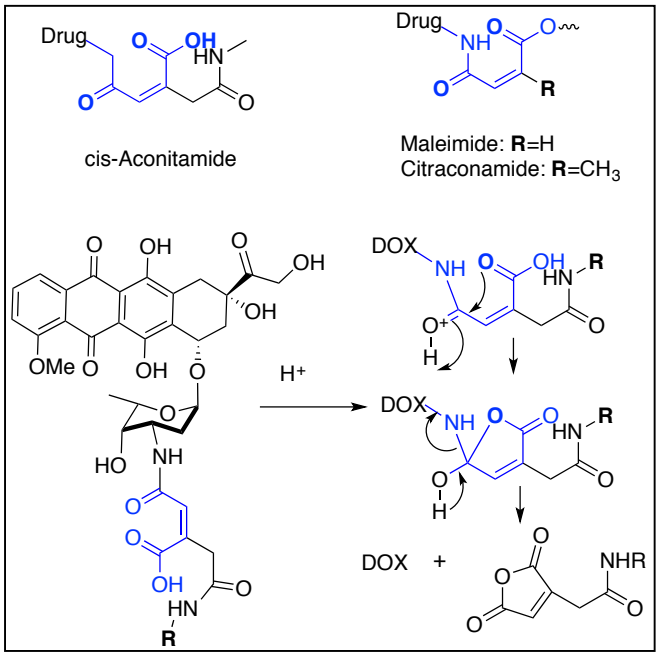

Figure 1.4 Structure of pH sensitive amide linkers (top) and illustration of a proposed acid catalyzed cleavage mechanism for a *cis*-aconityl amide linker, leading to doxorubicin release (bottom).

Non-enzymatic cleavage of amide linkers can be facilitated by certain classes of specialized linkers attached to drug molecules through an amide bond have been shown to be responsive to low pH environments. These linkers mainly contain groups such as maleic acid frameworks like citraconyl, *cis*-aconityl, and maleyl groups. The application of these linkers has been demonstrated by amide conjugation (figure 1.4) of the *cis*–aconityl[49] group to doxorubicin at its daunosamine sugar. Incubation of this conjugate in citrate-phosphate buffers at various pHs and 37°C, amide linker was hydrolyzed to release free doxorubicin with half-lives at pH 4, 5, and 6 of <3, 6, and 96 h, respectively. This amide linker was extremely stable at pH 7 and negligible hydrolysis was observed even after a 4-day incubation. Therefore, cleavage of this *cis*-aconityl linker is highly pH-dependent, that facilitates controlled release of the doxorubicin to be regulated by the pH of the environment. As compared to two other structurally analogous linkers that were designd for doxorubicin conjugation, the *cis*-aconityl linker was hydrolyzed at a faster rate than the maleyl linker at the same pH, but slightly lower than that of the citraconyl linker, which showed rapid

hydrolysis within 3 h at pH 4.2. The above rate of hydrolysis pattern is in good agreement with the later study performed on emetine, an anticancer natural product, which had rates of hydrolysis of the same order at both pH 5.5 and 6.5 (citraconyl > aconityl > maleyl amide).

Hydrazone hydrolysis

a) Biochemical mechanism of hydrazone-linked drugs

Hydrazone is class of linkers that are terminated with acyl hydrazone, alkoxy carbonyl hydrazone, and benzenesulfonyl hydrazone. This linkage type has been applied for numerous classes of anticancer drugs including doxorubicin, paclitaxel, platinum-based agents, auristatin, and calicheamicin. This conjugation chemistry is suitable for a particular class of drug molecules or their derivatives where a chemical handle such as a ketone or aldehyde group that can be coupled to a hydrazine terminated linker. Hydrazone linkage is fairly stable at physiological pH (7.4) and hence hydrazone-linked drug molecules carried by the conjugate remain attached during systemic circulation. However, the hydrazone linkage is cleavable at lower pH environment, providing a controlled mechanism of drug release. The optimal condition for triggering linker cleavage is at pH $\leq$ 5. Thus, drug release occurs mainly after endocytosis and exposure to the acidic environments of endosomes and lysosomes (pH 6.5− 5.5).

b) Representative example of hydrazone-linked drug

A Couple of synthetic methods has been developed for hydrazone conjugation of a ketone/ aldehyde group-containing drug molecule to nanocarriers as summarized in figure 1.5 first, a hydrazine-terminated linker is incorporated onto the surface of nanoparticle prior to the conjugation reaction with the drug of interest (method 1)[50]. This method is represented by doxorubicin conjugation through its ketone. This method is preferred for certain types of drug molecules that have structures, which contain nucleophilic functional groups such as amines as

found in the daunosamine aminoglycoside of doxorubicin. If the nanoparticle is modified by nonhydrazine functionality such as a carboxylic acid instead, the amine from the drug will act competitively in the conjugation reaction with the nanocarrier, resulting in an amide linkage.

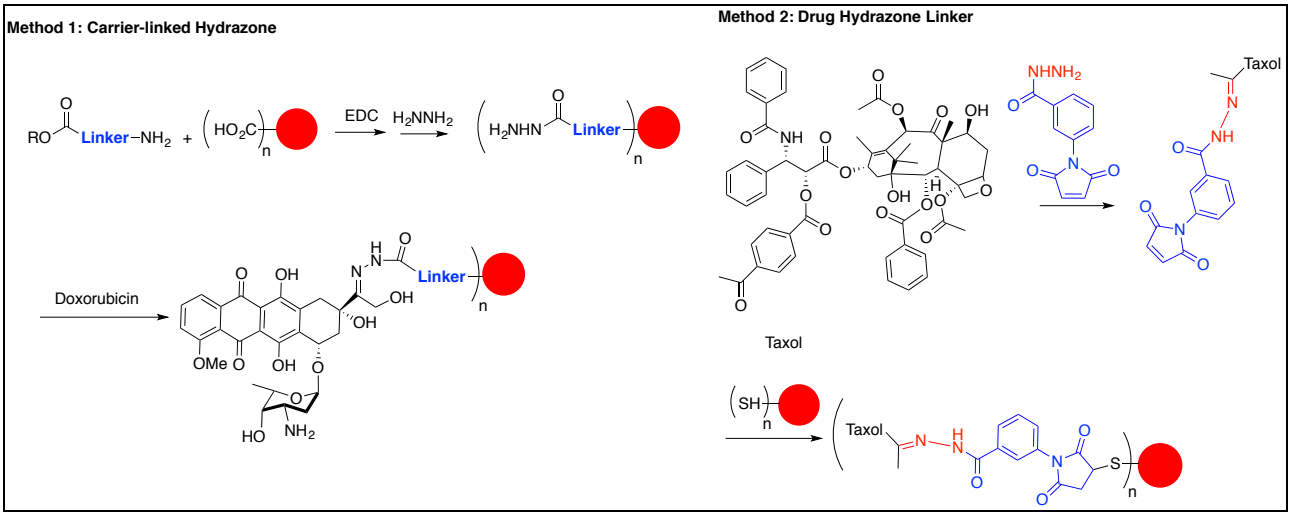

Figure 1.5 Illustrative examples for the drug conjugation via hydrazone linkage.

However, the amide linker is extremely stable and hence significant amount of drug molecules linked through an amide linkage is not cleavable even upon exposure to acidic subcellular compartments. In the Second method[51], a hydrazone linker is preinstalled on the drug molecule by reaction with a hydrazine linker and then the resulting drug-linker is attached to the carrier such as antibody by a chemoselective reaction with the linker. This route is validated by paclitaxel conjugation in which a bifunctional linker composed of an acyl hydrazine and maleimide group is utilized. The maleimide group reacts chemoselectively with the thiol expressed on the surface of the antibody as a carrier, and hence bioorthogonal to the hydrazine reacting with the ketone modified paclitaxel.

Disulfide Exchange

a) Biochemical mechanism of disulfide exchange

Disulfide linkers are one of the important classes of linkers that have been employed for drug conjugation in targeted drug delivery. Unlike linkers such as amide, ester, and hydrazone chemistry, the disulfide bond is not susceptible to hydrolytic cleavage. In this case, disulfide bond undergoes cleavage reaction through an electrochemical reduction process to yield the respective thiol or disulfide exchange reactions. This electrochemical reduction can also occur through a chemical mechanism triggered by an endogenous thiol molecule such as cysteine, homocysteine, N-acetyl cysteine, glutathione (L-γ-glutamyl-L-cysteinyl-L-glycine; GSH), other cysteine-containing peptides, and thioglycolic acid[52]. Drug attached through disulfide linker is stable enough for targeted intracellular uptake of the drug-linked nanovehicle since the disulfide exchange reaction occurs mainly in the cytoplasm after their endocytosis. Moreover, it is important to note that drug release via cleavage of the disulfide linker is not contributed by redox machinery located on the cell surface but through the thiol triggered intracellular reactions.

Glutathione (GSH) being an important player in the cleavage of disulfide-linked drugs:

Glutathione (GSH) is a major player in cancer cell-specific drug release. GSH exists mainly in the reduced form inside the cell, and its total cellular distribution is localized in the various compartments as cytoplasm (2-10 mM; ≤ 85%), mitochondria (≤ 30%), and nucleus (≤ 10%)[53]. Such a high cytoplasmic concentrations of GSH are mainly associated with cellular detoxification mechanisms such as the formation of GSH conjugates with cytotoxic chemotherapeutic and redox reactions with genotoxic reactive oxygen species. Moreover, its cellular expression level is subject to change and can be increased up to 10-14 mM. In many cancer cells, GSH is often exploited as a counter strategy to reduce the cytotoxicity of anticancer drugs and has been found to be responsible for drug resistance to certain cancer cell types. However, such a higher expression and reactivity of GSH in cancer cells has been utilized

successfully to design prodrugs that can respond to the controlled release of drugs targeted toward these types of cancer cells.

b) Representative example of disulfide-linked drug

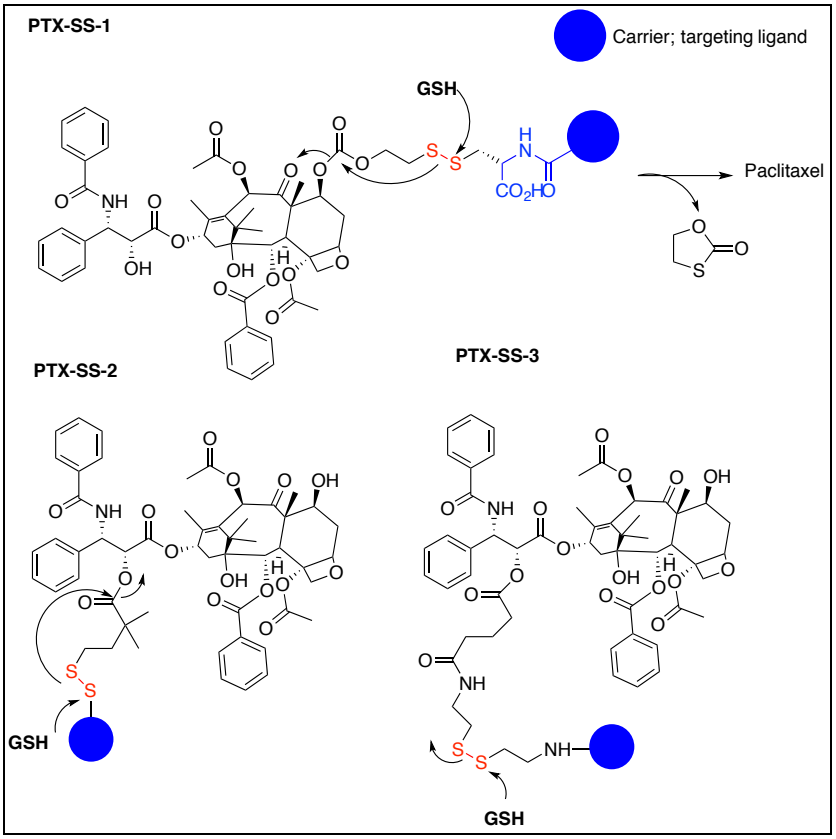

Figure 1.6 Design of disulfide-tethered taxol constructs, and mechanisms for GSH-triggered, the self-immolative release of paclitaxel.

Controlled drug release in a targeted delivery via disulfide linkage has been extensively studied for a group of many cytotoxic compounds including those used currently in the clinic such as paclitaxel, gemcitabine, mitomycin, maytansine, and calicheamicin. The introduction of disulfide in most anticancer molecules to a nanocarrier or cancer-specific antibody is performed by indirect methods since each drug molecule lacks a free thiol or disulfide functional group in its chemical structure. Paclitaxel-disulfide linked molecules such as PTX-SS-1[54]; PTX-SS-2[54], and PTX-SS-3[55] demonstrate this strategy as shown in Figure 1.6. In above examples disulfide

spacer is attached to paclitaxel at its C-7, and C-2 side chain attached via carbonate or ester functionality. This variation of functional groups in the linker is designed for enabling the release of the free drug since a disulfide exchange reaction with GSH will trigger the release of drug molecule that is terminated with a thiol moiety. However, the ester or carbonate is reactive to the nucleophilic thiol, the transient drug intermediate can subsequently undergo a thiol-mediated intramolecular cyclization reaction, and free paclitaxel is released as a result of the formation of 2-oxathiolane (PTX-SS-1) or a five-membered thiolactone (PTX-SS-2).

Hypoxia activation

a) Biochemical mechanism for the release of hypoxia-induced drugs

Hypoxia is mainly characterized by a state of abnormally low oxygen supply in tissues and cells. Similarly, like an acidosis (pH 6.5− 6.9), it constitutes one of the hallmarks of solid tumors, as the growth of new immature vessels results in poor perfusion and in oxygen deprivation. Tumor microenvironments are often associated with low oxygen levels, hence the equilibrium of the enzymatic activities of oxidoreductases are shifted mainly favoring the reduction of substrates. Using this feature of cancer cells, they can be selectively targeted by prodrugs that are only activated by such enzymes, which are activated in hypoxic conditions as the oxidoreductase and also referred to as hypoxia-specific enzymes[56]. Activation of many drugs (mitomycin C, apaziquone (EO9), TH-302, banoxantrone (AQ4N), PR104A, and RH1) using oxidoreductase has been well documented in the literature.

b) Representative example of hypoxia-induced release of drug

Reductive activation of prodrugs catalyzed by oxidoreductases has been employed in the design of certain linker-drug constructs where the linker is cleaved in response to hypoxia,

resulting in drug release in the tumor. These hypoxia-dependent linkers have been classified based on core functionality of the substrate including quinone-trimethyl lock systems[57], indolequinone, nitroaromatic heterocyclics (nitroimidazole, nitrofuran, nitrothiofuran), and N-oxides (tirapazamine).

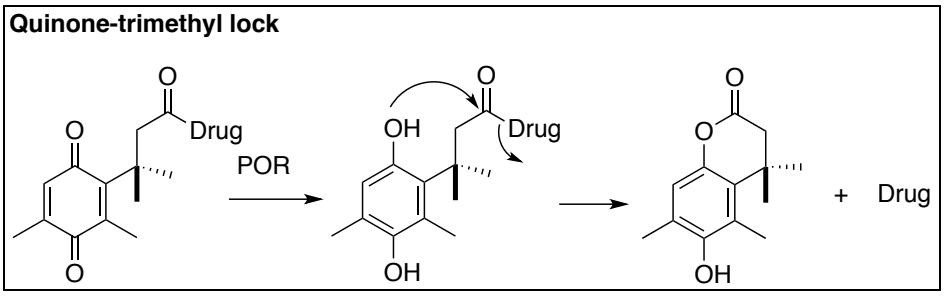

Figure 1.7 Mechanism of drug release triggered by oxidoreductase, POR= cytochrome P450 oxidoreductase.

In case of quinone-trimethyl lock system, cleavage of this linker in cancer cell is mediated by cytochrome P450 oxidoreductase (POR) via a two-electron ($2e^-$) reduction mechanism, and the resulting hydroquinone intermediate undergoes an intramolecular six-membered-ring cyclization, leading to release of the drug molecule as a leaving group (Figure 1.7). The role played by three methyl groups is the real highlight for this design since the extended spacer was aimed to lock the conformation of the drug linker in a more favorable position for intramolecular attack by the phenol group and, thus, facilitate the rate of drug release.

Mannich base

a) Biochemical mechanism for the release of drug through mannich reaction

The Mannich reaction is the aldehyde-mediated condensation between primary or secondary amine molecule and a nucleophilic molecule including amines, phenols, carboxamides, and ketones. The release of using mannich base system serves as an important strategy for targeted drug delivery but has never been very popular than other methods. However, The product of this reaction, (commonly called a Mannich base), serves as a prodrug

for the parent drug molecule and is effective for improving its solubility and pharmacokinetics. Moreover, this strategy has numerous synthetic advantages such as chemo-selective conjugation to amines and high tolerance of the conjugation reaction to the presence of diverse functional groups. Finally, the reaction is performed in aqueous-alcoholic conditions that are unique and are important for the solubilization of many drug molecules, which are most of the times polar and charged.

b) Representative example of mannich base mediated drug release

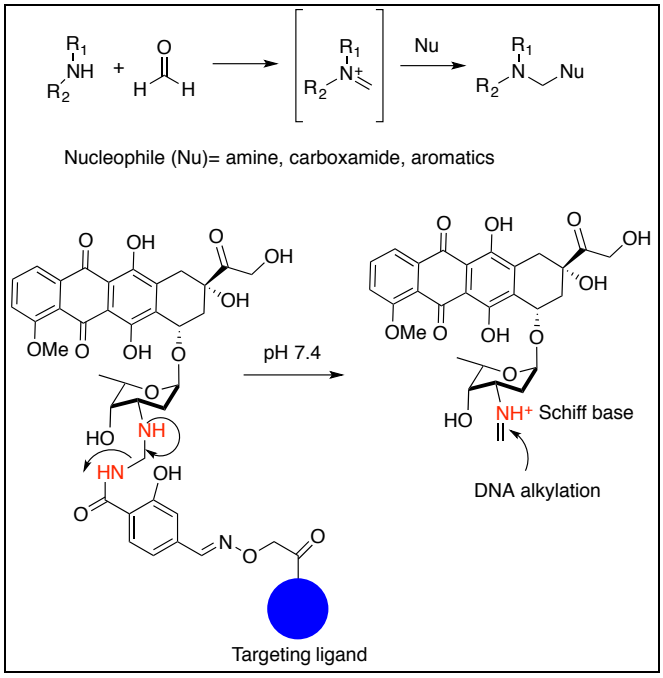

Figure 1.8 Structure of a doxorubicin molecule tethered to an Arg-Gly-Asp (RGD) targeting ligand through a Mannich linker based on salicylamide.

Doxorubicin is conjugated through a formaldehyde-derived linkage to a small Arg-Gly-Asp (RGD)[58] peptide ligand targeting a $\alpha_v\beta_3$ integrin receptor. This work showed that Mannich linker undergoes hydrolytic cleavage and converted into its Schiff base (“ imine”) form in the

cytosol that follows up with hydrolysis to give free doxorubicin. Importantly, construct showed higher cytotoxicity than unmodified one in both drugs sensitive and drug-resistant tumor cells. A remarkable activity is due to its additional mode of action such as covalent modification of DNA base pairs by the released doxorubicin Schiff base.

Self-immolative linkers

a) Biochemical mechanisms of self-immolation

Self-immolative linkers are emerging class of reactions that bring about a cascade of spontaneous, intramolecular reactions that occur in response to an applied external stimulus trigger. These linker types have found wide utility in the targeted drug delivery applications. These linkers incorporate dual functional features in its structural design with a triggering moiety linked to a self-immolative spacer rather than direct attachment to the drug molecule. Thus, the drug release mechanism is different than of direct release linkers due to the presence of the intervening spacer. Each of these triggering moiety is rationally designed for specific cleavage in response to the application of certain external stimuli with respect to the drug structure. This includes mainly (Figure 1.9)[45] enzymatic triggers of glycosidases, plasmin, cathepsin B, other peptidase, and β-lactamase. Other triggers can be thiol-disulfide exchange, low pH, bioreduction, and light.

This triggering mechanism is based on following principle. Once the triggering moiety is removed from the terminus of the linker, the free spacer group is activated and undergoes spontaneous cyclization or electronic cascade reactions, leading to drug release. Each of such cascade reactions is based on 1,4 or 1,6 elimination reactions. This subsequently undergoes cyclization of an amine-terminated spacer to a five-membered urea and carbamate fragment, and cyclization of a mercapto ester or " trimethyl lock" spacer to a lactone moiety. Other features of

above linkers system are due to extended spacer length. Presence of such extra spacer provides relief from steric clashes between the triggering moiety and a bulkier drug molecule and is highly essential for efficient cleavage of the trigger group by macromolecular enzymes such as glycosidases, peptidases, and bioreductive DT diaphorase illustrated here in figure 9.

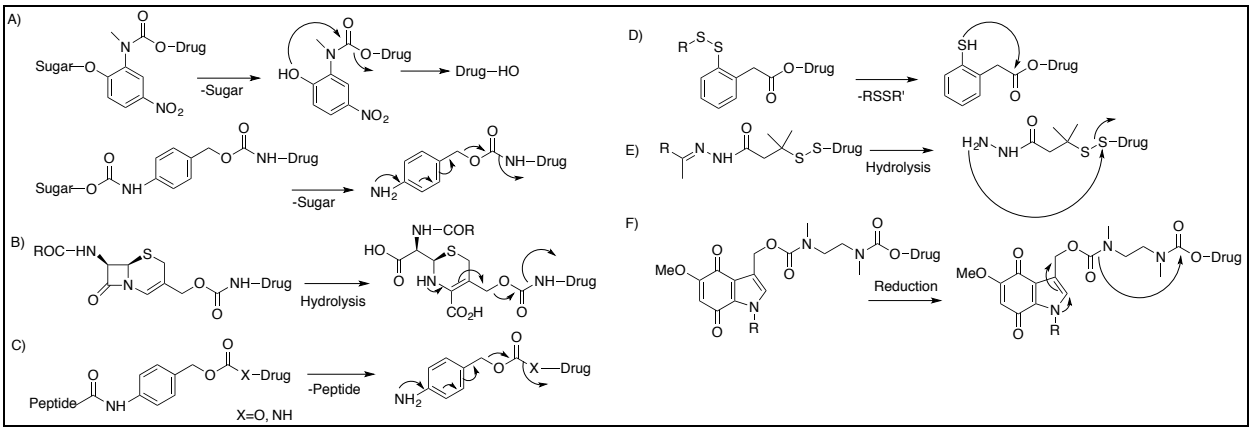

Figure 1.9 Types of self-immolative linkers and spontaneous release reactions triggered by glycosidase (A), cephalosporin's or β-lactamase (B), peptidase (C), glutathione (D), low pH (E), and bioreduction (F).

Photochemistry

a) Mechanism of drug release through photoirradiation

A key aspect of drug delivery science is the ability to control the timeframe of release after uptake of the drug conjugate by the targeted cell. Many of the release mechanisms discussed earlier mainly depends upon either chemical or enzymatic cleavage of the linker to which drug is attached. Such a drug release mechanism is mainly influenced by specific factors or stimuli highly selective to linker type or tumor environment. Photochemistry, however, brings about orthogonal release approach where light is applied to actively trigger drug release (Figures 1.10). In chemistry this approach is termed as photocaging[59]. In this method, a drug molecule is temporarily inactivated by derivatization with a photocleavable trigger group (photocage). This photocaged molecule releases its parent drug molecule. Controlling this drug release using light

as a trigger is very difficult and requires sophisticated methods. Photochemical means of drug release has been applied to numerous drugs such as doxorubicin, methotrexate, 5-fluorouracil, paclitaxel, camptothecin, doxycycline, and tamoxifen. Many of these photochemical linkers are based on UV-light-responsive aromatic rings comprised of o-nitrobenzyl (ONB), coumarin, quinoline, xanthene, and benzophenone[45].

b) Representative example of photochemical drug release

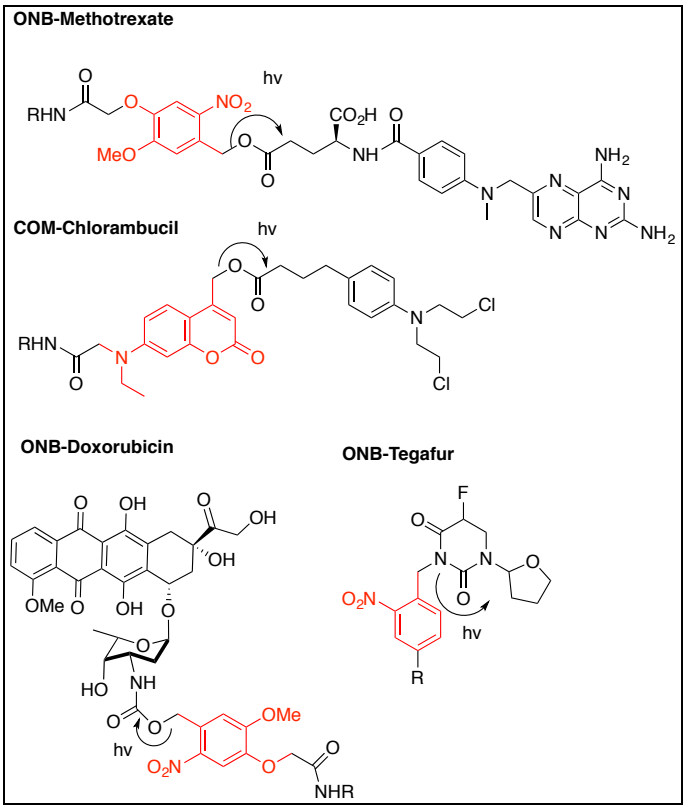

Figure 1.10. Examples of photo-controlled release of drugs using o-nitrobenzyl and coumarin-based linkers.

Figure 1.10 represents detail structures of some of the main photocleavable linkers. Out of these, the ONB group has been most commonly employed for drug attachment to nanocarriers including PAMAM dendrimers[60] and AuNP[61]. Synthetically, ONB linker provides greater flexibility in its aromatic ring substitution and further derivatization and allows facile modifications for use in linker installation and drug attachment. ONB can be easily cleaved by

one-photon (254-365 nm) and two-photon (710 nm, 750 nm) excitation wavelengths. Coumarin-based linkers represent one of the major classes of photon-cleavable linkers where drug of interest is covalently attached to a methyl group located at the C-4 position of 7-dialkylaminocoumarin or 6-bromo-7-hydroxycoumarin. These linkers are amenable to cleavage at one-photon (365 nm, 475 nm) as well as by two-photon (740 nm, 800 nm) wavelength with an advantage of providing a greater cross-section of two-photon absorption for uncaging than the ONB class for more efficient drug release. In summary, light acts as an effective mode of drug release. It is potentially applicable for those therapeutic and diagnostic applications *in vivo* that require noninvasive or spatiotemporal drug/probe activation. One of the technical problem facing such applications *in vivo* relates to the poor tissue penetration of UV or visible light, which makes it less efficient than *in vitro*. Recently, upconversion nanocrystals (UCNs)[62] open up promising opportunities for the photochemical control of drug release. Certain classes of UCNs show unique optical properties that allow them to emit light in the UV range upon excitation by near-infrared (NIR) light at 980 nm.

Azo reduction

a) Biochemical mechanism for azo reduction

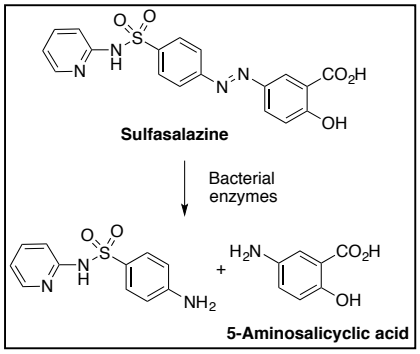

Figure 1.11. Bacterial enzyme mediated cleavage of an azo linker.

The azo reduction is often achieved through incorporation of azo linker that can be cleaved through biological mechanism. This type of linker chemistry has been employed for the activation of an anti-inflammatory class of azo-linked prodrugs[63]. This mainly includes sulfasalazine, balsalazide, ipsalazide, and olsalazine. For example, sulfasalazine undergoes reductive cleavage of its azo linker by bacterial enzymes in the colon to an active metabolite, 5-amino salicyclic acid (ASA) shown in figure 1.11.

Antibody-drug conjugates

It is well established that cancer cells possess specific molecular markers that play an important role in tumor growth or progression and has opened the door to specifically target these markers, also called tumor associated antigens. They mainly comprised of cell surface proteins, glycoproteins, or carbohydrates. Ideally, the antigen may be overexpressed or present in mutated form on cancer cells. Immunization of mice with human cancer cells or purified antigens elicits a target-specific antibody response in the sera of these animals. However, they are often obtained in low yields and as a mixture that contains antibodies against non-specific antigen targets. An advance in the hybridoma and recombinant DNA technology has enabled production of large amounts of a single purified antibody to the antigen of interest[64]. Highly specific and less immunogenic antibodies were produced by replacing protein sequences of the murine antibody with sequences naturally occurring in human antibodies, without affecting the

specific binding of the antibody to its target antigen. In the first generation constructs, molecular biologists merely replaced the entire constant regions of the murine antibody with the corresponding human constant region sequences, while retaining the murine variable domains (Fv) responsible for antigen binding (figure 1.12).

These so-called chimeric versions of antibodies still possess some murine residues that can lead to non-specific binding or interactions. So, antibody-engineering methods have advanced to a great extent and led to new humanization methods wherein the humanized antibody, only the essential antigen recognition murine residues encompassing the complementarity-determining regions (CDRs) within the Fv domains are preserved, while the remainder of the murine Fv is replaced with human Fv sequences. Further, phage display technology[65] and transgenic mice bearing the human repertoire introduced new avenues for generating fully human antibodies requiring no additional engineering for human therapeutic development. With these developments, it has been possible to reduce or eliminate the immune response previously noted with murine antibodies and also the circulation half-life of these new constructs is significantly longer ($T_{1/2}$ up to three weeks) than that of their murine versions (typically two to three days). Typically, antibodies are macromolecular Y-shaped protein approximately 150 kDa and above. The efficiency of tumor cell killing by antibodies can range widely, from poor to high depending on the nature of the target antigen.

In general, antibodies can induce cancer cell death by a multitude of mechanisms, including a) immune-mediated functions, such as antibody-dependent cellular cytotoxicity (ADCC), b) complement dependent cytotoxicity (CDC), c) antibody-dependent phagocytosis, d) interference with tumor-cell signaling pathways, often achieved through receptor blockage, e) depletion of circulating tumor cells by direct binding to the antibody, f) apoptosis, and g)

immune modulation of T-cell function[66].

There are very few examples in current literature where antibody alone has been employed for the treatment of various cancers[2]. For instance, ipilimumab, an antibody that activates the immune system by targeting CTLA-4, has been approved for the treatment of patients with late-stage melanoma. Ipilimumab represents one of the few antibodies with sufficient activity to be used as a single agent in the treatment of solid tumors. Many of these antibody-based therapeutics are administered in combination with chemotherapeutic agents such as the anti-EGF receptor antibodies cetuximab and panitumumab are used in combination with chemotherapy for the treatment of colorectal and head and neck cancers. High specificities of antibodies have received much attention in cancer treatment in recent years as they greatly reduce 'off-target' toxicity.

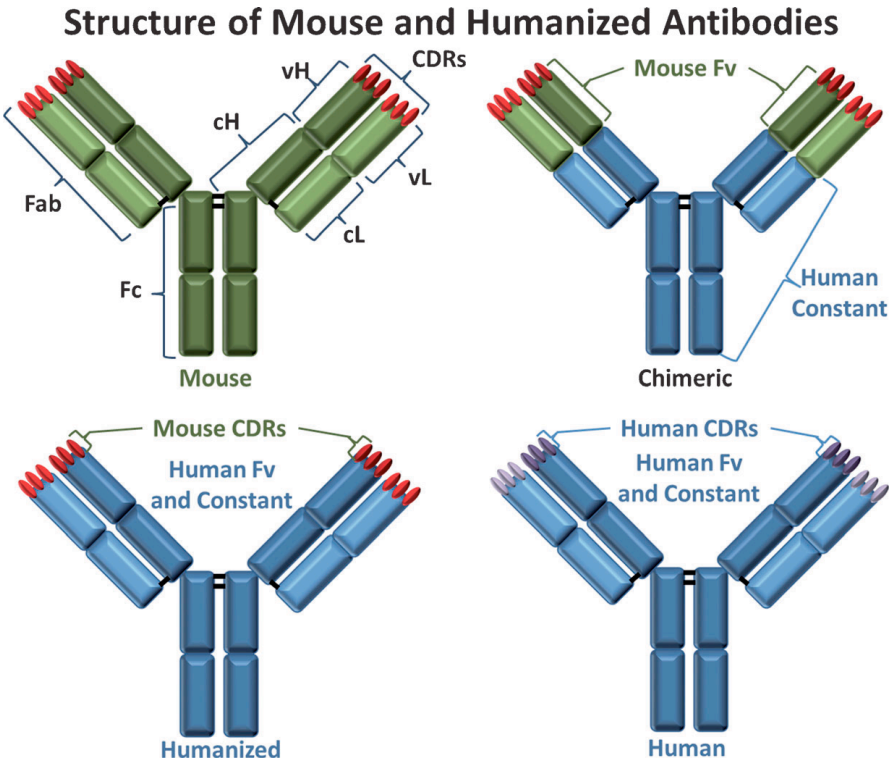

Figure 1.12 A cartoon representation of mouse (green), chimeric, humanized, and human (blue) antibodies. The antibody subdomains are marked, including Fab, Fc, heavy-chain variable (vH), light-chain variable (vL), heavy-chain constant (cH), light-chain constant (cL), and the complementarity-determining regions (CDRs).

Antibody-drug conjugates (ADCs) mainly composed of an antibody armed with covalently linked potent cytotoxic drugs using various conjugation and linker chemistries. The antibody's binding region allows selective targeting of certain cell types and discriminates healthy tissues from diseased ones and the potent cytotoxic drug element effects cell killing independently of antibody-dependent cell-mediated cytotoxicity. Hence, ADCs offer the prospect for delivery of a toxic payload directly to a target, with minimal off-target toxicity[2]. Although Paul Ehrlich[7] envisioned the concept of "magic bullet" in 1913, it took 45 years to construct such an entity in the form of ADC. The first generation of ADCs was mostly constructed using murine and chimeric antibodies to improve the tumor selectivity of clinically used anticancer drugs such as methotrexate, vinblastine, doxorubicin, and melphalan. It was recognized early on, that the nature of the linker connecting the monoclonal antibody and drug was important. Once internalized into a target cell, some intracellular release mechanism should cleave the linker to release the active drug. In most of these conjugates, acid-labile hydrazone linkers were utilized that relied on the acidic pH value ≈5 of the intracellular compartment, the endosome, and enzyme-labile linkers that relied on lysosomal enzymes, such as peptidases and esterase's, for cleavage.

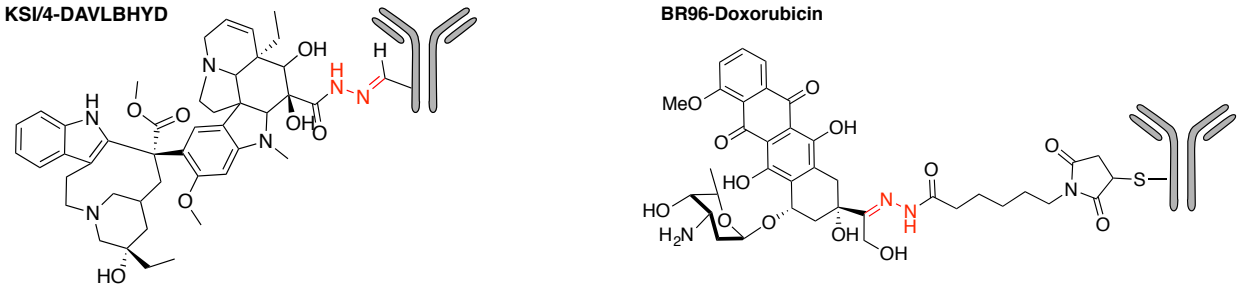

Figure 1.13. Structures of first-generation antibody-drug conjugates.

Particularly, anti-tumor activity of ADCs constructed using doxorubicin[67] and vinblastine[68] (figure 1.13) through acid-labile hydrazone linkers was found to be superior as

compared to corresponding free or unconjugated drugs both *in vitro* and *in vivo*. A Radiolabelled version of these conjugates showed 15% accumulation per gram of tumor compared with the injected dose of conjugate and provided concrete evidence of tumor localization in the patients. The toxicity profile of the conjugate was markedly different from that of the unconjugated drug, suggesting that antibody-mediated delivery can indeed alter the biodistribution of the drug, However, many of these conjugates, in general, were only moderately potent and often less active than the parent drug and despite the strong preclinical data, wherein the conjugated doxorubicin was shown to be superior to free doxorubicin, the conjugate failed to demonstrate clinically meaningful therapeutic activity. Since many of these preclinical trials were carried out using either chimeric or murine antibodies it has lead to development of immune responses in about 50% of the evaluable patients. This lack of clinical success with early ADCs, that make use of existing anticancer drugs as the "payload", initially dampened the enthusiasm in this area of research. However, a careful analysis of each component of these early ADCs led to the identification of several factors that may have led to their failure.

General design principles for the antibody-drug conjugates

a) The cytotoxic molecule

Lack of sufficient *in vitro* potency was one of the key drawbacks for early generation ADCs and the finding that conjugation often led to decreased potency compared to the parent free drug[69]. This compromised potency is mainly attributed to the differential uptake properties of unconjugated and conjugated drug. Delivery of the cytotoxic molecule by an antibody is limited by two factors: a) moderate number of antigen molecules on the cell surface to which the antibody can bind (typically $\approx 10^5$ receptors/cell), and b) internalization of cell-surface bound antigen–antibody complex, or intracellular processing to release the active drug may not be

efficient and the number of molecules of a moderately potent cytotoxic drug required to effect cell kill could be very high (>10^6 molecules/cell). Based on these calculations, therapeutically active ADC can only be created by making use of cytotoxic molecules that possess potency in subnanomolar to picomolar range. Also, cytotoxic molecule should be stable and water-soluble upon conjugation with antibody. Another major challenge is chemically modifying the drug to introduce functional groups that are amenable to conjugation reactions with antibodies. The site and nature of the modification have to be carefully selected so as to preserve the potency of the parent drug.

b) The Linker

Many first-generation preclinical candidates were prepared by merely mixing a drug bearing carboxylic acid with the antibody in aqueous solution in the presence of the coupling agent EDC (N-ethyl-N'-(3-dimethylaminopropyl)carbodiimide hydrochloride) to enable amide bond formation with amino groups of the antibody. As antibodies possess amino acid residues with free carboxyl groups (aspartate, glutamate) and free amino groups (lysine), EDC-mediated coupling can result in both intra and intermolecular amide bond formation between amino acid residues of the antibody. Analytical tool at that time was not well developed to evaluate the biochemical characterization of these conjugates prior to clinical evaluation. The first improvement was development of acid-labile linkers that can be cleaved under acidic environments such as in endosome or lysosomes. Efficient release of drugs was observed when ADCs were incubated at acidic pH. However, incubation of ADCs at pH 7.4, 37^{o}C resulted in time-dependent premature release of drug[70]. This premature release can cause systemic toxicity hence it was reasoned that effective linker design has to balance good stability during several days in circulation and efficient cleavage upon delivery into the target cell.

c) The antibody

One of the key functions of antibody is to bind preferentially to the antigen of interest and accumulate linked cytotoxic molecule at the tumor site. Typically, the antibody should be selected to cell-surface targets in such a way that the antigen is expressed in high copy numbers ($>10^5$/cell). In addition, homogeneous expression of antigen on all cells of the tumor is highly desired as determined by IHC staining of tumor tissue biopsies. The binding affinity of the antibody to its antigen is still debatable. A high binding affinity (KD<1 nm) has ensured good tumor localization, but some *in vivo* studies have suggested that antibodies with lower binding affinity have shown better penetration in solid tumors[71]. The immunogenicity issue of ADCs that used murine antibodies has been solved with the use of fully humanized antibodies.

With these design principles led finally approval of to the first US Food and Drug Administration (FDA) approved ADC, gemtuzumab ozogamicin (trade name, Mylotarg)[72]. Despite promising preliminary results, Pfizer Inc. voluntarily withdrew Mylotarg from the market in June 2010 as post-approval clinical trials for patients with acute myeloid leukemia showed that the ADC offered no clinical benefit over standard chemotherapy. However, it was reapproved by US-FDA in 2017 for the treatment of relapsed or refractory B-cell precursor acute lymphoblastic leukemia (ALL). This first approval nevertheless showed considerable promise in the following years with two ADCs gaining FDA approval- brentuximab vedotin (trade name, Adcetris)[73] in 2011 and trastuzumab emtansine (trade name, Kadcyla)[74] in 2013 for the treatment of patients suffering from relapsed Hodgkin lymphoma, anaplastic large-cell lymphoma and metastatic breast cancers respectively. It has been expected that the market for ADC research will grow rapidly in coming years.

Modifying accessible lysine residues on the surface of the desired antibody generated

Kadcyla and Mylotarg ADCs[73-74]. In fact, drug is conjugated to the antibody through lysine modification in many of these ADC clinical candidates. However, with ~90 accessible lysine's, non-selective chemical modification has the potential to generate complex mixtures, with up to 106 distinct species statistically possible when targeting drug-to-antibody ratios of 2–4. Such heterogeneous mixtures of ADCs may give random conjugation and uncontrolled drug loading and this can result in a narrow therapeutic window[75] with major pharmacokinetic implications. The promising case of Adcetris was obtained by reacting some of the eight free cysteine's obtained by reduction of the four interchain disulfides of an antibody. However, this method still creates ~15 different species when targeting typical average drug-to-antibody ratios of 2–4, it offers a significant improvement over lysine modification strategies in terms of reduced heterogeneity but still very challenging to control selective reduction of four interchain disulfides. Although this non-specific conjugation technology has been used in all FDA-approved ADC, the use of non-selective approaches is now considered suboptimal for developing next-generation ADCs, and there is a growing appreciation of the importance of developing site-specific methods[76], with several reports highlighting the advantages for generating near homogenous conjugates due to a well-defined and improved pharmacokinetic profile.

Site-specific conjugation technology

Site-specific conjugation using engineered antibodies

With a rapid progress in the field of protein engineering approaches has made it possible to site-specifically functionalize antibodies of interest. This mainly includes three main methods to obtain site-specifically modified ADCs with re-engineered antibodies: i) insertion of cysteine residues in the antibody sequence by mutagenesis, ii) enzymatic conjugation, and iii) insertion of

unnatural amino acids containing functional groups that can be chemo-selectively reacted.

a) Engineered cysteines

Nucleophilicity of thiol moiety of the cysteine side chain has been highest amongst all amino acid functional groups. This makes it an ideal target for the selective and site-specific modification of antibodies. Moreover, site-directed mutagenesis of cysteine residues can readily be inserted at a specific position on a protein. Junutula et al. described[77] a method for the incorporation of additional cysteine residues on antibodies. This method suffers from the formation of protein dimers or scrambled disulfides of engineered cysteine residues that can pair with other free cysteines that could reduce its activity. This problem has been addressed by screening conjugation sites on an antibody against the ovarian cancer antigen MUC16; an engineered thio-antibody (THIOMAB) containing two new cysteine sites for attachment was generated successfully. This method also suffers from formation of mixed disulfides due to cross-reactivity with a glutathione. To solve this, mild re-oxidation of the interchain disulfides with a gentle oxidant such as copper sulfate to afford an antibody with all of its native disulfide bonds intact, and two reduced engineered cysteines were generated to create ADC with drug to antibody ratio of 2.

b) Enzyme-mediated modification

This method relies upon the ability of enzymes that react with a particular amino acid in a specific amino acid sequence that in turn can be used to site-specifically attached drug molecules. Transglutaminases (TGs) can mediate the covalent crosslinking of proteins[78], where they catalyze the formation of amide bonds between the primary amine of a lysine and the amide group of a glutamine. In 2010, the Schibli group[79] showed site-specific functionalization of IgGs (rituximab and the anti-L1-CAM chCE7) using an amide bond forming transglutaminase.

After the deglycosylation of N-glycan using glycosidases (PNGaseF) of antibodies, various amine-containing substrates were coupled to Q295 by isopeptide bond formation. Using a chemoenzymatic two-step variant of the transglutaminase technology, they were able to produce homogenous Trastuzumab-MMAE conjugates with a DAR of 2 functionalized at Q295. In another method, Rinat-Pfizer[76] placed the amino-acid tag LLQA to several positions to the heavy and light chain of anti-EGFR, anti-HER2 and anti-M1S1 antibodies and conjugated fluorophores and auristatin derivatives using a transglutaminase from *Streptoverticillium mobaraense* resulting in DAR of 1.2–2.

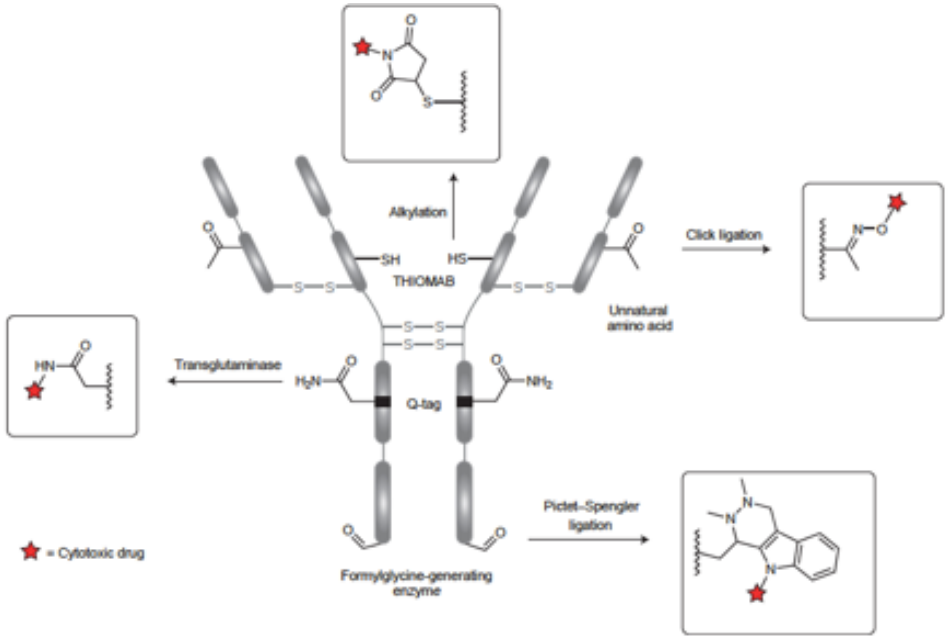

Figure 1.14 The engineering methods highlighted consist of: THIOMAB cysteine engineering followed by alkylation; unnatural amino acid incorporation followed by click ligation; Glutamine tag (Q-tag) insertion followed by transglutaminase functionalization; and use of formylglycine-generating enzyme to generate an aldehyde followed by hydrazino-iso-Pictet–Spengler functionalization.

Another chemoenzymatic strategy where formylglycine-generating enzymes (FGE) oxidizes the cysteine side chain of the peptide sequence CXPXR to a formylglycine. The

resulting aldehyde can then be readily reacted with aminooxy or hydrazine-functionalized molecules[80]. In addition to this hydrazino-iso-Pictet–Spengler (HIPS) chemistry was performed to conjugate a cytotoxic maytansine derivative (a potent microtubule-targeted agent) at three different positions[81]. Unfortunately, this method suffers from the hydration of the aldehyde from formylglycine in water to form an unreactive gem-diol, which lowers the yield of the process[82].

c) Unnatural amino acid incorporation

Introduction of unnatural amino acids into proteins have presented opportunities for the site-selective modification of antibodies[83].P-acetylphenylalanine and p-azidophenylalanine, have been successfully incorporated into proteins. In turn, oxime ligation and azide–alkyne cycloaddition have been utilized to introduce drug of interest. Zimmerman[84] et al. incorporated p-azidomethyl-phenylalanine into trastuzumab and using strain-promoted azide–alkyne cycloaddition to conjugate monomethyl auristatin F (a potent tubulin inhibitor). Unnatural amino acids methods offer the possibility of generating homogenous conjugates by attachment of a drug at virtually any accessible site on antibodies. However, the potential immunogenicity of unnatural amino acids is not yet fully understood and more studies are required to ensure the safety.

Site-specific modification of native antibodies

Producing homogeneous ADCs described in the previous section was highly attractive. However, they require site-directed mutagenesis and optimization of cell culture conditions, which can increase the overall manufacturing cost of an ADC. Therefore, significant efforts have been directed to design ways to avoid the requirement for re-engineering by modifying native form of antibody.

a) Targeting interchain disulfides

Antibody possesses 4 interchain disulfides typically, which upon reduction generates 8 nucleophilic cysteine residues. Moreover, reduction of native interchain disulfide bonds has shown to have a limited effect on antibody structure and stability since assembly of light and heavy chains do not depend primarily on covalent disulfide linkages, but rather on non-covalent interactions. Doronina[85] et al. initially reduced the 4 interchain disulfide bonds of anti-CD30 antibody and conjugated the liberated cysteines to monomethyl auristatin E (MMAE) using a maleimide linker. Resulting ADC was potent and selective for CD30-positive haematologic malignancies. However, further analysis by Hamblett[75] et al. and Beckley[86] et al. showed that drug to antibody ratio of 8 had a significant impact on conjugate pharmacokinetics such as poor tolerability, high plasma clearance rate, decreased efficacy in vivo and propensity to aggregate, and that a lower drug-to-antibody ratio resulted in a larger therapeutic window.

With these issues in mind, a screening of various reduction/re-oxidation strategies resulted in Adcetris, with an average drug-to-antibody ratio of 4 with isomeric homogeneities up to 75%. But, major drawback of this strategy is choice of thiol-maleimide chemistry. Bioconjugation through above chemistry has shown to undergo retro-addition reactions with serum protein thiols such as albumin, resulting in the transfer of drug to thiol-bearing proteins and thus leading to off-target toxicity. However, recently many strategies have been developed to obtain more stable version of thiol-maleimide adduct.

To make ADCs with DAR of 4, Badescu[87] et al. explored the reduction of the interchain disulfide bridges followed by functional re-bridging of the disulfide (Fig. 1.15). This would allow insertion of a single cytotoxic payload per disulfide and maintain a covalent attachment between drug and antibody chains. This method was invented based on bis-cysteine-selective

sulfone reagents that allow for an addition–elimination–addition sequence onto the reduced disulfide bonds of either Fab arms or antibody of choice. Using MMAE and T-DM1 as a payload they successfully demonstrated increased efficacy over drug alone whilst retaining binding and antigen-selective cytotoxicity *in vitro* and *in vivo*. Chudasama[88] and Caddick[89] et al. in a combined effort have developed dibromopyridazinediones and dithiomaleimides reagents that allow efficient functional re-bridging of interchain disulfides of antibody Fab fragments generating near homogeneous ADCs.

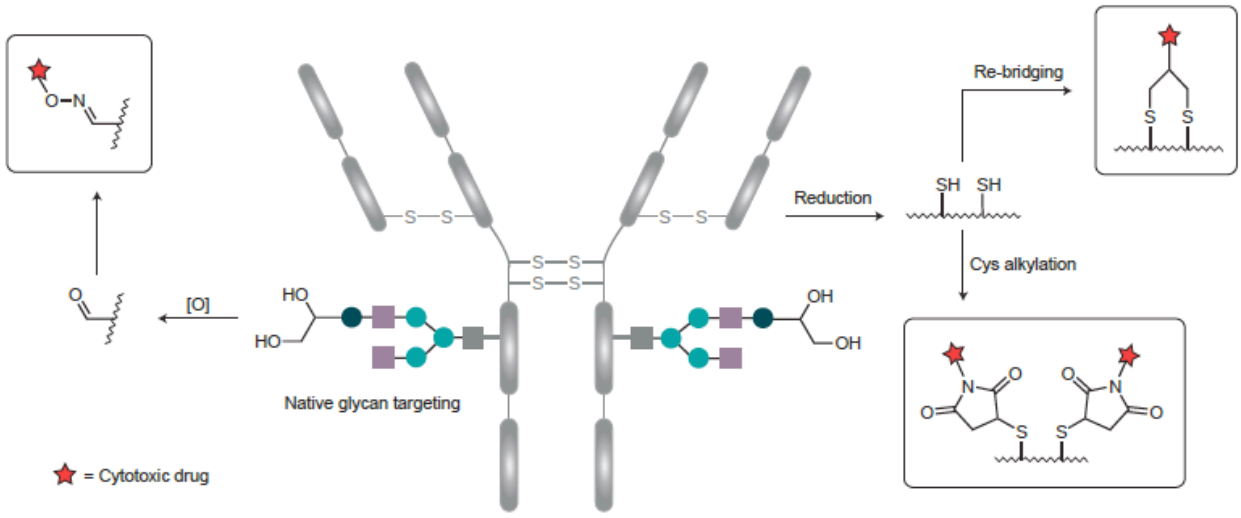

Figure 1.15 The methods highlighted: native glycan targeting to yield aldehyde-modified antibody by oxidation followed by reductive amination or O-substituted oxime functionalization, and disulfide reduction followed by either cysteine alkylation using maleimide or functional disulfide re-bridging.

b) Selective glycan modifications

All antibodies possess highly glycosylated at conserved N-glycosylation site at the N297 residue of the Fc region. Over the year this site has been explored for the antibody modifications. Typically, Sodium periodate at high concentration has been used to oxidize carbohydrate residues in the native glycans to provide aldehydes which are ligated with hydrazine modified drug to afford relatively homogenous ADCs. However, major side reaction that can occur due to harsh oxidizing reagent was oxidation of methionine residues located close to the FcRn binding

site. This over-oxidation has shown to affect FcRn binding and compromised half-life in serum[90]. To overcome this problem many mild enzymatic methods have been developed.

Stan[91] et al. through sequential treatment of neuraminidases cleave the glycosidic linkages of sialic acids and galactose oxidase to oxidize the galactose residues of an anti-CEA antibody. Site-specific attachment of doxorubicin using reductive amination on the generated aldehydes produces ADCs with DAR of 3.7 approximately was four times more potent *in vitro* than its counterpart generated by lysine conjugation with a DAR of 7.8. This example demonstrates the importance of site-specific conjugation while constructing ADCs. In another study[92], site-specific modification was achieved through sequential use of galactosyltransferase and sialyltransferase to transfer galactose and sialic acid residues onto the native glycans. However, sialic acid residues were further oxidized to yield aldehyde-functionalized trastuzumab. This oxidation treatment resulted in partial oxidation of the methionines residues proximal to the FcRn binding regions, which compromised FcRn binding by ~25% but had a negligible effect on serum half-life. The resulting aldehyde containing sialic acids was conjugated with MMAE or MMAF through oxime ligation with DAR of 1.6. These glyco-conjugated ADCs exhibited efficacious activity both *in vitro* and *in vivo*. Boons[93] et al. developed a more elegant approach that avoids the oxidation step. Sequential modification of N-glycans using galactosyltransferase and sialyltransferase could introduce various chemical reporters such as azido-modified sialic acid on the native antibodies. The azide, which is absent in biological system, then can undergo strain-promoted azide–alkyne-cycloaddition reaction to introduce a suitable cytotoxic drug of interest. This approach has recently been applied to an anti-CD22 antibody using a suitable doxorubicin derivative resulting in a near homogeneous ADC that has been shown to selectively target and kill lymphoma cells.

The major drawback of these glycan-based modifications arises from the heterogeneous population of glycans in an antibody, and their dependence on the presence of galactose on an IgG. These characteristics may reduce the homogeneity of the final ADC products and could add additional steps to homogenize the glycan population hence, making the large-scale manufacturing process complicated[94].

Payloads for next generation of ADCs

Payloads that possess high potency, stability, and adequate solubility in the aqueous media after conjugation to antibody are highly desirable. There are two main classes of payloads that are widely explored in ADC[2] field 1) Anti-mitotic and 2) DNA damaging agents. Maytansinoids[95], vinca alkaloids (e.g. vincristine, vinblastine), paclitaxel, docetaxel[96], and auristatins (e.g. MMAE, MMAF)[97] are anti-mitotic agents that bind to tubulin and disrupt normal microtubule formation and dynamics. They can also stabilize altered microtubule structures, thus interfering with their normal degradation during cell division. Calicheamicins[98], duocarmycins[99], camptothecin[100], and pyrrolobenzodiazepine (PBD)[101] are DNA damaging agents. In general, above agents exert high potency by tight binding to minor groove of DNA in highly sequence-specific manner or by sequence-specific alkylation of DNA.

Conclusion and perspective

The concept of targeted drug delivery has witnessed a rapid development for improving safety and efficacy profiles of currently existing therapeutic agents. In this context, nanoparticles (nanostructures such as liposomes, nanoemulsions, polymeric micelles, and dendrimers) are attractive drug carriers (for passive and active targeting) because they can be made from a variety of materials engineered to possess properties that allow loading and precise delivery of drug bound molecules. Currently, dozens of polymer-based nanotherapeutics have been

approved or evaluated in clinical trials. However, the progress of these clinical candidates towards FDA approval has been sluggish due to complexity, design inflexibility, lack of detail mode of action at mechanistic level, manufacturing reproducibility at nanoscale proven in the clinic, lack of consistent or reproducible results in various animal models. In the past, most of the preclinical work has been performed using nude mice bearing subcutaneous tumor xenografts, which is questionable since these cancer cells possess characteristic differentiated from human cancer cells. In addition, most of the candidates of this class have failed due to suboptimal design features such as lack of targeting ligands, non-specific uptake and drug release mechanisms or combination of these factors. Despite these limitations, two active targeting and one passively targeted polymeric nanoformulations such as PK2, BIND-014 and Xyotax have been translated to the clinical evaluation of patients with liver and prostate cancers respectively. It has been anticipated that in the next 10 years, a growing number of targeted nanoparticulate drugs will enter the different phases of clinical trials.

In contrast to the nanoparticle-based drug delivery, antibody-drug conjugates (ADCs) have gathered significant excitement due to approval of 4 ADCs namely brentuximab vedotin, ado-trastuzumab emtansine, gemtuzumab ozogamicin, and inotuzumab ozogamicin for the treatment of various cancers. The Clinical success of ADC can be attributed to the use of humanized antibodies (non-immunogenic), linkers that are stable in circulation and cleavable upon tumor internalization, and emergence of site-specific conjugation technology that allows the preparation of ADC with well-defined drug to antibody ratio (DAR). However, many ADCs in the clinical pipeline still suffer from non-specific uptake properties (such as pinocytosis), off-target toxicities, compromised PK/PD properties, and reduced half-life in circulation. These effects are mainly associated with non-selectivity of antibodies for a given target and interaction

with Fcγ receptors. Moreover, in general antibodies with drug to antibody (DAR) ratio of 4 and above showed compromised PK/PD profiles and faster clearance over unmodified IgG. Medicinal chemists and biologists are working together to optimize these features of ADC.

The future design of ADCs will be focused not only on preferential accumulation at tumor site resulting in effective eradication of solid tumors but also selectively recognize and kill circulating metastatic tumor cells, drug-resistant tumor cells as well as slowly dividing cancer stem cells.

References

[1] V. T. DeVita and E. Chu, *Cancer Research* **2008**, *68*, 8643-8653.

[2] R. V. J. Chari, M. L. Miller and W. C. Widdison, *Angewandte Chemie International Edition* **2014**, *53*, 3796-3827.

[3] B. A. Chabner and T. G. Roberts, *Nat Rev Cancer* **2005**, *5*, 65-72.

[4] R. Cairns, I. Papandreou and N. Denko, *Molecular Cancer Research* **2006**, *4*, 61-70.

[5] a) H. Clevers, **2011**, 313; b) L. Zitvogel, O. Kepp and G. Kroemer, *Nat Rev Clin Oncol* **2011**, *8*, 151-160.

[6] L. M. Parker, C. T. Griffiths, R. A. Yankee, G. P. Canellos, R. Gelman, R. C. Knapp, C. M. Richman, J. S. Tobias, R. S. Weiner and E. Frei, *Cancer* **1980**, *46*, 669-674.

[7] P. Ehrlich, *British Medical Journal* **1913**, *2*, 353-359.

[8] a) I. Brigger, C. Dubernet and P. Couvreur, *Advanced Drug Delivery Reviews* **2002**, *54*, 631-651; b) D. Peer, J. M. Karp, S. Hong, O. C. Farokhzad, R. Margalit and R. Langer, *Nat Nano* **2007**, *2*, 751-760.

[9] a) M. E. Davis, Z. Chen and D. M. Shin, *Nat Rev Drug Discov* **2008**, *7*, 771-782; b) A. Z. Wang, R. Langer and O. C. Farokhzad, *Annual Review of Medicine* **2012**, *63*, 185-198.

[10] a) M. Elsabahy and K. L. Wooley, *Chemical Society Reviews* **2012**, *41*, 2545-2561; b) N. Wiradharma, Y. Zhang, S. Venkataraman, J. L. Hedrick and Y. Y. Yang, *Nano Today* **2009**, *4*, 302-317.

[11] a) L. Brannon-Peppas and J. O. Blanchette, *Advanced Drug Delivery Reviews* **2004**, *56*, 1649-1659; b) J. Fang, H. Nakamura and H. Maeda, *Advanced Drug Delivery Reviews* **2011**, *63*, 136-151.

[12] T.-Y. Kim, D.-W. Kim, J.-Y. Chung, S. G. Shin, S.-C. Kim, D. S. Heo, N. K. Kim and Y.-J. Bang, *Clinical Cancer Research* **2004**, *10*, 3708-3716.

[13] Y. Matsumura, T. Hamaguchi, T. Ura, K. Muro, Y. Yamada, Y. Shimada, K. Shirao, T. Okusaka, H. Ueno, M. Ikeda and N. Watanabe, *Br J Cancer* **2004**, *91*, 1775-1781.

[14] T. Hamaguchi, K. Kato, H. Yasui, C. Morizane, M. Ikeda, H. Ueno, K. Muro, Y. Yamada, T. Okusaka, K. Shirao, Y. Shimada, H. Nakahama and Y. Matsumura, *Br J Cancer* **2007**, *97*, 170-176.

[15] R. Plummer, R. H. Wilson, H. Calvert, A. V. Boddy, M. Griffin, J. Sludden, M. J. Tilby, M. Eatock, D. G. Pearson, C. J. Ottley, Y. Matsumura, K. Kataoka and T. Nishiya, *Br J Cancer* **2011**, *104*, 593-598.

[16] Y. Nakamura, A. Mochida, P. L. Choyke and H. Kobayashi, *Bioconjugate Chemistry* **2016**, *27*, 2225-2238.

[17] R. Korsmeyer, *Regenerative Biomaterials* **2016**, *3*, 143-147.

[18] T. M. Allen, *Nat Rev Cancer* **2002**, *2*, 750-763.

[19] a) H. Koo, M. S. Huh, I.-C. Sun, S. H. Yuk, K. Choi, K. Kim and I. C. Kwon, *Accounts of Chemical Research* **2011**, *44*, 1018-1028; b) J. Nicolas, S. Mura, D. Brambilla, N. Mackiewicz and P. Couvreur, *Chemical Society Reviews* **2013**, *42*, 1147-1235.

[20] J. D. Byrne, T. Betancourt and L. Brannon-Peppas, *Advanced Drug Delivery Reviews* **2008**, *60*, 1615-1626.

[21] Y. Zhong, F. Meng, C. Deng and Z. Zhong, *Biomacromolecules* **2014**, *15*, 1955-1969.

[22] N. Kamaly, Z. Xiao, P. M. Valencia, A. F. Radovic-Moreno and O. C. Farokhzad, *Chemical Society Reviews* **2012**, *41*, 2971-3010.

[23] Y. Zhang, G. Wang and J. Huang, *Journal of Polymer Science Part A: Polymer Chemistry* **2010**, *48*, 5974-5981.

[24] a) Z. Amoozgar and Y. Yeo, *Wiley Interdisciplinary Reviews: Nanomedicine and Nanobiotechnology* **2012**, *4*, 219-233; b) C.-M. J. Hu, R. H. Fang, B. T. Luk, K. N. H. Chen, C. Carpenter, W. Gao, K. Zhang and L. Zhang, *Nanoscale* **2013**, *5*, 2664-2668.

[25] K. Kataoka, A. Harada and Y. Nagasaki, *Advanced Drug Delivery Reviews* **2001**, *47*, 113-131.

[26] a) C. Deng, Y. Jiang, R. Cheng, F. Meng and Z. Zhong, *Nano Today* **2012**, *7*, 467-480; b) Y. Matsumura and K. Kataoka, *Cancer Science* **2009**, *100*, 572-579.

[27] Y. H. Bae and H. Yin, *Journal of Controlled Release* **2008**, *131*, 2-4.

[28] V. Ortiz, S. O. Nielsen, D. E. Discher, M. L. Klein, R. Lipowsky and J. Shillcock, *The Journal of Physical Chemistry B* **2005**, *109*, 17708-17714.

[29] F. Meng, Z. Zhong and J. Feijen, *Biomacromolecules* **2009**, *10*, 197-209.

[30] F. X. Gu, R. Karnik, A. Z. Wang, F. Alexis, E. Levy-Nissenbaum, S. Hong, R. S. Langer and O. C. Farokhzad, *Nano Today* **2007**, *2*, 14-21.

[31] a) R. K. O'Reilly, C. J. Hawker and K. L. Wooley, *Chemical Society Reviews* **2006**, *35*, 1068-1083; b) S. C. Owen, D. P. Y. Chan and M. S. Shoichet, *Nano Today* **2012**, *7*, 53-65.

[32] G. P. Adams, R. Schier, A. M. McCall, H. H. Simmons, E. M. Horak, R. K. Alpaugh, J. D. Marks and L. M. Weiner, *Cancer Research* **2001**, *61*, 4750-4755.

[33] a) J. F. Kukowska-Latallo, K. A. Candido, Z. Cao, S. S. Nigavekar, I. J. Majoros, T. P. Thomas, L. P. Balogh, M. K. Khan and J. R. Baker, *Cancer Research* **2005**, *65*, 5317-5324; b) P. S. Low, W. A. Henne and D. D. Doorneweerd, *Accounts of Chemical Research* **2008**, *41*, 120-

129; c) I. J. Majoros, C. R. Williams, A. Becker and J. R. Baker, *Wiley Interdisciplinary Reviews: Nanomedicine and Nanobiotechnology* **2009**, *1*, 502-510.

[34] E. Burakowska, J. R. Quinn, S. C. Zimmerman and R. Haag, *Journal of the American Chemical Society* **2009**, *131*, 10574-10580.

[35] Z. Liu, S. M. Tabakman, Z. Chen and H. Dai, *Nat. Protocols* **2009**, *4*, 1372-1381.

[36] a) B. Chertok, A. E. David and V. C. Yang, *Biomaterials* **2010**, *31*, 6317-6324; b) A. K. Gupta and M. Gupta, *Biomaterials* **2005**, *26*, 3995-4021.

[37] C. R. Patra, R. Bhattacharya, D. Mukhopadhyay and P. Mukherjee, *Advanced Drug Delivery Reviews* **2010**, *62*, 346-361.

[38] L. A. Mitchell, F. T. Lauer, S. W. Burchiel and J. D. McDonald, *Nat Nano* **2009**, *4*, 451-456.

[39] B. S. Zolnik, A. f. González-Fernández, N. Sadrieh and M. A. Dobrovolskaia, *Endocrinology* **2010**, *151*, 458-465.

[40] A. M. Alkilany, P. K. Nagaria, C. R. Hexel, T. J. Shaw, C. J. Murphy and M. D. Wyatt, *Small* **2009**, *5*, 701-708.

[41] S. Hong, P. R. Leroueil, E. K. Janus, J. L. Peters, M.-M. Kober, M. T. Islam, B. G. Orr, J. R. Baker and M. M. Banaszak Holl, *Bioconjugate Chemistry* **2006**, *17*, 728-734.

[42] T. P. Thomas, I. J. Majoros, A. Kotlyar, J. F. Kukowska-Latallo, A. Bielinska, A. Myc and J. R. Baker, *Journal of Medicinal Chemistry* **2005**, *48*, 3729-3735.

[43] SoodA, SalihS, RohD, L. Lacharme Lora, ParryM, HardimanB, KeehanR, GrummerR, WinterhagerE, P. J. Gokhale, P. W. Andrews, AbbottC, ForbesK, WestwoodM, J. D. Aplin, InghamE, PapageorgiouI, BerryM, LiuJ, A. D. Dick, R. J. Garland, WilliamsN, SinghR, A. K. Simon, LewisM, HamJ, RogerL, D. M. Baird, L. A. Crompton, M. A. Caldwell, SwalwellH, M.

Birch Machin, G. Lopez Castejon, RandallA, LinH, M. S. Suleiman, W. H. Evans, NewsonR and C. P. Case, *Nat Nano* **2011**, *6*, 824-833.

[44] Y. Zhang, Y. Bai, J. Jia, N. Gao, Y. Li, R. Zhang, G. Jiang and B. Yan, *Chemical Society Reviews* **2014**, *43*, 3762-3809.

[45] P. T. Wong and S. K. Choi, *Chemical Reviews* **2015**, *115*, 3388-3432.

[46] I. J. Majoros, T. P. Thomas, C. B. Mehta and J. R. Baker, *Journal of Medicinal Chemistry* **2005**, *48*, 5892-5899.

[47] M. W. Duffel, *Journal of Medicinal Chemistry* **2004**, *47*, 2714-2715.

[48] A. Page-McCaw, A. J. Ewald and Z. Werb, **2007**, *8*, 221.

[49] W.-C. Shen and H. J. P. Ryser, *Biochemical and Biophysical Research Communications* **1981**, *102*, 1048-1054.

[50] M. Prabaharan, J. J. Grailer, S. Pilla, D. A. Steeber and S. Gong, *Biomaterials* **2009**, *30*, 5757-5766.

[51] J. Kalia and R. T. Raines, *Angewandte Chemie International Edition* **2008**, *47*, 7523-7526.

[52] W. Zhang, P. Li, Q. Geng, Y. Duan, M. Guo and Y. Cao, *Journal of Agricultural and Food Chemistry* **2014**, *62*, 5845-5852.

[53] R. M.Green, M. Graham, M. R.O'Donovan, J. K. Chipman and N. J.Hodges, *Mutagenesis* **2006**, *21*, 383-390.

[54] V. M. Vrudhula, J. F. MacMaster, Z. Li, D. E. Kerr and P. D. Senter, *Bioorganic & Medicinal Chemistry Letters* **2002**, *12*, 3591-3594.

[55] J. Lim, A. Chouai, S.-T. Lo, W. Liu, X. Sun and E. E. Simanek, *Bioconjugate Chemistry* **2009**, *20*, 2154-2161.

[56] J. M. Brown and W. R. Wilson, *Nat Rev Cancer* **2004**, *4*, 437-447.

[57] M. N. Levine and R. T. Raines, *Chemical Science* **2012**, *3*, 2412-2420.

[58] P. S. Cogan and T. H. Koch, *Journal of Medicinal Chemistry* **2003**, *46*, 5258-5270.

[59] G. Mayer and A. Heckel, *Angewandte Chemie International Edition* **2006**, *45*, 4900-4921.

[60] S. Ki Choi, T. Thomas, M.-H. Li, A. Kotlyar, A. Desai and J. J. R. Baker, *Chemical Communications* **2010**, *46*, 2632-2634.

[61] S. S. Agasti, A. Chompoosor, C.-C. You, P. Ghosh, C. K. Kim and V. M. Rotello, *Journal of the American Chemical Society* **2009**, *131*, 5728-5729.

[62] M. Haase and H. Schäfer, *Angewandte Chemie International Edition* **2011**, *50*, 5808-5829.

[63] M. A. Peppercorn, *Annals of Internal Medicine* **1984**, *101*, 377-386.

[64] G. Köhler and C. Milstein, *The Journal of Immunology* **2005**, *174*, 2453-2455.

[65] A. L. Nelson, E. Dhimolea and J. M. Reichert, *Nat Rev Drug Discov* **2010**, *9*, 767-774.

[66] a) R. K. Oldham and R. O. Dillman, *Journal of Clinical Oncology* **2008**, *26*, 1774-1777; b) A. M. Scott, J. D. Wolchok and L. J. Old, *Nat Rev Cancer* **2012**, *12*, 278-287.

[67] A. W. Tolcher, S. Sugarman, K. A. Gelmon, R. Cohen, M. Saleh, C. Isaacs, L. Young, D. Healey, N. Onetto and W. Slichenmyer, *Journal of Clinical Oncology* **1999**, *17*, 478-478.

[68] a) B. H. Petersen, S. V. DeHerdt, D. W. Schneck and T. F. Bumol, *Cancer Research* **1991**, *51*, 2286-2290; b) D. Schneck, F. Butler, W. Dugan, D. Littrell, B. Petersen, R. Bowsher, A. DeLong and S. Dorrbecker, *Clinical Pharmacology & Therapeutics* **1990**, *47*, 36-41.

[69] P. Trail, D. Willner, S. Lasch, A. Henderson, S. Hofstead, A. Casazza, R. Firestone, I. Hellstrom and K. Hellstrom, *Science* **1993**, *261*, 212-215.

[70] B. C. Laguzza, C. L. Nichols, S. L. Briggs, G. J. Cullinan, D. A. Johnson, J. J. Starling, A. L. Baker, T. F. Bumol and J. R. F. Corvalan, *Journal of Medicinal Chemistry* **1989**, *32*, 548-555.

[71] S. I. Rudnick, J. Lou, C. C. Shaller, Y. Tang, A. J. P. Klein-Szanto, L. M. Weiner, J. D. Marks and G. P. Adams, *Cancer Research* **2011**, *71*, 2250-2259.

[72] M. L. Linenberger, T. Hong, D. Flowers, E. L. Sievers, T. A. Gooley, J. M. Bennett, M. S. Berger, L. H. Leopold, F. R. Appelbaum and I. D. Bernstein, *Blood* **2001**, *98*, 988-994.

[73] a) P. D. Senter and E. L. Sievers, *Nat Biotech* **2012**, *30*, 631-637; b) A. Younes , N. L. Bartlett , J. P. Leonard , D. A. Kennedy , C. M. Lynch , E. L. Sievers and A. Forero-Torres *New England Journal of Medicine* **2010**, *363*, 1812-1821.

[74] S. Verma, D. Miles, L. Gianni, I. E. Krop, M. Welslau, J. Baselga, M. Pegram, D.-Y. Oh, V. Diéras, E. Guardino, L. Fang, M. W. Lu, S. Olsen and K. Blackwell, *New England Journal of Medicine* **2012**, *367*, 1783-1791.

[75] K. J. Hamblett, P. D. Senter, D. F. Chace, M. M. C. Sun, J. Lenox, C. G. Cerveny, K. M. Kissler, S. X. Bernhardt, A. K. Kopcha, R. F. Zabinski, D. L. Meyer and J. A. Francisco, *Clinical Cancer Research* **2004**, *10*, 7063-7070.

[76] P. Strop, S.-H. Liu, M. Dorywalska, K. Delaria, Russell G. Dushin, T.-T. Tran, W.-H. Ho, S. Farias, Meritxell G. Casas, Y. Abdiche, D. Zhou, R. Chandrasekaran, C. Samain, C. Loo, A. Rossi, M. Rickert, S. Krimm, T. Wong, Sherman M. Chin, J. Yu, J. Dilley, J. Chaparro-Riggers, Gary F. Filzen, Christopher J. O'Donnell, F. Wang, Jeremy S. Myers, J. Pons, David L. Shelton and A. Rajpal, *Chemistry & Biology* **2013**, *20*, 161-167.

[77] J. R. Junutula, S. Bhakta, H. Raab, K. E. Ervin, C. Eigenbrot, R. Vandlen, R. H. Scheller and H. B. Lowman, *Journal of Immunological Methods* **2008**, *332*, 41-52.

[78] C. S. Greenberg, P. J. Birckbichler and R. H. Rice, *The FASEB Journal* **1991**, *5*, 3071-3077.

[79] S. Jeger, K. Zimmermann, A. Blanc, J. Grünberg, M. Honer, P. Hunziker, H. Struthers and R. Schibli, *Angewandte Chemie International Edition* **2010**, *49*, 9995-9997.

[80] P. Wu, W. Shui, B. L. Carlson, N. Hu, D. Rabuka, J. Lee and C. R. Bertozzi, *Proceedings of the National Academy of Sciences* **2009**, *106*, 3000-3005.

[81] P. M. Drake, A. E. Albers, J. Baker, S. Banas, R. M. Barfield, A. S. Bhat, G. W. de Hart, A. W. Garofalo, P. Holder, L. C. Jones, R. Kudirka, J. McFarland, W. Zmolek and D. Rabuka, *Bioconjugate Chemistry* **2014**, *25*, 1331-1341.

[82] D. Rabuka, J. S. Rush, G. W. deHart, P. Wu and C. R. Bertozzi, *Nat. Protocols* **2012**, *7*, 1052-1067.

[83] J. Y. Axup, K. M. Bajjuri, M. Ritland, B. M. Hutchins, C. H. Kim, S. A. Kazane, R. Halder, J. S. Forsyth, A. F. Santidrian, K. Stafin, Y. Lu, H. Tran, A. J. Seller, S. L. Biroc, A. Szydlik, J. K. Pinkstaff, F. Tian, S. C. Sinha, B. Felding-Habermann, V. V. Smider and P. G. Schultz, *Proceedings of the National Academy of Sciences* **2012**, *109*, 16101-16106.

[84] E. S. Zimmerman, T. H. Heibeck, A. Gill, X. Li, C. J. Murray, M. R. Madlansacay, C. Tran, N. T. Uter, G. Yin, P. J. Rivers, A. Y. Yam, W. D. Wang, A. R. Steiner, S. U. Bajad, K. Penta, W. Yang, T. J. Hallam, C. D. Thanos and A. K. Sato, *Bioconjugate Chemistry* **2014**, *25*, 351-361.

[85] S. O. Doronina, B. E. Toki, M. Y. Torgov, B. A. Mendelsohn, C. G. Cerveny, D. F. Chace, R. L. DeBlanc, R. P. Gearing, T. D. Bovee, C. B. Siegall, J. A. Francisco, A. F. Wahl, D. L. Meyer and P. D. Senter, *Nat Biotech* **2003**, *21*, 778-784.

[86] N. S. Beckley, K. P. Lazzareschi, H.-W. Chih, V. K. Sharma and H. L. Flores, *Bioconjugate Chemistry* **2013**, *24*, 1674-1683.

[87] G. Badescu, P. Bryant, M. Bird, K. Henseleit, J. Swierkosz, V. Parekh, R. Tommasi, E. Pawlisz, K. Jurlewicz, M. Farys, N. Camper, X. Sheng, M. Fisher, R. Grygorash, A. Kyle, A.

Abhilash, M. Frigerio, J. Edwards and A. Godwin, *Bioconjugate Chemistry* **2014**, *25*, 1124-1136.

[88] J. P. M. Nunes, M. Morais, V. Vassileva, E. Robinson, V. S. Rajkumar, M. E. B. Smith, R. B. Pedley, S. Caddick, J. R. Baker and V. Chudasama, *Chemical Communications* **2015**, *51*, 10624-10627.

[89] A. Maruani, M. E. B. Smith, E. Miranda, K. A. Chester, V. Chudasama and S. Caddick, **2015**, *6*, 6645.

[90] W. Wang, J. Vlasak, Y. Li, P. Pristatsky, Y. Fang, T. Pittman, J. Roman, Y. Wang, T. Prueksaritanont and R. Ionescu, *Molecular Immunology* **2011**, *48*, 860-866.

[91] A. C. Stan, D. L. Radu, S. Casares, C. A. Bona and T.-D. Brumeanu, *Cancer Research* **1999**, *59*, 115-121.

[92] Q. Zhou, J. E. Stefano, C. Manning, J. Kyazike, B. Chen, D. A. Gianolio, A. Park, M. Busch, J. Bird, X. Zheng, H. Simonds-Mannes, J. Kim, R. C. Gregory, R. J. Miller, W. H. Brondyk, P. K. Dhal and C. Q. Pan, *Bioconjugate Chemistry* **2014**, *25*, 510-520.

[93] X. Li, T. Fang and G.-J. Boons, *Angewandte Chemie International Edition* **2014**, *53*, 7179-7182.

[94] R. Jefferis, *Nat Rev Drug Discov* **2009**, *8*, 226-234.

[95] A. I. Meyers, P. J. Reider and A. L. Campbell, *Journal of the American Chemical Society* **1980**, *102*, 6597-6598.

[96] M. Abal, J. M. Andreu and I. Barasoain, *Current Cancer Drug Targets* **2003**, *3*, 193-203.

[97] S. O. Doronina, B. A. Mendelsohn, T. D. Bovee, C. G. Cerveny, S. C. Alley, D. L. Meyer, E. Oflazoglu, B. E. Toki, R. J. Sanderson, R. F. Zabinski, A. F. Wahl and P. D. Senter, *Bioconjugate Chemistry* **2006**, *17*, 114-124.

[98] P. R. Hamann, L. M. Hinman, C. F. Beyer, D. Lindh, J. Upeslacis, D. A. Flowers and I. Bernstein, *Bioconjugate Chemistry* **2002**, *13*, 40-46.

[99] D. L. Boger, C. W. Boyce, R. M. Garbaccio and J. A. Goldberg, *Chemical Reviews* **1997**, *97*, 787-828.

[100] S.-J. Moon, S. V. Govindan, T. M. Cardillo, C. A. D'Souza, H. J. Hansen and D. M. Goldenberg, *Journal of Medicinal Chemistry* **2008**, *51*, 6916-6926.

[101] J. Mantaj, P. J. M. Jackson, K. M. Rahman and D. E. Thurston, *Angewandte Chemie International Edition* **2017**, *56*, 462-488.

CHAPTER 2

CONTROLLED MULTI-FUNCTIONALIZATION FACILITATES TARGETED DELIVERY OF NANOPARTICLES TO CANCER CELLS

2016, *Chem. Eur. J,* 22, 1415-1423, Reprinted here with permission of publisher

Abstract

A major objective of nanomedicine is to combine in a controlled manner multiple functional entities into a single nanoscale device to target particles with great spatial precision, thereby increasing the selectivity and potency of therapeutic drugs. A multifunctional nanoparticle is described for controlled conjugation of a cytotoxic drug, a cancer cell targeting ligand, and an imaging moiety. The approach is based on the chemical synthesis of polyethylene glycol that at one end is modified by a thioctic acid for controlled attachment to a gold core. The other end of the PEG polymers is modified by a hydrazine, amine, or dibenzocyclooctynol moiety for conjugation with functional entities having a ketone, activated ester, or azide moiety, respectively. The conjugation approach allowed the controlled attachment of doxorubicin through an acid-labile hydrazone linkage, an Alexa Fluor dye through an amide bond, and a glycan-based ligand for the cell surface receptor CD22 of B-cells using strain promoted azide-alkyne cycloaddition. The incorporation of the ligand for CD22 led to rapid entry of the nanoparticle by receptor-mediated endocytosis. Covalent attachment of doxorubicin via hydrazone linkage caused pH-responsive intracellular release of doxorubicin and significantly enhanced the cytotoxicity of nanoparticles. A remarkable 60-fold enhancement in cytotoxicity of CD22 (+) lymphoma cells was observed compared to nontargeted nanoparticles.

Introduction

Nanomaterials are emerging as promising devices for drug delivery.[1] These carriers can increase longevity of a drug in the blood stream, solubilize hydrophobic drugs, offer controlled release by environmental-sensitive or external stimuli, and accumulate in solid tumors by enhanced permeability and retention effect.[2] The therapeutic efficiency of nanomaterials can further be improved by surface functionalization by, for example, a tissue-targeting ligand,[3] a

cell-penetrating molecule,[4] or by a signaling peptide for organelle targeting.[5] Moreover, therapeutic targeting can be combined with imaging by attachment of an appropriate contrast agent.[6]

Polymeric micelles are especially promising for targeted drug delivery because of their chemical versatility, stealth properties, and their ability to carry high payloads.[3] The most commonly used polymeric micelles are composed of polyethylene glycol (PEG) grafted to poly-d,l-lactide-co-glycolide (PLGA), polylactic acid, poly-g-caprolactone (PCL), and poly-alkylcyanoacrylates.[7] These amphiphilic molecules self-assemble in water to create micelles that have an apolar core that can be used for drug loading and a polar corona that provides stealth properties.[8] Polymeric micelles are entering clinical evaluation and for example PEG-poly(glutamic acid) polymeric micelles carrying cisplatin (NC-6004, Nanoplatin®)[9] were examined in a phase 1 clinical trial. Compared to the free drug, the nanodelivery device was associated with less toxicity and nausea, and the disease control rate was encouraging. A number of other synthetic polymer nanocarriers have been evaluated in clinical trials, including doxorubicin-loaded polymeric micelles[10] and mitoxantrone-loaded polybutylcyanoacrylate nanoparticles.[11] Although polymeric micelles are effective at encapsulation of hydrophobic drugs, the entrapment of hydrophilic drugs leads in general to poor drug loading.[12] Furthermore, these delivery systems suffer from premature drug release,[12,13] resulting in rather modest increase of selectivity over free drug. In addition, these formulations can cause burst release of a drug leading to a reduced therapeutic efficiency.[14] These issues have been addressed by the covalent attachment of drugs to polymeric nanoparticles. Although promising results have been achieved by using this type of nanoparticle, it has been difficult to combine covalent drug attachment with targeted delivery due to a lack of orthogonal conjugation chemistries. This challenge has been

addressed by individual attachment of drug and a targeting module to a polymer followed by self- assembly. For example, doxorubicin and a folate receptor[15] were each attached to PLGA-amino-PEG through amide coupling and the resulting polymers were employed for micelle formation. Drawbacks of this approach include possible interference of the functional groups on micelle formation and amide bond chemistry can only be employed for the attachment of a limited number of entities.[16] Moreover, attachment of doxorubicin through acylation is not ideal as it cannot readily be released and therefore compromises its activity.[17] Post-nanoparticle functionalization is a more attractive approach, and, for example, random amide coupling has been used to attach a peptide that binds the urokinase plasminogen activator receptor (Upar)[18] and functionalized gemcitabine to the polymeric surface of iron oxide nanoparticles. This type of conjugation lacks selectivity and the resulting particles do not have a corona that provides stealth properties. A more elegant and controlled coupling approach involved the preparation of amphiphilic co-polymers that contain several reactive groups for selective functionalization. For example, a polymer was prepared having pendant enol ethers and a terminal furan for coupling of drugs and a targeting agent by thiolene and reverse Diels–Alder reactions, respectively.[13b] Although conceptually elegant, having both functionalities at the same polymer may make it difficult to generalize the approach because of difficulties of properly presenting a targeting ligand at the surface of the particles.

We report here a novel approach for the controlled covalent attachment of a drug and targeting ligand by employing poly (ethylene glycol) (PEG) functionalization at one end with a thioctic acid for covalent attachment to a gold core to form stable nanoparticles, and at the other end by a reactive functional group for drug, probe, or targeting ligand attachment. We have found that hydrazine, amine, and dibenzocyclooctynol (DIBO),[19] which can be ligated to ketones, activated

esters, and azides, respectively (Figure 2.1), are attractive for attachment of three different entities in a controlled manner. These conjugation reactions are orthogonal and do not require toxic reagents. The methodology was applied to the preparation of a multifunctional nanoparticle that is modified by a carbohydrate-based ligand for CD22,[20] which is expressed on B-cells, and is attractive for the treatment of B-cell lymphomas. Additionally, the reactive groups were exploited for the attachment of doxorubicin and Alexa Fluor 568. It was found that attachment of the glycan ligand for CD22 and a cytotoxic drug resulted in a remarkable approximately 60-fold increase in cytotoxicity. An additional advantage of such a delivery devise containing drug molecules covalently bound to a gold core is that it may overcome multidrug resistance.[21]

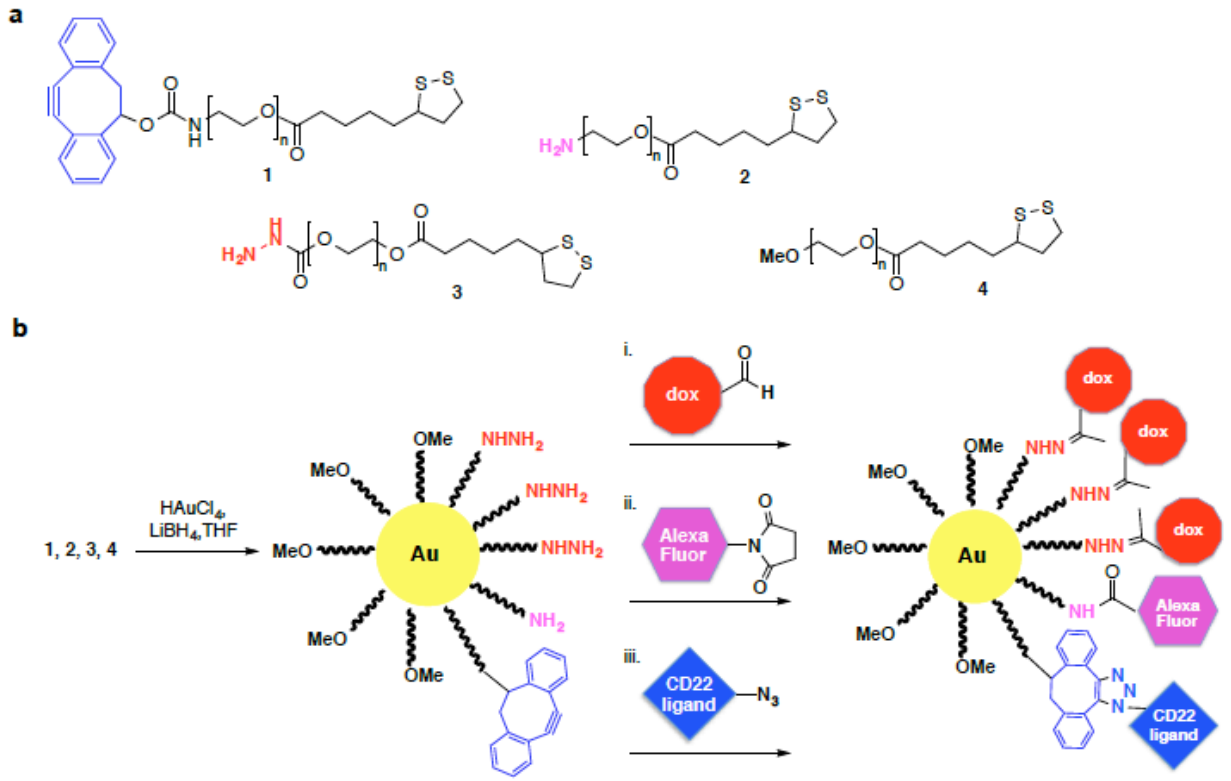

Figure 2.1 Chemical synthesis of multifunctional AuNPs targeting CD22 receptors of B-cells a) One end of PEG is modified with thioctic acid for tethering to AuNPs and another end by a

functional group for post-synthesis modification. b) Multifunctional AuNPs were synthesized by a modified Burst method. Three bioorthogonal functional groups are present for post-synthesis modification. Hydrazines can selectively react with the ketone of doxorubicin to give a hydrazone-linked drug. Amines can react with an active ester of Alexa Fluor 568 to give an amide bound fluorophore, and finally, DIBO can react with an azide of the CD22 targeting ligand by strain promoted azide-alkyne cycloaddition (SPAAC) to provide a triazole-linked module.

Results and Discussion

Chemical synthesis of heterobifunctional PEG derivatives

Gold nanoparticles (AuNPs) are attractive drug delivery vehicles owing to their ease of synthesis, chemical inertness, and flexibility of covalent surface functionalization that can offer high affinity binding interactions through multivalent display of therapeutic molecules.[1b] Heterobifunctional polymers **1**, **2** and **3** were prepared starting from a α-hydroxy-ω-azido-poly (ethylene glycol) (**6**, HO-PEG-N_3, MW≈2000 Da) for attachment to a gold core. Thus, the alcohol of 6 was esterified with thioctic acid in the presence of N, N'-dicyclohexylcarbodiimide (DDC), 4-(dimethylamino) pyridine (DMAP), and triethylamine to give PEG derivative **7** having a terminal thioctic acid moiety (Scheme 2.1). The azide of **7** was reduced to an amine using triphenylphosphine in a mixture of THF and water at 50^{o}C to give polymer **2**. FTIR spectra of **7** confirmed the presence of azido moiety (2098 cm^{-1}) and this signal had disappeared in the reduced product **2** (see the Supporting Information). Polymer **2** was modified with activated carbonate **5** in the presence of triethylamine to yield polymer **1**. The ^{1}H NMR spectrum of **1** showed aromatic proton signals typical for DIBO (7.18–7.38 ppm) that had appropriate integrations compared to the PEG signals (3.58–3.75 and 4.12–4.25 ppm), indicating complete

functionalization (see the Supporting Information). Polymer **3** was synthesized starting from α-hydroxy-ω-amino-poly (ethylene glycol) (**8**, HO-PEG-NH_2, MW≈2000 Da) that was coupled with thioctic acid to give **9** (TA-PEG-OH). The hydroxyl group of compound **9** was activated with p-nitrophenyl chloroformate to generate compound **10**, which was treated with hydrazine monohydrate to provide hydrazine-functionalized polymer **3**. Finally, polymer **4** containing nonreactive methyl ether was synthesized using a reported approach to control the density of various reactive functionalities at the nanoparticle surface.[13d]

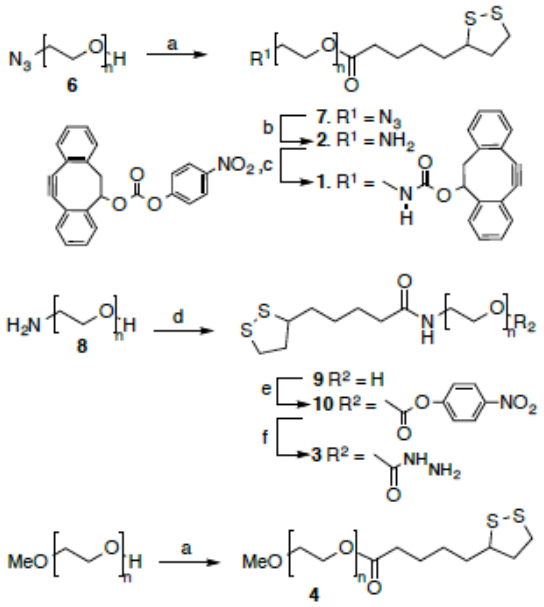

Scheme 2.1 Synthesis of heterobifunctional polymers **1**–**4**. Reagents and conditions: a) thioctic acid, DCC, DMAP, Et_3N, CH_2Cl_2; b) PPh_3, THF, 50°C, H_2O; c) **5**, Et_3N, CH2Cl2; d) thioctic acid, DCC, NHS, Et_3N, CH_2Cl_2; e) p-nitrophenylchloroformate, Et_3N, CH_2Cl_2; f) hydrazine monohydrate, CH_2Cl_2.

Chemoenzymatic synthesis of CD22 targeting ligand for strain-promoted azide-alkyne cycloaddition (SPAAC)

Trisaccharide **14**, which contains a sialic acid modified at C9 by a biphenylcarbonyl moiety, is a high affinity ligand for CD22.[20] This compound contains an anomeric azidopentyl linker for conjugation to the DIBO moiety[19] of the nanoparticles. The target glycan was synthesized by a chemoenzymatic approach employing acceptor **12** and a convenient one-pot two-enzyme sialylation system using a modified literature procedure (Scheme 2.2).[22] This enzyme system does, however, not tolerate bulky substituents at C9 of sialic acid and therefore a strategy was used by which CMP-sialic acid modified by a C9 amino function was employed for transfer which was followed by acylation of the amine of sialic acid to give target compound **14**.

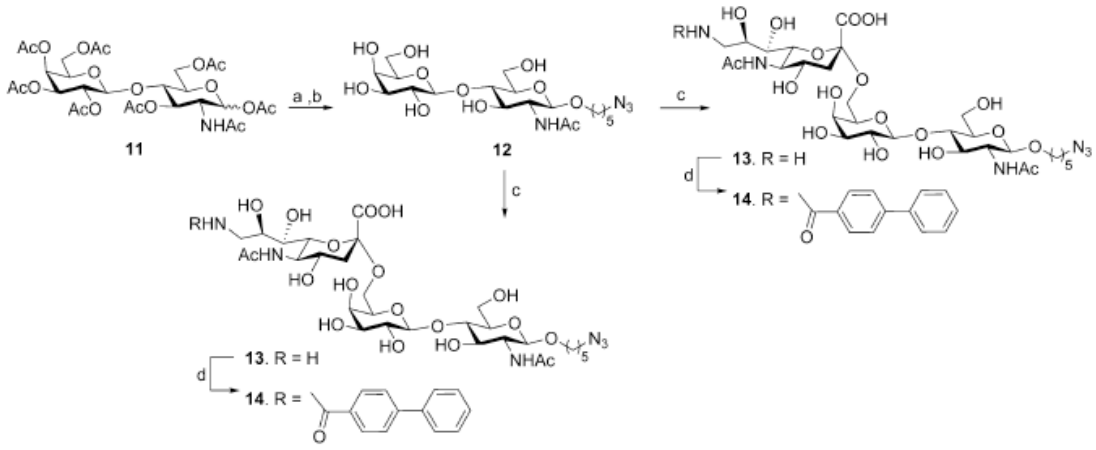

Scheme 2.2 Chemoenzymatic synthesis of the glycan ligand of CD22 Reagents and conditions: a) TMSOTf, 1,2-dichloroethane, 5-azidopentanol, 60^{o}C, 18 h; b) NaOMe, MeOH, 1 h (74 %, two steps); c) Neu5Ac9NH$_2$, CTP, Pd(2,6)ST, NmCSS, pH.9.5, 37^{o}C, overnight (53%); d) 4-biphenylcarbonyl-NHS ester, Et3N, DMF, 24 h (81%).

Acceptor **12** was prepared in high overall yield by treatment of per-O-acetylated LacNAc **11** with 5-azidopentanol in the presence of trimethylsilyl trifluoromethanesulfonate (TMSOTf) to

give a glycoside that was deacetylated with sodium methoxide in methanol. Next, C9-amino sialic acid was introduced by in-situ formation of CMP-Neu5Ac9NH_2 by condensation of Neu5Ac9NH_2 with CTP in the presence of Neisseria meningitides CMP-sialic acid synthetase (NmCSS) followed by the addition of compound **12** and α (2,6)-sialyltransferase (Pd (2,6) ST) derived from Photobacterium damselae to give the desired sialoside **13** in a yield of 53 %. Treatment of 13 with 4-biphenylcarbonyl-Nhydroxysuccinimide in DMF gave 14 in an excellent yield of 81%.

Synthesis and characterization of multifunctional AuNPs

AuNPs **A**-containing PEG derivatives (Figure 2.1) having three different surface reactive functional groups, were prepared by a modified literature procedure,[23] whereby $LiBH_4$ was added drop wise to a vigorously stirred mixture of polymers **1**–**4** (ratio of 1/2/3/4 is 10:10:30:50) and $HAuCl_4$ in anhydrous THF under a nitrogen atmosphere in the dark. After a reaction time of 3 h, methanol was added to quench the excess of reducing agent. The PEG-stabilized nanoparticles were soluble in THF, which made it possible to remove uncomplexed polymers and inorganic salts by dialysis applying a 12–14 kDa molecular weight cut-off membrane. An aqueous solution of AuNPs was obtained by concentrating the THF solution under reduced pressure, which was followed by the addition of water and extensive dialysis against water for three days. The resulting nanoparticles were characterized by ultraviolet–visible (UV/Vis) absorption spectroscopy, showing a λ_{max} at 518 nm (Supporting Information, Figure S1), which is a characteristic surface plasmon resonance band for AuNPs. Dynamic light scattering of the resulting AuNPs showed a mean diameter of 21(±1) nm (Supporting Information, Figure S2 and Table S1). Furthermore, transmission electron microscopy (TEM) images revealed that the gold core had an average diameter of 5–8 nm (Supporting Information, Figure S4).

Thermogravimetric analysis (TGA) of nanoparticle A gave a weight ratio of gold-to-organic matter of approximately 22:78 (Supporting Information, Figure S5). Interestingly, the heterobifunctional PEG derivatives lacking hydrophobic PCL did not show any structural heterogeneity and instability that we observed for PCL-PEO based block polymers.[13d]

Multi-functionalization

Multifunctional nanoparticle **D** was prepared by subsequent conjugation of doxorubicin (**15**), Alexa Fluor 568 (**16**), and glycan ligand (**14**; Figure 2.3a). It was anticipated that the ketone moiety of doxorubicin could be selectively ligated to the hydrazine moiety of particle A to give hydrazone-linked doxorubicin.[24] This linker was expected to be stable at physiological pH but to hydrolyze and release free doxorubicin after endocytosis and entry into endosomes and lysosomes that have an acidic environment. The amines of the particles can be reacted with activated esters such as Alexa Fluor derivative **16**, and finally glycan ligand **14** is modified by an azido moiety that can be exploited for strain-promoted cycloaddition with the DIBO moiety of the particles.

Thus, particle A was incubated with doxorubicin in the presence of a catalytic amount of trifluoroacetic acid (TFA) in the dark for 48 h to form hydrazone-linked AuNPs B. The solution was dialyzed against water to remove free doxorubicin. To quantify the conjugated doxorubicin, AuNPs **B** were suspended in acetate buffer at pH 5 and stirred for 30 h. The resulting nanoparticle solution was centrifuged (Milipore, centrifugation filters) to remove the gold particles and the free doxorubicin was quantified by HPLC analysis, which revealed a conjugation efficiency of 86% (Supporting Information, Figure S6).

To examine drug release in more detail, nanosurface energy transfer (NSET) effect was utilized.[25] As previously reported, the emission spectrum of doxorubicin (λ_{em} at 565 nm)

overlaps with the UV/Vis absorption spectrum of AuNPs, resulting in a decrease of fluorescence intensity of doxorubicin due to energy transfer to AuNPs.[21] The fluorescence of doxorubicin will, however, recover once it is released from nanoparticles by hydrolysis of the hydrazone bond. Thus, AuNP **B** was incubated in acetate buffer of pH 5 and PBS buffer of pH 7.4 and fluorescence emission was measured over different time intervals. As shown in Figure 2.2, incubation of AuNPs **B** at pH 5 resulted in rapid recovery of fluorescence, whereby after 15 h no further increase was observed, indicating doxorubicin had been completely released. However, incubation of AuNPs **B** at pH 7.4 did not exhibit significant fluorescence recovery even after prolonged periods of time, indicating that doxorubicin will only be released when entering acidic compartments of cells.

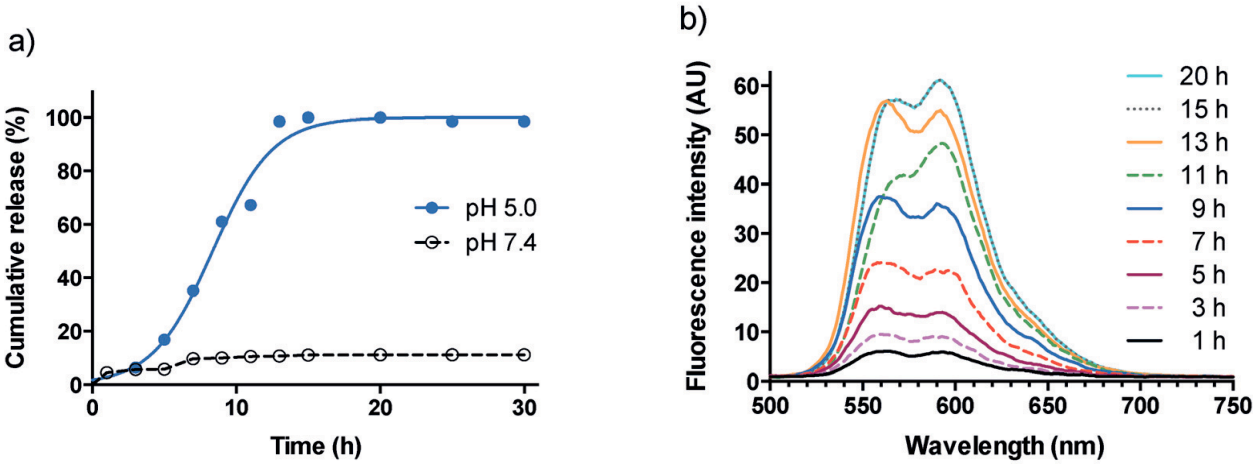

Figure 2.2 Fluorescence recovery after the hydrolysis of hydrazone bonds of AuNPs **B**. a) Quantitative analyses of the cumulative release of doxorubicin at 37°C from AuNPs **B** at pH 7.4 or 5.0 (complete release of doxorubicin was assumed when no further increase of fluorescence was observed over time and set at 100 %). b) Fluorescence emission spectra of AuNPs **B** in acetate buffer (pH 5.0) over time. Note: spectra at 15 and 20 h overlap.

Next, attention was focused on further conjugation reactions to obtain AuNPs **D**. Thus, the solution containing AuNPs **B** was adjusted to pH 8 by the addition of aqueous $NaHCO_3$, and

active ester **16** was added. After a reaction time of 24 h, the solution was dialyzed against water to remove free Alexa Fluor 568 (AuNPs **C**), and then azide **14** was added for a strain promoted azide-alkyne cycloaddition with the DIBO moieties of nanoparticle **C** to attach the glycan ligand through a triazole moiety. After 24 h, the solution was dialyzed to give nanoparticle **D** (Figure 2.3). The degree of functionalization for Alexa Fluor 568 was determined by measuring the fluorescence intensity showing a 94% efficiency of conjugation. It is important to note that the degree of functionalization may even be higher as some fluorescence quenching by the gold core of the nanoparticles is possible.[26] Quantitative monosaccharide analysis was performed by treatment of the particles with TFA at 100^{o}C to cleave glycosidic linkages followed by analysis by high-pH anion-exchange chromatography (HPAEC; Supporting Information, Figure S7). It was found that the level of glycan functionalization was approximately 85%. Collectively, these results demonstrate that the conjugation approach is highly efficient. Dynamic light scattering (Supporting Information, Figure S2 and Table S1) showed a slight increase in size (29(±2) nm) due to the three consecutive chemical transformations on the surface of nanoparticles, while TEM indicated no significant change in the size and morphology of the gold core (Supporting Information, Figure S4).

Previous studies, in which liposomes were modified with a glycan such as **14**, had indicated that optimal targeting was achieved when approximately 5% of the surface molecules were modified with the targeting agent.[20c] Furthermore, previously we had found that 10% surface modification of polymeric micelles with a fluorescent tag is appropriate for various visualization purposes.[13d] Thus, the accomplished conjugation efficiencies for **14** and the fluorophore was expected to be appropriate. Furthermore, the drug loading was limited to 30% of the surface molecules to avoid unwanted effects due to the hydrophobicity of the drug.

a)

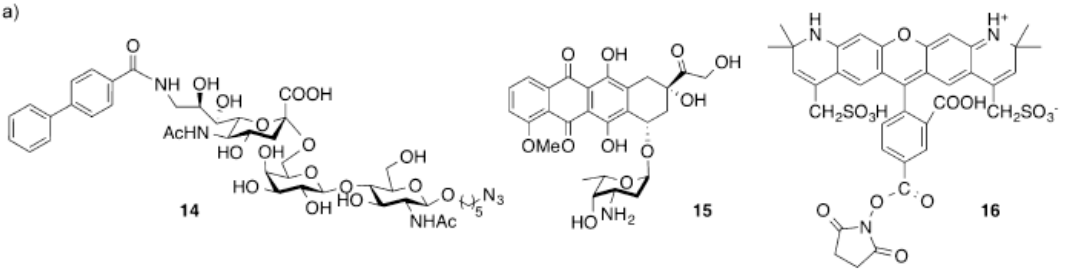

b)

AuNPs	Starting composition (%)				Conjugation efficiency (%)		
	1	**2**	**3**	**4**	**14**	**15**	**16**
A	10	10	30	50			
B	10	10	30	50		25.8	
C	10	10	30	50		25.8	9.4
D	10	10	30	50	8.5	25.8	9.4

Figure 2.3 Compounds for surface modification and chemical composition of AuNPs. a) The chemical structures of compounds **14**–**16** used for surface modification of the nanoparticles. b) Chemical composition of AuNPs **A**–**D**.

In vitro cytotoxicity, cellular uptake, and intracellular localization of AuNPs

CD22, which is a validated target for the treatment of B-cell lymphoma, undergoes receptor-mediated endocytosis,[27] and hence is an attractive target for delivery of drug loaded nanoparticles.[20b] The glycan moiety of AuNPs **D** is a high affinity ligand of CD22, and thus it was anticipated that particles endowed with this functionality should preferentially be endocytosed by cells expressing CD22. Daudi Burkitt's lymphoma cells, which express CD22, were incubated with AuNPs **B** (non-targeted NPs), AuNPs **D** (targeted NPs), and free doxorubicin at varying concentrations. After 48 h, cell viability was measured by MTT assay. As can be seen in Figure 2.4a), targeted AuNP **D** (IC_{50}=0.48 μM) exhibited a 60-fold increase in cytotoxicity compared to AuNP **B** (IC_{50}=27 μM) indicating that the glycan moiety greatly facilitates selective uptake and that the hydrazone-linked doxorubicin can be cleaved intracellularly to cause cytotoxicity. With respect to the latter, the basicity of the amine of doxorubicin is important for toxicity,[28] and therefore, the hydrazone linkage needs to be cleaved

before the drug can exert its effect. The low toxicity of AuNP **B** is probably caused by nonspecific cellular uptake. Importantly, control AuNPs modified only with targeting glycan **14** did not show any toxicity at corresponding concentrations (Supporting Information, Figure S8).

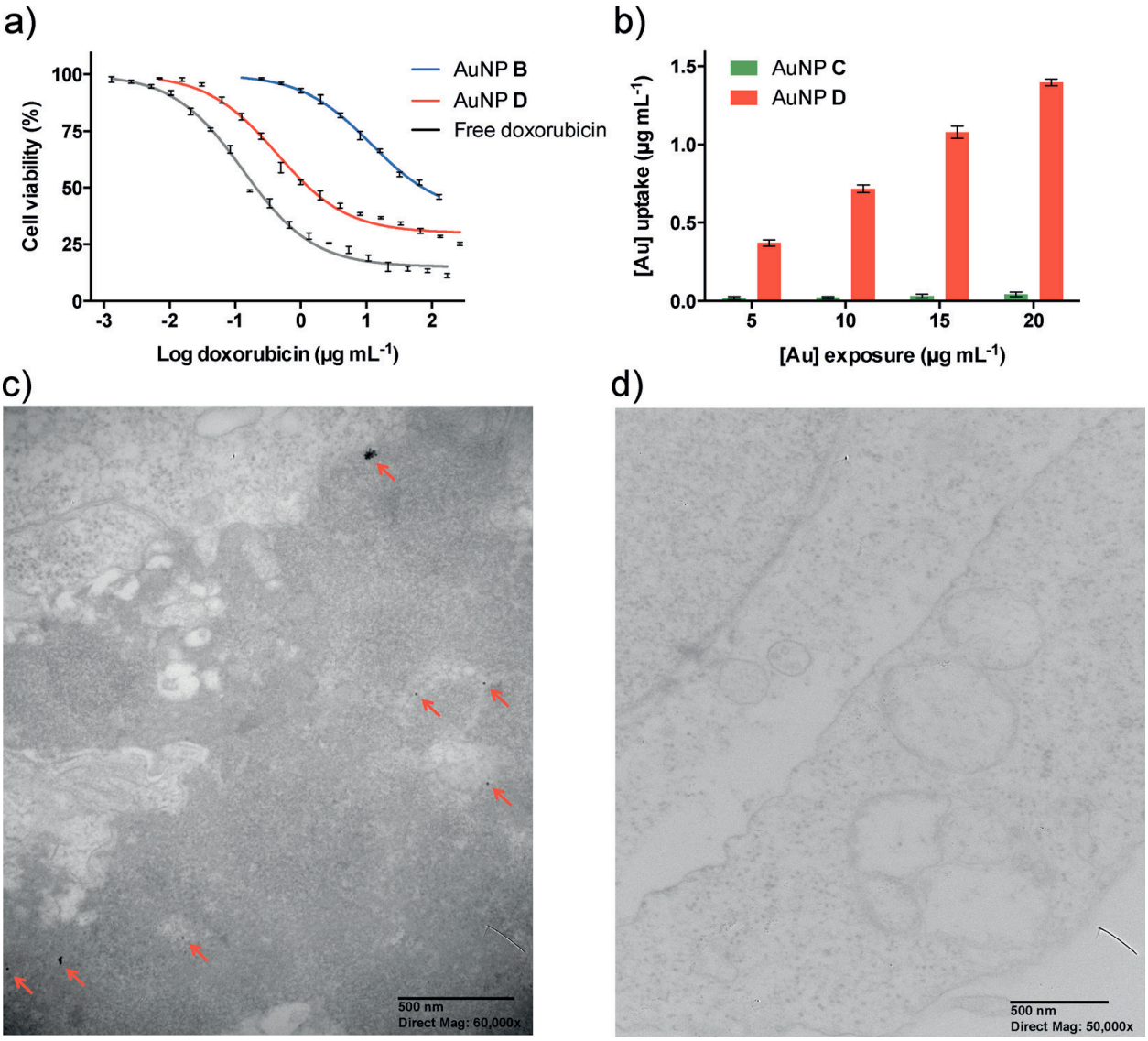

Figure 2.4 Biological examination of AuNPs **B**, **C**, and **D**. a) Cytotoxicity of doxorubicin tethered AuNPs **B** and **D** on Daudi Burkitt's cells. Data shown are mean ±SD (n=3). b) Daudi Burkitt's cells were exposed to nanoparticles **C** and **D** at 5–20 μgmL^{-1} gold for 2 h. After the cells were washed and lysed, fluorescence intensity (absorbance 578 nm, emission 603 nm) was

measured and using corresponding calibration curves uptake was calculated as mean ±SD (n=3). c, d) TEM images of representative sections of Daudi Burkitt's cells that were incubated with AuNPs **C** and **D** at 100 μgmL^{-1} gold for 10 h. c) Most AuNPs **D** were freely dispersed in the cytoplasm (shown with red arrows) as single nanoparticles, while some were found to be aggregated. d) AuNPs **C** did not exhibit any internalization.

Alexa Fluor 568-conjugated AuNPs **C** and **D** were employed to study in more detail cellular uptake. CD22-expressing Daudi Burkitt's lymphoma cells and CD22 non-expressing Jurkat cells were exposed to different concentrations of AuNPs **C** and **D**, and after incubation time of 2 h, cell lysates were analyzed for fluorescence intensity. As expected, the glycan ligand (**14**) of AuNPs **D** led to a significant increase in cellular uptake compared to the treatment with non-targeted nanoparticles **C** (Figure 2.4b) and Supporting Information, Figure S9). Importantly, the Jurkat cells did not show significant uptake of AuNPs **D** under similar experimental conditions, demonstrating excellent targeting properties of the new AuNPs.

The intracellular localization of nanoparticles **D** and **C** was examined by TEM, to visualize the gold core of the nanoparticles. Daudi Burkitt's cells were exposed to AuNPs **C** and **D** for 10 h. The use of targeted AuNPs **D** showed a significant number of internalized nanoparticles (Figure 2.4c) and Supporting Information, Figure S10). The internalized nanoparticles **D** were predominantly dispersed in the cytosol as individual nanoparticles, whereas few were found in aggregated form. Thus, it appears that the particles can escape vesicular structures after internalization.[29] As expected, cells treated with AuNPs **C** did not show internalized nanoparticles (Figure 2.4d and Supporting Information, Figure S11).

Conclusion

Although active targeted delivery of cytotoxic drugs to cancer cells is an attractive concept to overcome poor selectivity's of cytotoxic drugs, results are often disappointing due to premature release of a drug from nanocarrier delivery systems.[12,13] Covalent attachment of a drug to a nanoparticle is an attractive approach to overcome this problem.[30] This technology has, however, not matured due to difficulties of preparing nanoparticles that have good stability, a polar corona for stealth properties and which allow controlled conjugation of a drug and targeting device. The multifunctional AuNP platform described here has a unique feature in that it is composed of a polar PEG corona modified with hydrazine, amine and azide-reactive functional groups for post-synthesis modification by hydrazone bond formation, amide bond chemistry, and SPAAC, respectively. These conjugation methods are highly selective and allow the attachment of three different functional entities with high efficiency. The particles exhibit excellent stability because at one end they are modified by thiotic acid for attachment to a gold core by a modified Brust approach. The three functional groups of the polymers are compatible with the reducing conditions employed in this reaction. The resulting nanoparticles are small (5–8 nm), which is attractive for drug delivery, and exhibit excellent water solubility and were stable for a prolonged period of time. In this respect, recent studies have shown that PEG-coated gold nanoparticles with size ranging from 15–60 nm exhibit liver, kidney and spleen toxicity in mice.[31] Nanoparticles that have diameters of ≤5.5 nm are also not attractive for in vivo use because these are rapidly cleared by the renal route.[32] Other attractive features of the new platform include excellent control over ligand density and the targeting ligand is well assessable by binding to cell surface receptors. As a proof-of-principle, we have demonstrated that a nanoparticle modified by a glycan ligand for CD22 for targeting B-cells, doxorubicin attached via a pH-sensitive

hydrazone linkage for cytotoxicity, and a fluorophore for measuring uptake, exhibits a 60-fold increase in cytotoxicity of CD22 expressing B-cells compared to similar non-targeting particles. The pH responsive nature of drug release was studied in detail and free doxorubicin was only observed in acidic conditions. It is expected that the new nanoparticle platform can be employed for the combinatorial attachment of various cell targeting devices and drug molecules.

Experimental section

General reagents and materials

Polyethylene glycol (PEG, number average molecular weight, Mn≈2000 Da), polyethylene glycol monomethyl ether (Mn ca. 2000 Da), p-toluenesulfonyl chloride, sodium azide, dimethylformamide (DMF, 99.8 %), 4-(dimethyl amino) pyridine (DMAP, 99%), 1,3-dicyclohexyl carbodiimide (DCC, 99%), hydrogen tetrachloroaurate (III) trihydrate ($HAuCl_4 \cdot 3H_2O$, 99.9 %), triethylamine (99.5 %), thioctic acid (98 %), N-hydroxysuccinamide (NHS, 99 %), p-nitrophenyl chloroformate (96 %), hydrazine monohydrate (98 %), 1,2 dichloroethane, sodium methoxide, and 4-biphenyl-carboxylic acid were purchased from sigma Aldrich, Neu5Ac were purchased from Carbosynth LLC, and lithium aluminium hydride ($LiAlH_4$, 95%) was obtained from Aldrich. Alexa Fluor 568 carboxylic acid succinimidyl ester was obtained from Invitrogen. Doxorubicin hydrochloride was purchased from LC Laboratories. A 0.25m $LiBH_4$ solution in tetrahydrofuran (THF) was freshly prepared by diluting commercial 2M $LiBH_4$ (Aldrich) with freshly distilled THF. PEG was dried by azeotropic distillation from toluene followed by storage in vacuo at 60^{o}C for 24 h. Dichloromethane (CH_2Cl_2, 99%+, Fisher Scientific) was distilled from CaH_2 prior to use. All other chemicals and solvents were of analytical grade and were used as received. Column chromatography was performed on 70–230 mesh silica gel. Thin-layer chromatography was performed using Kiesel gel 60 F254 (Merck) and visualized using UV, I2 adsorption, and/or H_2SO_4/heat. Dialysis membrane Spectra/Pro 2 (molecular weight cut-off 12–14 kDa) and Spectra/pro 7 (molecular weight cut-off 50 kDa) were purchased from Spectrum Laboratories, Inc. All other reagents and solvents were of analytical grade.

General methods for compound characterization

^{1}H and ^{13}C NMR spectra ($CDCl_3$ or D_2O) were recorded using a Varian Merc-300 spectrometer equipped with Sun workstations at 300 K with the residual 1H solvent peak as reference and the solvent carbon signal as standard, respectively. COSY, HSQC, and HMBC experiments were used to assist assignment of the sugar products. Multiplicities are quoted as singlet (s), doublet (d), doublet of doublets (dd), triplet (t), or multiplet (m). NMR signals were assigned on the basis of 1H NMR, 13C NMR, gCOSY, and gHSQC spectroscopy experiments. Chemical shifts are quoted on the d scale in parts per million (ppm). Residual solvent signals were used as an internal reference. FT-IR spectra were recorded on a Shimadzu IR Prestige-21 spectrophotometer. MALDI-TOF MS spectra were recorded on an Applied Biosystems 5800 MALDI-TOF in the positive ion mode by using 2,5-dihydroxy-benzoic acid in acetonitrile (10 $mgmL^{-1}$) as a matrix. Thermogravimetric analyses (TGA) were conducted on a Perkin–Elmer Pyris 1 thermogravimetric analyzer at a heating rate of $10^{o}C\ min^{-1}$ under nitrogen. UV/Vis spectra were recorded on a Beckman Coulter DU 800 spectrophotometer, between 200 and 800 nm wavelength. Fluorescent spectroscopy was carried on a BMG Labtech POLAR star OPTIMA reader. Reverse phase HPLC studies were carried out using Agilent 1100 series (Eclipse XDB-C18 column, 5 μM, 4.6×250 mm). Sugar analysis was conducted by high-pH anion-exchange chromatography (HPAEC) using an ICS-3000 ion chromatography system (Dionex, Sunnyvale) with deionized water and 200 mM NaOH as eluent. TEM observations were made using a Philips/FEI Tecnai 20 instrument operating at an accelerating voltage of 200 kV. DLS measurements were performed on a zeta potential and particle size analyzer (Malvern Zetasizer Nano ZS system).

General procedure for the preparation of AuNPs A

Glassware used for the preparation of Au nanoparticles was washed three times with aqua regia followed by copious amounts of nanopure water and finally dried in an oven at 150°C for 24 h. To a solution of $HAuCl_4 \cdot 3H_2O$ (16 mg, 0.040 mmol) in anhydrous THF (12 mL) was added polymer 1 or a mixture of 1–4 (0.200 g, 1/2/3/4, 1:1:3:5, w/w/w/w). After stirring the mixture in the dark under a nitrogen atmosphere for 22 h, $LiBH_4$ in THF (0.25m, 0.5 mL, ≈3 equiv to $HAuCl_4$) was added drop wise under vigorous stirring. After stirring the reaction mixture for 3 h, ethanol (3 mL) was added and stirring was continued for 12 h. The solution was dialyzed against THF by using a 50-kDa molecular weight cut-off membrane (Spectra/pro 7) until no unassociated polymer was detected by thin-lay chromatography (eluent: $CHCl_3/CH_3OH$, 9:1). The solution was concentrated to a small volume (1.5–3.5 wt%) and then slowly added (25 mLmin¢1) to a fourfold excess of sterile water with vigorous stirring. The mixture was then dialyzed (12–14 kDa MWCO) against sterile water and then lyophilized. UV/Vis, TEM, dynamic light scattering, TGA, and zeta potentials were used for particle characterization.

Procedure for the preparation of AuNPs B-D

AuNPs **A** (30 mg) stabilized by polymers 1–4 (1/2/3/4, 1:1:3:5, w/w/w/w), compound 15 (5.31 mg, 3–4 equiv), and TFA (25 mL) were dissolved in anhydrous 6 mL (1:1) THF/MeOH. The reaction mixture was stirred in the dark at RT for 48 h. The solution was then dialyzed against tetrahydrofuran (THF) by applying a 50-kDa molecular weight cut-off membrane (Spectra/pro 7) until no fluorescence intensity (from doxorubicin) was detected in the dialysate. The solution was concentrated to a small volume (1.5–2%) and then slowly added to a fourfold excess of sterile water with vigorous stirring. The mixture was stirred for another hour and then dialyzed

(12–14 kDa MWCO) against sterile water to obtained AuNPs **B**. The pH of the solution was then adjusted to 8 by the addition of $NaHCO_3$. To the solution, N-hydroxysuccinamide-modified Alexa Fluor 568 (compound 16, 1.1 mg, 1.5 equiv) was added to react with the amines. The reaction mixture was stirred in the dark at room temperature at 24 h and was then dialyzed against water for 2 days until no fluorescence was detected. Compound **14** (1.9 mg, 2 equiv) was added and stirred for 24 h in the dark at RT and the resulting mixture was dialyzed against water for 2 days to give nanoparticle **D**. Dynamic light scattering, TEM, zeta potential, sugar and HPLC analysis were used to characterize these AuNPs.

Measurement of release of doxorubicin from AuNPs B

To quantitatively determine the release of doxorubicin, AuNPs B were suspended in phosphate buffer (pH 7.4) or acetate buffer (pH 5.0) at 1.5 mgmL¢1 and stirred for 30 h. The fluorescence emission spectra were recorded every 2 h. Next the nanoparticle solution was centrifuged (Milipore, centrifugation filters) to remove supernatant that contained released doxorubicin. This was further lyophilized and the amount of doxorubicin in given nanoparticle preparations was quantified using HPLC with solvent gradient from 20 to 50% (0.01M TFA/acetonitrile) for 25 min per injection. The amount of doxorubicin was in agreement with the fluorescence intensity measurements.

Quantitative sugar analysis

Sugar analysis was conducted by high-pH anion-exchange chromatography (HPAEC) using an ICS-3000 ion chromatography system (Dionex, Sunnyvale) with deionized water and 200 mm NaOH as eluent. The system consists of a SP gradient pump with an AS autosampler, ICS-3000 thermal compartment, and an ICS-3000 electrochemical detector equipped with an amperometry cell. The cell consists of a gold electrode, a combination reference electrode of glass and

Ag/AgCl (3m KCl) and titanium counter electrode consisting of the cell body. Separation was carried out using the CarboPac PA 20 column set consisting of a guard column (50 mm×4 mm I.D.) and an analytic column (150 mm×3 mm I.D.). The column and the electrochemical detection cell were placed inside the ICS-3000 thermal compartment for temperature control. The chromatographic system control, data acquisition, and analysis were carried out using Chromeleon Software (Dionex). Sample preparation: 0.5–1.0 mg of nanoparticle sample and sugar standard, such as compound 12 were treated with 2M TFA in water (250 μL) at 100^{o}C for 4 h. Sample and standard were dried by spinvacuo centrifugation, resuspended in 0.5 mL of water and passed through a C18 Cartridge (Waters), dried by spin-vacuo centrifugation, redissolved in a quantitative volume of water. The sugar content in the sample was determined based on the calibration curves of standards.

Cell line and culture conditions

Human B lymphoblasts Daudi Burkitt's cells (CCL-213, ATCC) and human Jurkat cells (Clone E6-1; ATCC) were cultured in ATCC-formulated RPMI-1640 medium with l-glutamine (2 mm), sodium bicarbonate (1.5 gL^{-1}), glucose (4.5 gL^{-1}), HEPES (10 mm) and sodium pyruvate (1.0 mm). The medium was supplemented with penicillin (100 U mL^{-1}) and streptomycin (100 $mgmL^{-1}$, Mediatech) and fetal bovine serum (FBS, 10%, BenchMark). Cells were maintained in a humid 5% CO_2 atmosphere at 37^{o}C and subcultured every 2–3 days.

Cytotoxicity assay

Cytotoxicity was determined using the MTT assay. On the day of exposure, exponentially growing cells were plated as 1×10^5 cells per well in 180 μL in 96-well tissue culture plates (Nunc). Cells were then incubated with medium (control), free doxorubicin, AuNPs **B**, and AuNPs **D** (20 μL, 10x in cell culture medium) for 2 h at 37^{o}C. Next the plate was centrifuged and

the supernatant was replaced with fresh medium (200 μL per well), which allowed for an additional 48 h of incubation. The viability was measured by quantifying the cellular ability to reduce the water-soluble tetrazolium dye 3-4,5-dimethylthiazole-2,5-diphenyl tetrazolium bromide (MTT) to its insoluble formazan salt as follows. At 44 h, MTT (5 $mgmL^{-1}$ in PBS, 20 μL per well) was added to the wells and the cells were further incubated for 4 h. At 48 h the supernatant was carefully removed and the water-insoluble formazan salt was dissolved in DMSO (120 mL per well). The absorbance was measured at 545 nm using a microplate reader (BMG Labtech). Data points were collected in triplicate and expressed as normalized values of untreated control cells (100 %). Data were fitted using Prism software (GraphPad Software, Inc.).

Measurement of cellular uptake

Daudi Burkitt's cells and Jurkat cells as control were harvested and added to tubes as 1×10^6 cells in 320 μL medium. AuNPs **C** or **D** (80 μL, 5x in cell culture medium) was added to give a final volume of 400 μL per tube. After incubation for 2 h, the supernatant was discarded and the cells were washed three times with Dulbecco's phosphate buffered saline. Next, the cells were lysed in Passive Lysis Buffer 1x (100 μL; Promega) and the fluorescence (excitation 578 nm, emission 603 nm) was measured in black 96-well plates using a fluorescent microplate reader (BMG Labtech). Calibration curves of the appropriate Alexa Fluor 568 conjugated AuNPs **C** or **D** in Passive Lysis Buffer 1x were used to calculate total cellular uptake. The data are presented as mean ±SD of triplicate treatments, with each experiment being repeated three times.

Intracellular localization of AuNPs by transmission electron microscopy (TEM)

Daudi Burkitt's cells were plated at 1×10^6 cells per well in 96-well plates and the cells were incubated with AuNPs **C** or **D** in culture medium (100 μgmL^{-1} of Au). After 10 h, the medium

was removed and the cells were washed twice with Dulbecco's phosphate buffered saline and then fixed with 2% glutaraldehyde in phosphate buffered saline (PBS; 0.1M, pH 7.4) for 1 h in Eppendorf tube. Samples were then washed three times with PBS to remove excess glutaraldehyde (10 min each wash). Cells were then post-fixed with 1% OsO_4/0.1 M PBS for 1 h, centrifuged, and rinsed with buffer and then washed three times for 10 min with distilled water to remove excess salts before dehydration in ethanol series. Next, the cells were dehydrated through a graded ethanol series of 25, 50, and 75 for 10 min each and 100% for 10 min thrice. This was followed by transition into (1:1) propylene oxide (PO)/ethanol twice for 10 min. The cells were infiltrated with Embed 812 through graded (resin/PO) series of 25, 50, and 75 with 1 h between each step. Samples were then kept in fresh 100% Embed 812 resin and polymerized at 60^{o}C for 48 h. Samples were then sectioned with a Diatome diamond knife on a RMC MT-X ultramicrotome (Boeckeler Instruments, Inc.). Ultrathin sections (≈100 nm) were collected on 300 mesh Cu grids. Sections were then post-stained with uranyl acetate (30 min) and lead citrate (5 min). The samples were viewed with a JEOL JEM-1200 TEM equipped with an AMT XR41C bottom-mount CCD camera using 80 kV accelerating voltage.

Procedure for chemical synthesis of polymers 1-4

Synthesis of N_3-PEG-TA (**7**): Compounds **6** (1.5 g, 0.75 mmol), thioctic acid (0.77 g, 3.75 mmol), DMAP (46 mg, 0.38 mmol), and anhydrous Et_3N (0.09 mL, 0.63 mmol) were dissolved in dichloromethane (50 mL) under an atmosphere of nitrogen. The mixture was cooled to 0^oC and DCC (0.83 g, 4.05 mmol) was added. The reaction mixture was stirred at 0°C for 1 h and then stirred at room temperature for an additional 24 h. The precipitated byproduct (1,3-dicyclohexyl urea) was removed by filtration and the filtrate was concentrated in vacuo. The crude product was dissolved in a small amount of dichloromethane/methanol (1:1, v/v) and purified on a LH20 size exclusion column using dichloromethane/methanol (1:1, v/v) as eluent. Fractions containing pure N_3-PEG-TA were collected and combined. Next, the solvent was removed under reduced pressure to obtain compound **7** as a light-yellow solid (1.24 g, 74%). ^1H NMR (500 MHz, D_2O) δ 4.12-4.2 (2H, m, CH_2O), 3.58-3.75 (180H, m, CH_2O), 3.38-3.43 (2H, m, $N_3CH_2CH_2O$), 3.05-3.20 (2H, m, CH_2CH_2S), 2.30-2.45 (3H, m, CH_2CHS), 1.62-1.95 (2H, m, CH2), 1.46-1.63 (4H, m, CH_2CH_2), 1.31-1.41 (2H, m, CH_2). FTIR: 2864 (C-H), 2098 (N=N=N),1722 (C=O), 1455, 1341, 1283 (C-H), 1100 (C-O) cm^{-1}.

Synthesis of MeO-PEG-TA (**4**): Compounds **11** (1.5 g, 0.75 mmol), thioctic acid (0.77 g, 3.75 mmol), DMAP (46 mg, 0.38 mmol), and anhydrous Et_3N (0.09 mL, 0.63 mmol) were dissolved in dichloromethane (50 mL) under an atmosphere of nitrogen. The mixture was cooled to 0^oC and DCC (0.83 g, 4.05 mmol) was added. The reaction mixture was stirred at 0°C for 1 h and then stirred at room temperature for an additional 24 h. The precipitated byproduct (1,3-dicyclohexyl urea) was removed by filtration and the filtrate was concentrated in vacuo. The crude product was dissolved in a small amount of dichloromethane/methanol (1:1, v/v) and

purified on a LH20 size exclusion column using dichloromethane/methanol (1:1, v/v) as eluent. Fractions containing pure MeO-PEG-TA were collected and combined. Next, the solvent was removed under reduced pressure to obtain compound **3** as a white solid (1.16 g, 71%).

^{1}H NMR (500 MHz, $CDCl_3$) δ 4.12-4.2 (2H, m, CH_2O), 3.52-3.85 (180H, m, CH_2O), 3.32-3.45 (3H, s, CH_3O and 2H, m, $CH_3CH_2CH_2O$), 3.05-3.20 (2H, m, CH_2CH_2S), 2.25-2.52 (3H, m, CH_2CHS),1.75-2.00 (2H, m, CH_2), 1.52-1.75 (4H, m, CH_2CH_2), 1.31-1.48 (2H, m, CH_2).

Synthesis of NH_2-PEG-TA (**2**): Compound **7** (1 g, 0.45 mmol) and triphenylphosphine (592 mg, 2.25 mmol) were dissolved in anhydrous THF (40 mL) and placed under an atmosphere of argon. The mixture was heated at 50^{o}C and stirred vigorously for 24 h. Then, 6 mL water was added and the reaction mixture was stirred for 5 h. The solvents were evaporated under reduced pressure and excess of triphenylphosphine was removed by filtration because it is insoluble in water and the filtrate was concentrated in vacuo. The crude product was dissolved in small amount of dichloromethane and purified on silica gel column chromatography using methanol/dichloromethane (1:9, v/v). Fractions containing pure NH_2-PEG-TA were collected and combined to give polymer 2 as a light yellow solid (0.86 g, 87%) after evaporation of solvent under reduced pressure.

^{1}H NMR (500 MHz, $CDCl_3$) δ 4.12-4.2 (2H, m, CH_2O), 3.58-3.80 (180H, m, CH_2O), 3.32-3.53 (2H, m, $NH_2CH_2CH_2O$), 3.05-3.20 (2H, m, CH_2CH_2S), 2.30-2.50 (3H, m, CH_2CHS), 1.62-1.95 (2H, m, CH_2), 1.46-1.73 (4H, m, CH_2CH_2), 1.35-1.57 (2H, m, CH_2). FTIR: 2864 (C-H), 1722 (C=O), 1455, 1341, 1283 (C-H) cm^{-1}.

Synthesis of DIBO-PEG-TA (**1**): Compounds **2** (0.5 g, 0.23 mmol), **5** (131 mg, 0.34 mmol), and anhydrous Et_3N (catalytic amount) were dissolved in dichloromethane (25 mL) and placed under an atmosphere of nitrogen. This mixture was stirred for 24 h at room temperature, after which the solvents were removed under reduced pressure. The residue was dissolved in a small amount of dichloromethane/methanol (1:1, v/v) and purified on a LH20 size exclusion column using dichloromethane/methanol (1:1, v/v) as the eluent. Fractions containing pure DIBO-PEG-TA were collected and combined to give polymer **1** after removal of solvent under reduced pressure as a light yellow amorphous solid (0.48 g, 86%).

^{1}H NMR (500 MHz, $CDCl_3$) δ 7.18-7.38 (8H, aromatics), 5.45 (1H, dd, CHO), 4.12-4.25 (2H, m, CH_2O), 3.58-3.75 (180H, m, CH_2O), 3.32-3.43 (2H, m, $NHCH_2CH_2O$), 2.86-3.04 (2H, dd, CH_2), 3.05-3.20 (2H, m, CH_2CH_2S), 2.25-2.50 (3H, m, CH_2CHS), 1.85-2.1 (2H, m, CH_2), 1.50-1.73 (4H, m, CH_2CH_2), 1.35-1.49 (2H, m, CH_2).

Synthesis of TA-PEG-OH (**9**): HO-PEG-NH_2 (1.0 g, 0.50 mmol) was dried by azeotropic distillation with toluene and dissolved in anhydrous dichloromethane. To this solution was added α-thioctic acid (135 mg, 0.65 mmol), N, N'-dicyclohexylcarbodiimide (DCC) (135 mg, 0.65 mmol), N-hydroxysuccinimide (NHS) (62 mg, 0.54 mmol) and triethylamine (117 mg, 1.16 mmol). The mixture was stirred at room temperature for 48 h, after which it was filtered to remove dicyclohexylurea. The filtrate was concentrated under reduce pressure and residue was dissolved in a small amount of dichloromethane/methanol (1:1, v/v) and purified on a LH20 size exclusion column using dichloromethane/methanol (1:1, v/v) as eluent. Tubes containing pure TA-PEG-OH were collected and combined to obtain desired compound **9** as a light yellow solid (0.74 g, 68%) after removal of solvent under reduced pressure.

^{1}H NMR (500 MHz, D_2O) δ 4.12-4.2 (2H, m, CH_2O), 3.58-3.75 (180H, m, CH_2O), 3.38-3.43 (2H, m, CH_2CH_2O), 3.05-3.20 (2H, m, CH_2CH_2S), 2.30-2.45 (3H, m, CH_2CHS), 1.62-1.95 (2H, m, CH_2), 1.47-1.63 (4H, m, CH_2CH_2), 1.30-1.40 (2H, m, CH_2).

Synthesis of TA-PEG-NPC (**10**): The hydroxyl group of compound **9** was activated by p-nitrophenyl chloroformate. TA-PEG-OH (0.4 g, 0.182 mmol) and triethylamine (43 mg, 0.424 mmol) were dissolved in 20 mL anhydrous dichloromethane and stirred at 0°C. To this solution was added drop wise p-nitrophenyl chloroformate (110 mg, 0.54 mmol) in 15 mL dichloromethane. The reaction mixture was stirred at 0 °C for 1 h and at room temperature for 24 h under N_2 atmosphere. The resultant solution was diluted by dichloromethane and washed with brine solution for three times. The organic phase was collected, dried with anhydrous magnesium sulfate, concentrated and precipitated into diethyl ether three times to give compound **10** (0.316 g 74%).

^{1}H NMR (500 MHz, $CDCl_3$) δ 8.25 (2H, dd, aromatics), 7.32 (2H, dd, aromatics), 4.12-4.2 (2H, m, CH_2O), 3.50-3.76 (180H, m, CH_2O), 3.28-3.43 (2H, m, CH_2CH_2O), 3.05-3.20 (2H, m, CH_2CH_2S), 2.15-2.45 (3H, m, CH_2CHS), 1.62-1.95 (2H, m, CH_2), 1.47-1.63 (4H, m, CH_2CH_2),1.30-1.40 (2H, m, CH_2).

Synthesis of NH_2-NH-PEG-TA (**3**): Compound **10** (350 mg, 0.15 mmol) was dissolved in 20 mL dichloromethane and reacted with hydrazine monohydrate (74.5 mg, 1.5 mmol). The solution was stirred for 24 h at room temperature. The resultant solution was washed three times with brine solution. The organic phase was collected, dried with anhydrous magnesium sulfate, concentrated and precipitated into diethyl ether three times to give compound **3** (239 mg, 71%).

^{1}H NMR (500 MHz, $CDCl_3$) δ 4.12-4.2 (2H, m, CH_2O), 3.58-3.80 (180H, m, CH_2O), 3.32-3.53 (2H, m, CH_2CH_2O), 3.05-3.20 (2H, m, CH_2CH_2S), 2.30-2.50 (3H, m, CH_2CHS), 1.62-1.95 (2H, m, CH_2), 1.46-1.73 (4H, m, CH_2CH_2), 1.35-1.57 (2H, m, CH_2).

Chemical synthesis of compounds 11-14

5-Azidopentyl-β-D-galactopyranosyl-(1→4)-2-acetamido-2-deoxy-β-D-glucopyranoside (12)

Per-acetate **11**[1] (500 mg, 0.74 mmol) was dissolved in anhydrous 1,2-dichloroethane (10 mL) under the atmosphere of argon. This solution was then treated with TMSOTf (200 μL, 1.11 mmol), followed by heating at 60°C overnight. 5-Azidopentanol[2] (480 mg, 3.7 mmol) was then added and stirring was continued at that temperature for 2 h, after which TLC (EtOAc) showed the reaction was complete. The mixture was then neutralized with Et_3N (1mL), and concentrated to dryness affording the crude product as orange oil. This intermediate was then dissolved in methanol (10 mL), after which a catalytic amount of sodium was added and the reaction mixture was stirred at room temperature for 1 h, after which TLC (EtOAc:MeOH:H_2O, 7:2:1) showed the deprotection was complete. The solution was then neutralized with AcOH (500 μL), concentrated to dryness, applied onto a column of silica gel, and purified using EtOAc: MeOH:H_2O (7:2:1) to give after lyophilization **12** as a white solid (298 mg, 74% over two steps). ^{1}H NMR (300 MHz, D_2O): δ 1.27 (2H, m, CH_2 linker), 1.47 (4H, m, CH_2 x 2 [linker]), 1.91 (3H, s, NHAc), 3.20 (2H, t, J = 6.7 Hz), 3.38 – 3.88 (12H, m, H-2 x 2, H-3 x 2, H-4 x 2, H-5 x 2, H-6 x 4), 4.34 (1H, d, H-1, J = 7.4 Hz), 4.40 (1H, d, H-1, J = 8.4 Hz). ^{13}C NMR (75 MHz, D_2O): δ 21.9, 22.5, 27.6, 27.9, 51.0, 55.0, 59.8, 60.8, 60.9, 60.9, 68.5, 70.2, 70.8, 72.4, 74.6, 75.2, 78.2, 100.8, 102.9.

5-Azidopentyl-5-acetamido-9-amino-3,5,9-trideoxy-D-glycero-α-D-galacto-2-nonulopyranosylonicacid-(2→6)-β-D-galactopyranosyl-(1→4)-2-acetamido-2-deoxy-β Dglucopyranoside (13)

Disaccharide **12** (30 mg, 0.06 mmol), 9-amino sialic acid[3] (28 mg, 0.09 mmol) and CTP (44 mg, 0.09 mmol) were dissolved in water (3 mL) in a 10 mL centrifuge tube containing Tris-HCl buffer (100 mM, pH~8.5) and $MgCl_2$ (20 mM). The resulting solution was then further adjusted to pH~8.5 using 1 M NaOH, after which an N. meningitides CMP sialic acid synthetase (20 U mL^{-1}, 500 μL) and a sialyltransferase Pd2,6ST (4 U mL^{-1}, 500 μL) were added and the reaction mixture was then incubated at 37°C overnight. After that time TLC (EtOAc:MeOH:H_2O, 7:2:1) showed the majority of the disaccharide was consumed into a slower moving product. Ice-cold EtOH was then added and the mixture was kept at 0°C for 30 min, followed by centrifugation. The supernatant was finally concentrated and passed through a Bio-gel P-2 gel filtration column with water to obtain **13** of analytical purity as a white solid (25 mg, 53%). R_f=0.05 (EtOAc:MeOH:H_2O, 7:2:1).

^{1}H NMR (300 MHz, D2O): δ 1.27 (2H, m, CH_2 [linker]), 1.47 (4H, m, CH_2 x 2 [linker]), 1.58 (1H, t, H-3ax, J = 12.2 Hz), 1.90 (3H, s, NHAc), 1.93 (3H, s, NHAc), 2.54 (1H, dd, H-3eq, J = 4.3, 12.2 Hz), 2.90 (1H, dd, J = 9.4, 13.1 Hz), 3.20 (2H, t, J = 6.9 Hz), 3.29 (1H, dd, J = 2.9, 13.1 Hz), 3.35 – 3.99 (19H, m), 4.32 (1H, d, J = 7.9 Hz), 4.43 (1H, d, J = 7.9 Hz). ^{13}C NMR (75 MHz, D_2O): δ 21.9, 21.9, 22.3, 22.4, 27.8, 39.8, 42.2, 50.9, 51.7, 54.8, 60.2, 63.1, 67.8, 67.9, 68.3, 69.9, 70.4, 72.3, 72.3, 73.4, 74.4, 80.5, 100.6, 103.5. MALDI HRMS: m/z 807.33 [M+Na^+]

Calcd for $C_{30}H_{52}N_6O_{18}$ 807.325.

5-Azidopentyl-5-acetamido-9-(4-biphenylcarbonylamido)-3,5,9-trideoxy-D-glycero-α-Dgalacto-2-nonulopyranosylonic acid-(2→6)-β-D-galactopyranosyl-(1→4)-2-acetamido-2-deoxy-β-D-glucopyranoside (14)

A mixture of trisaccharide **13** (25 mg, 0.0318 mmol) and 4-biphenyl carbonyl-N-hydroxysuccinimide ester (37 mg, 0.1274 mmol) was dissolved in anhydrous DMF (4 mL). Triethylamine (3 μL, 0.0318 mmol) was added and the reaction mixture was stirred for 24 h at room temperature. Solvents were evaporated under reduced pressure, and the crude product was purified by silica gel chromatography using EtOAc:MeOH:H_2O (7:2:1) as a mobile phase giving pure **14** as a white solid (25 mg, 81%).

^{1}H NMR (500 MHz, D_2O): δ 1.26 (2H, m, CH_2 [linker]), 1.46 (4H, m, CH_2 x 2 [linker]), 1.61 (1H, t, H-3ax, J = 12.5 Hz), 1.91 (3H, s, NHAc), 1.94 (3H, s, NHAc), 2.57 (1H, dd, H-3eq, J = 12.5, 4.7 Hz), 3.20 (2H, t, J = 6.8 Hz), 3.37 – 3.62 (11H, m), 3.64 – 3.77 (6H, m), 3.84 (2H, m), 3.90 (1H, t, J = 9.4 Hz), 3.98 (1H, ddd, J = 3.7, 8.1 Hz), 4.33 (1H, d, H-1, J = 8.0 Hz), 4.37 (1H, ad, H-1), 7.37 – 7.81 (9H, Ar-H). ^{13}C NMR (125 MHz, D_2O): δ 21.9, 22.4, 27.8, 39.9, 42.9, 50.9, 51.9, 54.9, 60.4, 63.3, 68.1, 68.2, 69.9, 70.0, 70.7, 72.4, 72.6, 74.4, 80.5, 100.7, 103.3, 127.0–129.3 (Ar-C). MALDI HRMS: 987.38 [M+Na^+]. Calcd for $C_{43}H_{60}N_6O_{19}$ 987.35.

Characterization methods for nanoparticles

Transmission electron microscopy (TEM): TEM observations were made using a Philips/FEI Tecnai 20 instrument operating at an accelerating voltage of 200 kV. Dilute solutions of the (1 mg mL^{-1}, freshly prepared in nano pure water and filtered through a 0.1 μm filter membrane) polymer-coated gold nanoparticles were deposited in copper grids coated with carbon (Electron Microscopy Science (EMS), Hatfield, PA). Excess water was removed by touching the edge of the grids with a small piece of filter paper (Whatman^{-1}). The grids were allowed to dry for 2 h at room temperature before measurements. TEM images were analyzed using Image J1.38 software developed at the National Institutes of Health.

Dynamic light scattering (DLS): DLS measurements were performed on a Zeta Potential and Particle Size Analyzer (Malvern Zetasizer Nano ZS system, USA). Dust-free vials were used for the aqueous solutions. Measurements were made at 25^{o}C with a scattering angle of 90^{o}. Five replicates were obtained to determine the average size and size distribution.

Calculation of conjugation yield: The amount of conjugation was calculated by the following equation:

$$\text{conjugation yield (\%)} = \frac{C \times V}{\frac{m \times p\%}{Mn} \times R\%} \times 100$$

where, C is defined as the concentration of the conjugated moieties (carbohydrate, Alexa Fluor, or doxorubicin) determined by sugar analysis or fluorescence measurement; V is the volume of the sample solution; m is the weight of the nanoparticles; p% is the polymer percentage of the nanoparticles determined by TGA; Mn is the number-average molecular weight of the polymer; and R% is the percentage of each functional group in the mixture of the polymers.

Quantification of doxorubicin by reverse phase HPLC: Amount of doxorubicin loaded on gold nanoparticles was estimated using Agilent 1100 series reverse phase HPLC (Eclipse XDBC18 column, 5 µm, 4.6×250 mm). Solvent system: Gradient from 20 to 50% (0.01 M TFA:acetonitrile) was used for 25 min/injection. Sample preparation: 1.5 mg mL^{-1} of nanoparticle and doxorubicin standards (25, 50, 100, 150 µg mL^{-1}) were incubated with pH 7.4 phosphate buffer and pH 5.0 acetate buffer for 30 h at room temperature. Doxorubicin content in the nanoparticles was determined based on the calibration curves of the free doxorubicin standards.

Figure S1. UV-Vis absorption spectrum of AuNPs **A** in H_2O

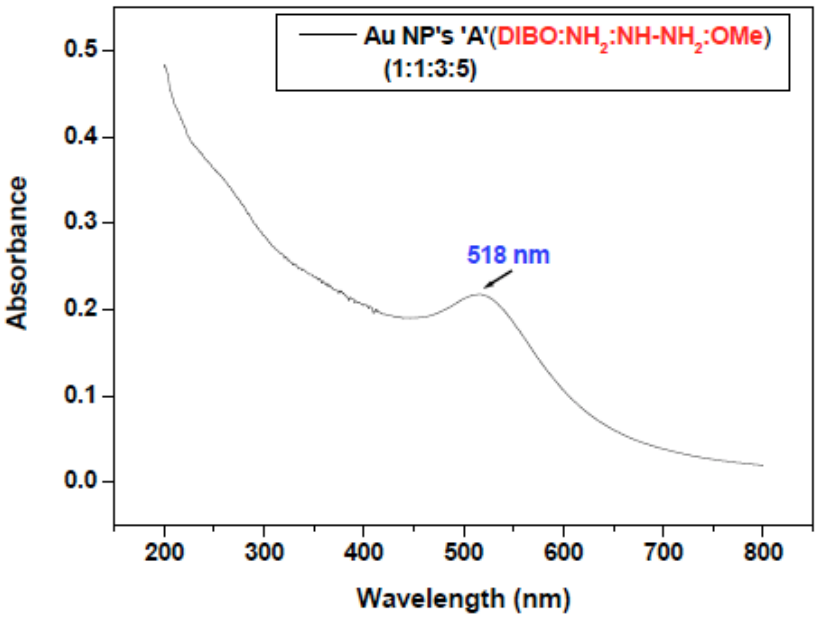

Figure S2. Size distribution histograms of nanoparticles **A-D** from DLS

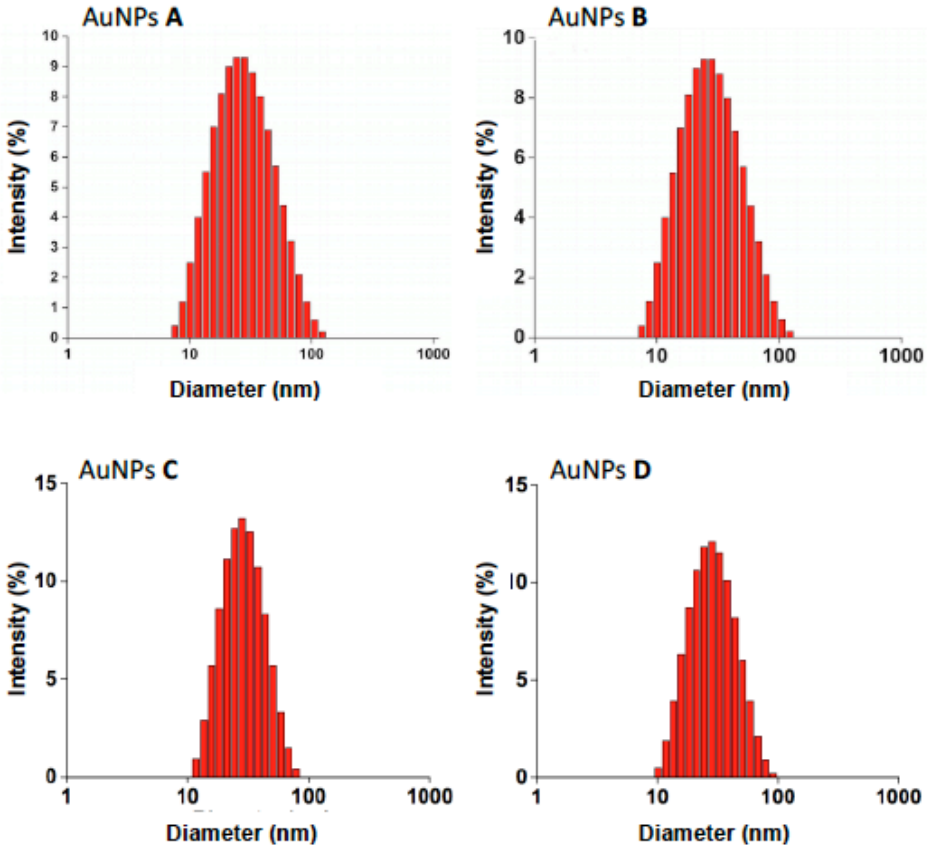

Table S1. Mean diameter and zeta potential of nanoparticles **A-D**

Nanoparticles	Mean diameter (nm)	Zeta potential (mV)
A	21.2 ± 0.97	-27.1 ± 1.23
B	23.4 ± 1.54	-22.1 ± 1.27
C	24.1 ± 0.87	-18.2 ± 2.14
D	28.6 ± 1.80	-15.1 ± 2.35

Figure S3. Stability study of AuNPs **A** (a) UV-vis spectra of AuNPs **A** in water up to 45 days. Multimodal size distribution of the nanoparticles at (b) day 0 and (c) day 45. Mean diameter was found to be 21.6 ± 1.03 nm (day 0) and 21.2 ± 0.86 nm (day 45).

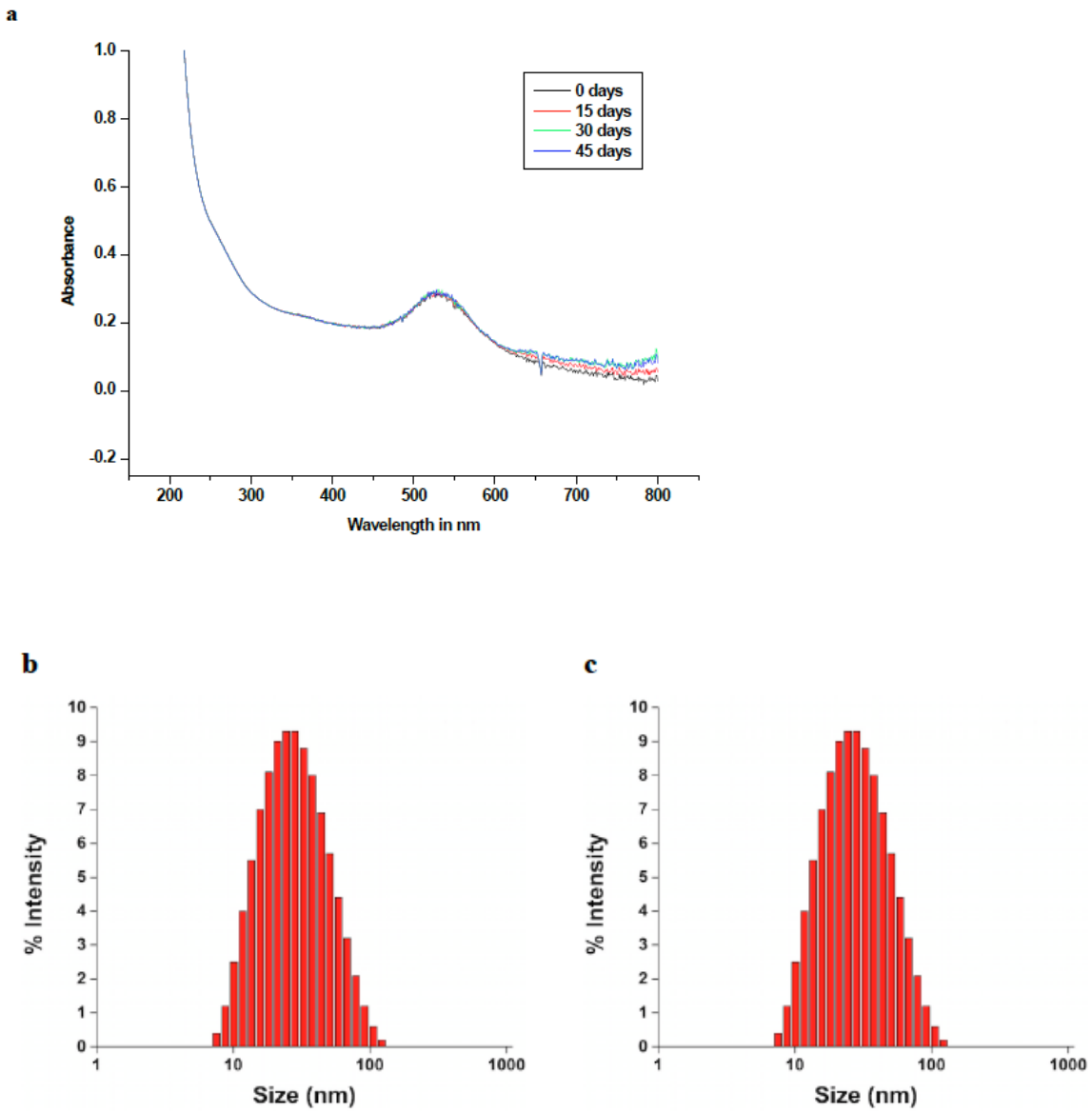

Figure S4. TEM images of AuNPs **A-D**

AuNPs **A**

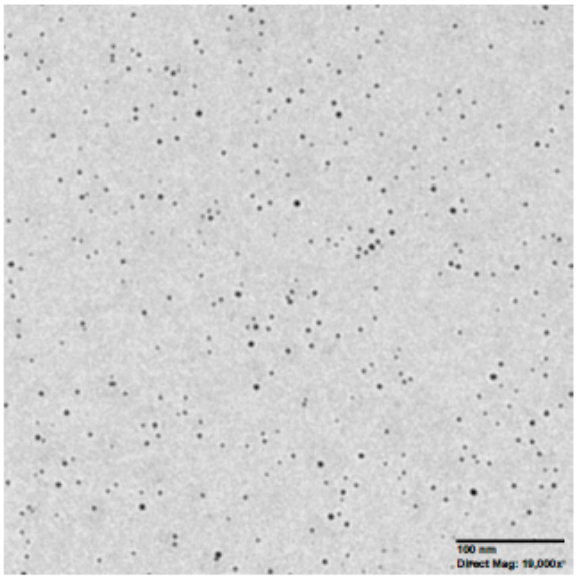

AuNPs **B**

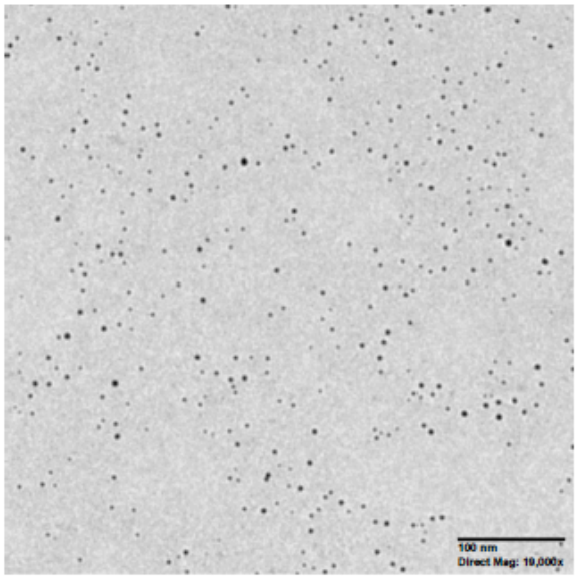

AuNPs **C**

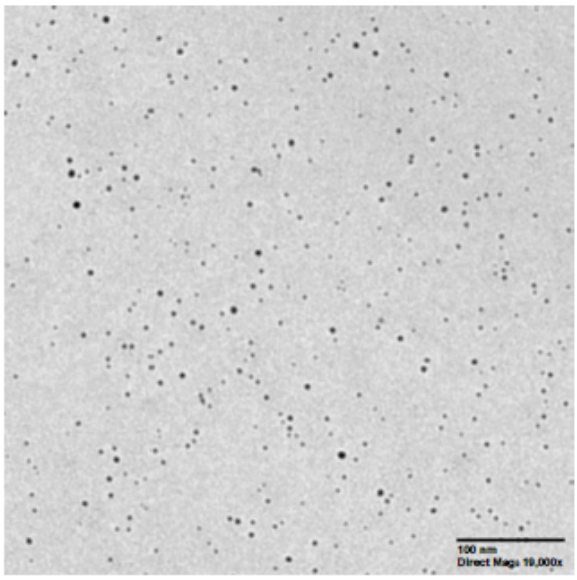

AuNPs **D**

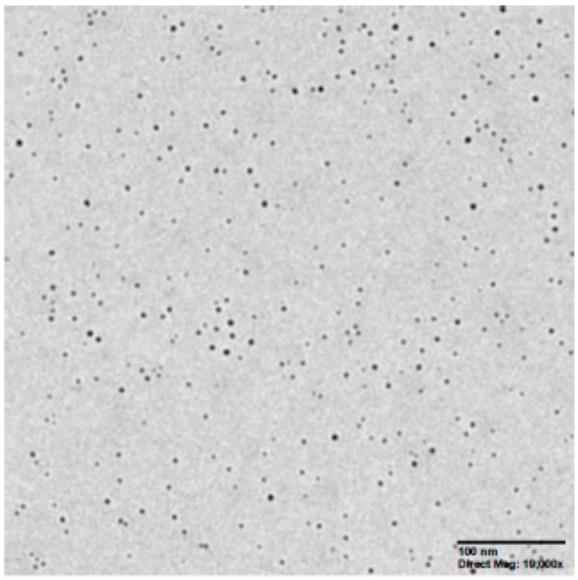

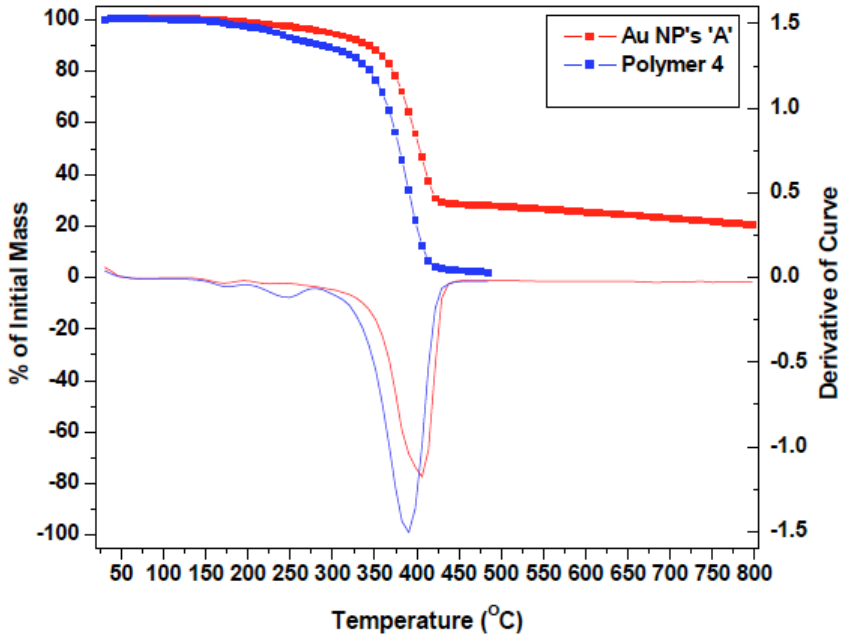

Figure S5. Thermo gravimetric analysis (TGA) of AuNPs **A** and polymer **4** AuNPs were lyophilized, dried completely, and then subjected to TGA analysis from 0 to 800°C.

These particles contain 78% polymer and 22% Au content. The maximum density at Au core was estimated[4] to be 3 polymer chains nm^{-2}. The compositional analysis, combined with the size of the gold core and average molecular weight of the polymers, suggests a density of 3.03 chains nm^{-2}. These results indicate that a significant percentage of polymer chains are attached to the metal surface.

Figure S6. Quantification of doxorubicin conjugated to AuNPs **B** (a) Reverse phase HPLC traces of doxorubicin standards at indicated concentrations and (b) the calibration curve. (c) HPLC trace of doxorubicin released from AuNPs B (1.5 mg mL^{-1}) after 30 h in acetate buffer pH 5, corresponding to 62.7 µg mL^{-1} doxorubicin.

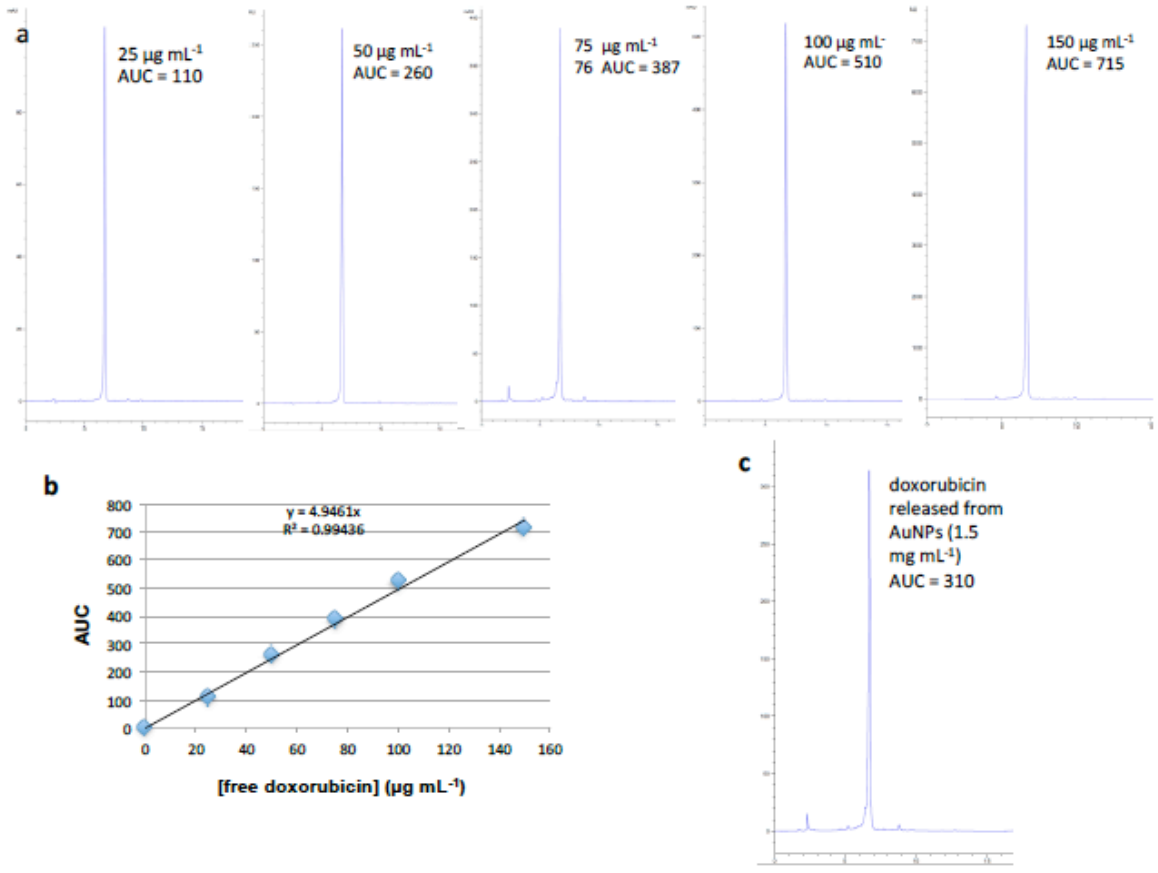

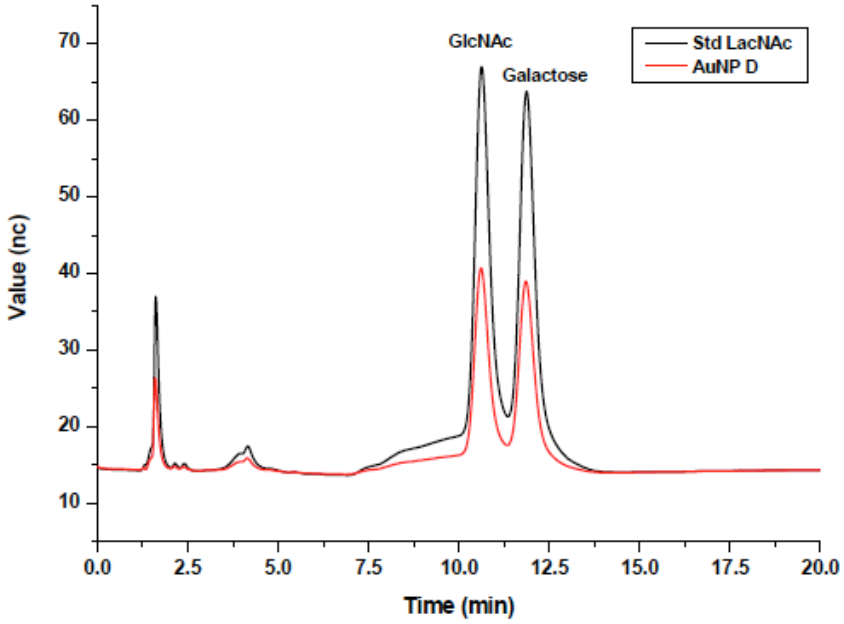

Figure S7. Monosaccharide analysis by HPAEC chromatography. The chromatogram represents a mixture of GlcNAc and galactose, monosaccharides obtained after sugar analysis of a LacNAc standard and AuNP **D**. The higher concentration of standard LacNAc (black) was used to assign the corresponding sugar peaks and the lower concentration of **D** (red) was used for comparison and quantification.

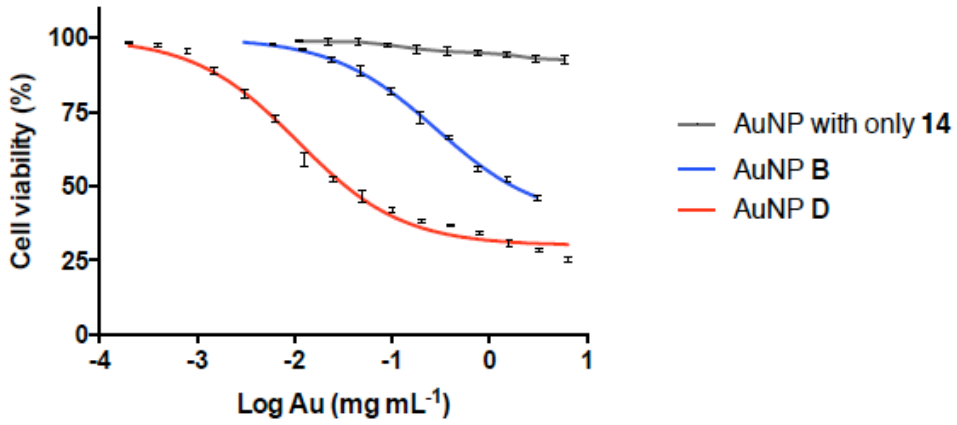

Figure S8. Cytotoxicity of AuNP. Daudi Burkitt's cells were exposed to doxorubicin tethered nanoparticles **B** and **D** and nanoparticles modified with only targeting glycan **14** at indicated concentrations gold for 2 h.

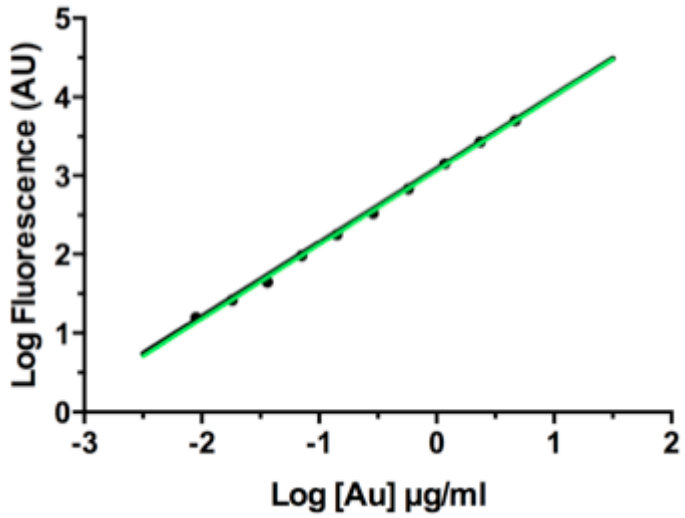

Figure S9. Fluorescence intensity calibration curves of nanoparticles **C** and **D**. Calibration curves of Alexa Fluor 568-conjugated AuNPs **C** (green) and **D** (black) in passive lysis buffer 1X. Data represent mean values ± SD. (n=3).

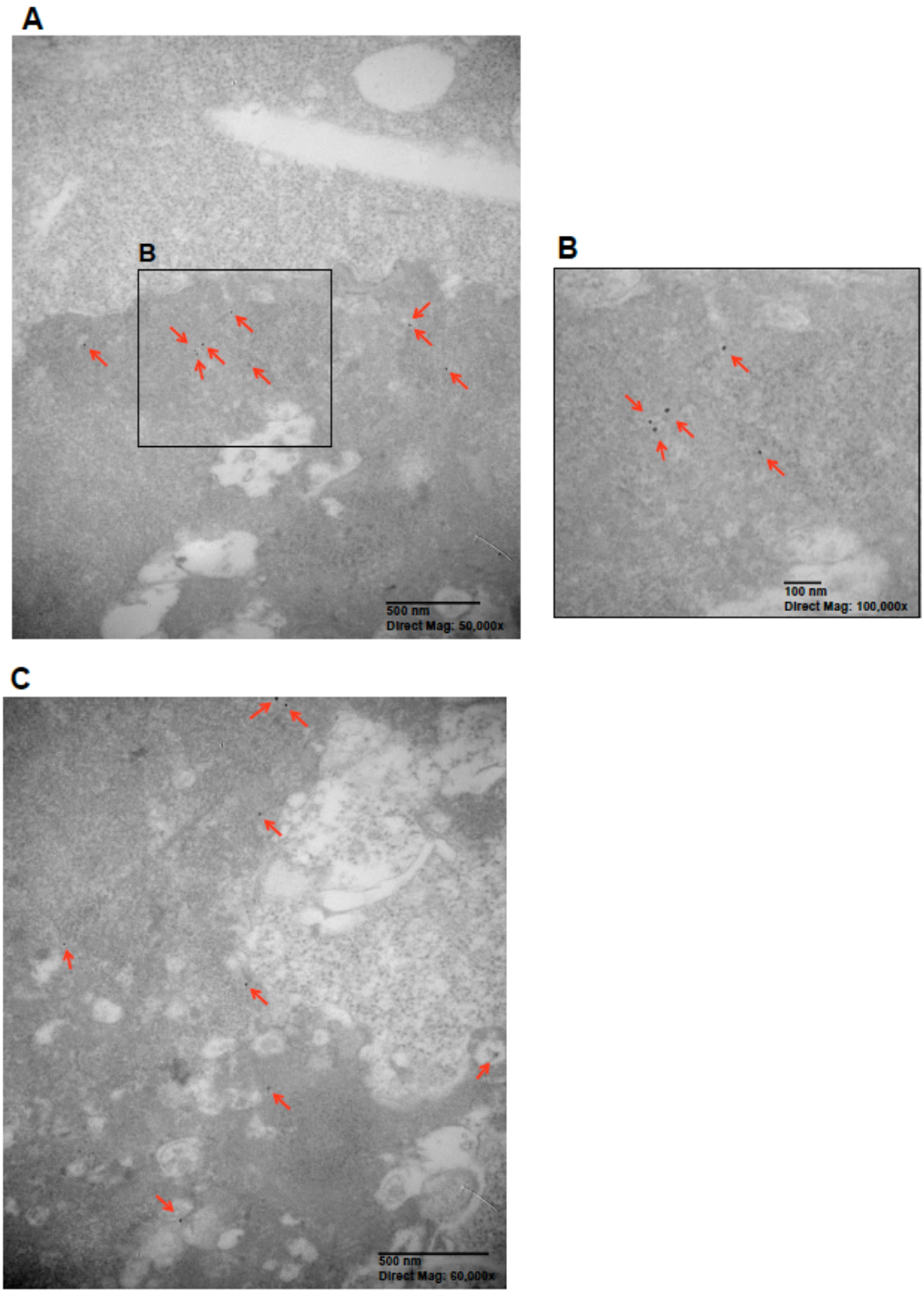

Figure S10. TEM images of representative sections of Daudi cells that were incubated with AuNPs **D** at 100 μg mL^{-1} gold for 10 h. Sections A, B, and C show freely dispersed nanoparticles in the cytosol of the cell. Image B is a magnified area from section A.

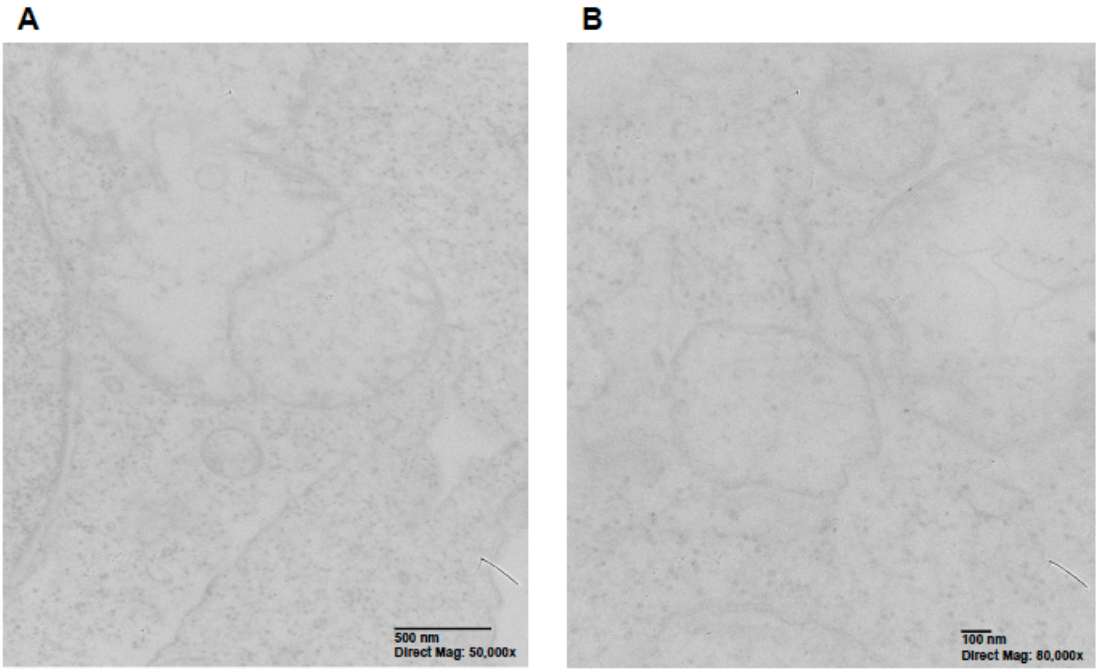

Figure S11. TEM images of representative sections of Daudi cells that were incubated with AuNPs **C** at 100 μg mL^{-1} gold for 10 h. No uptake of nanoparticles in the cells was observed. Images A and B were taken at two different magnifications, scale bars are 500 and 100 nm respectively.

Supplementary Information References

[1] Y.Gao, A. Eguchi, K. Kakehi, Y. C. Lee, *Bioorg. Med. Chem.* **2005**, 13, 6151-6157.

[2] M. J. Fer, S. Olatunji, A. Bouhss, S. Calvet-Vitale, C. Gravier-Pelletier, *J. Org. Chem.* **2013**, 78, 10088-10105.

[3] R. Isecke, R. Brossmer, *Tetrahedron* **1994**, 50, 7445-7460.

[4] T. Azzam, A. Eisenberg, *Langmuir* **2007**, 23, 2126-2132.

References

[1] a) C. J. Hawker, K. L. Wooley, *Science* **2005**, *309*, 1200–1205; b) D. Peer, J. M. Karp, S. Hong, O. C. Farokhzad, R. Margalit, R. Langer, *Nat. Nanotechnol.* **2007**, *2*, 751–760; c) V. P. Torchilin, *Pharm. Res.* **2006**, *24*, 1–16; d) S. F. M. van Dongen, H. P. M. de Hoog, R. J. R. W. Peters, M. Nallani, R. J. M. Nolte, J. C. M. van Hest, *Chem. Rev.* **2009**, *109*, 6212–6274; e) D. A. Giljohann, D. S. Seferos, W. L. Daniel, M. D. Massich, P. C. Patel, C. A. Mirkin, *Angew. Chem. Int. Ed.* **2010**, *49*, 3280–3294; *Angew. Chem.* **2010**, *122*, 3352–3366; f) R. A. Petros, J. M. DeSimone, *Nat. Rev. Drug Discovery* **2010**, *9*, 615–627; g) M. Elsabahy, K. L. Wooley, *Chem. Soc. Rev.* **2012**, *41*, 2545–2561; h) J. A. Hubbell, A. Chilkoti, *Science* **2012**, *337*, 303–305; i) A. Z. Wang, R. Langer, O. C. Farokhzad, *Annu. Rev. Med.* **2012**, *63*, 185–198; j) J. Nicolas, S. Mura, D. Brambilla, N. Mackiewicz, P. Couvreur, *Chem. Soc. Rev.* **2013**, *42*, 1147 1235; k) G. Zhang, X. Zeng, P. Li, *J. Biomed. Nanotechnol.* **2013**, *9*, 741–750.

[2] a) H. Maeda, G. Y. Bharate, J. Daruwalla, *Eur. J. Pharm. Biopharm.* **2009**, *71*, 409–419; b) J. Fang, H. Nakamura, H. Maeda, *Adv. Drug Delivery Rev.* **2011**, *63*, 136–151; c) L. Brannon Peppas, J. O. Blanchette, *Adv. Drug Delivery Rev.* **2012**, *64*, 206–212.

[3] M. A. Phillips, M. L. Gran, N. A. Peppas, *Nano Today* **2010**, *5*, 143–159.

[4] a) N. Nasongkla, X. Shuai, H. Ai, B. D. Weinberg, J. Pink, D. A. Boothman, J. Gao, *Angew. Chem. Int. Ed.* **2004**, *43*, 6323–6327; *Angew. Chem.* **2004**, *116*, 6483–6487; b) V. P. Torchilin, *Biopolymers* **2008**, *90*, 604–610.

[5] L. Rajendran, H. J. Knolker, K. Simons, *Nat. Rev. Drug Discovery* **2010**, *9*, 29–42.

[6] E. Boisselier, D. Astruc, *Chem. Soc. Rev.* **2009**, *38*, 1759–1782.

[7] N. Kamaly, Z. Xiao, P. M. Valencia, A. F. Radovic-Moreno, O. C. Farokhzad, *Chem. Soc. Rev.* **2012**, *41*, 2971–3010.

[8] F. X. Gu, R. Karnik, A. Z. Wang, F. Alexis, E. Levy-Nissenbaum, S. Hong, R. S. Langer, O. C. Farokhzad, *Nano Today* **2007**, *2*, 14–21.

[9] R. Plummer, R. H. Wilson, H. Calvert, A. V. Boddy, M. Griffin, J. Sludden, M. J. Tilby, M. Eatock, D. G. Pearson, C. J. Ottley, Y. Matsumura, K. Kataoka, T. Nishiya, *Br. J. Cancer* **2011**, *104*, 593–598.

[10] Y. Matsumura, T. Hamaguchi, T. Ura, K. Muro, Y. Yamada, Y. Shimada, K. Shirao, T. Okusaka, H. Ueno, M. Ikeda, N. Watanabe, *Br. J. Cancer* **2004**, *91*, 1775–1781.

[11] Q. Zhou, X. Sun, L. Zeng, J. Liu, Z. Zhang, *Nanomed. Nanotechnol. Biol. Med.* **2009**, *5*, 419–423.

[12] Y. Matsumura, *Adv. Drug Delivery Rev.* **2008**, *60*, 899–914.

[13] a) L. Bromberg, *J. Controlled Release* **2008**, *128*, 99–112; b) M. Shi, K. Ho, A. Keating, M. S. Shoichet, *Adv. Funct. Mater.* **2009**, *19*, 1689–1696; c) A. B. Ebrahim Attia, Z. Y. Ong, J. L. Hedrick, P. P. Lee, P. L. R. Ee, P. T. Hammond, Y. Y. Yang, *Curr. Opin. Colloid Interface Sci.* **2011**, *16*, 182-194; d) X. Li, J. Guo, J. Asong, M. A. Wolfert, G. J. Boons, *J. Am. Chem. Soc.* **2011**, *133*, 11147–11153; e) K. Cai, X. He, Z. Song, Q. Yin, Y. Zhang, F. M. Uckun, C. Jiang, J. Cheng, *J. Am. Chem. Soc.* **2015**, *137*, 3458–3461.

[14] J. Zeng, L. Yang, Q. Liang, X. Zhang, H. Guan, X. Xu, X. Chen, X. Jing, *J. Controlled Release* **2005**, *105*, 43–51.

[15] H. S. Yoo, T. G. Park, *J. Controlled Release* **2004**, *96*, 273–283.

[16] K. Ulbrich, T. Etrych, P. Chytil, M. Jelinkova, B. Rihova, *J. Controlled Release* **2003**, *87*, 33–47.

[17] P. T. Wong, S. K. Choi, *Chem. Rev.* **2015**, *115*, 3388–3432.

[18] G. Y. Lee, W. P. Qian, L. Wang, Y. A. Wang, C. A. Staley, M. Satpathy, S. Nie, H. Mao, L. Yang, *ACS Nano* **2013**, *7*, 2078–2089.

[19] X. H. Ning, J. Guo, M. A. Wolfert, G. J. Boons, *Angew. Chem. Int. Ed.* **2008**, *47*, 2253-2255; *Angew. Chem.* **2008**, *120*, 2285–2287.

[20] a) N. R. Zaccai, K. Maenaka, T. Maenaka, P. R. Crocker, R. Brossmer, S. Kelm, E. Y. Jones, *Structure* **2003**, *11*, 557–567; b) B. E. Collins, O. Blixt, S. Han, B. Duong, H. Li, J. K. Nathan, N. Bovin, J. C. Paulson, *J. Immunol.* **2006**, *177*, 2994–3003; c) W. C. Chen, G. C. Completo, D. S. Sigal, P. R. Crocker, A. Saven, J. C. Paulson, *Blood* **2010**, *115*, 4778–4786.

[21] F. Wang, Y. C. Wang, S. Dou, M. H. Xiong, T. M. Sun, J. Wang, *ACS Nano* **2011**, *5*, 3679-3692.

[22] a) H. Yu, H. A. Chokhawala, S. Huang, X. Chen, *Nat. Protoc.* **2006**, *1*, 2485–2492; b) E. Kaltgrad, M. K. O'Reilly, L. Liao, S. Han, J. C. Paulson, M. G. Finn, *J. Am. Chem. Soc.* **2008**, *130*, 4578–4579; c) M. K. O'Reilly, B. E. Collins, S. Han, L. Liao, C. Rillahan, P. I. Kitov, D. R. Bundle, J. C. Paulson, *J. Am. Chem. Soc.* **2008**, *130*, 7736–7745.

[23] a) M. Brust, J. Fink, D. Bethell, D. J. Schiffrin, C. Kiely, J. *Chem. Soc. Chem. Commun.* **1995**, 1655–1656; b) T. Azzam, A. Eisenberg, *Langmuir* **2007**, *23*, 2126–2132.

[24] A. Lau, G. Berube, C. H. Ford, M. Gallant, *Bioorg. Med. Chem.* **1995**, *3*, 1305–1312.

[25] a) G. K. Darbha, A. Ray, P. C. Ray, *ACS Nano* **2007**, *1*, 208–214; b) H. Lee, K. Lee, I. K. Kim, T. G. Park, *Biomaterials* **2008**, *29*, 4709–4718.

[26] a) V. N. Pustovit, T. V. Shahbazyan, *J. Chem. Phys.* **2012**, *136*, 204701; b) P. A. Ledin, N. Kolishetti, M. S. Hudlikar, G. J. Boons, *Chem. Eur. J.* **2014**, *20*, 8753–8760.

[27] A. Molina, *Annu. Rev. Med.* **2008**, *59*, 237–250.

[28] W. Priebe, *Curr. Pharma. Design* **1995**, *1*, 51–68.

[29] P. Nativo, I. A. Prior, M. Brust, *ACS Nano* **2008**, *2*, 1639–1644.

[30] a) X. Q. Zhang, X. Xu, R. Lam, D. Giljohann, D. Ho, C. A. Mirkin, *ACS Nano* **2011**, *5*, 6962–6970; b) L. Vigderman, E. R. Zubarev, *Adv. Drug Delivery Rev.* **2013**, *65*, 663–676.

[31] X. D. Zhang, D. Wu, X. Shen, P. X. Liu, N. Yang, B. Zhao, H. Zhang, Y. M. Sun, L. A. Zhang, F. Y. Fan, *Int. J. Nanomed.* **2011**, *6*, 2071–2081.

[32] H. Soo Choi, W. Liu, P. Misra, E. Tanaka, J. P. Zimmer, B. I. Ipe, M. G. Bawendi, J. V. Frangioni, *Nat. Biotechnol.* **2007**, *25*, 1165–1170.

CHAPTER 3

ORTHOGONAL GLYCOENGINEERING STRATEGY ENABLES PREPARATION OF DUAL-DRUG ANTIBODY-DRUG CONJUGATES DESIGNED TO BYPASS MULTIDRUG RESISTANCE IN CANCER CELLS

Hudlikar, Manish. Li, Xiuru. Sun, Tiantian. Boons, Geert-Jan.

To be submitted to *Angewandte Chemie*

Abstract

The concept of antibody-drug conjugates (ADCs) containing multiple drugs hold great promise as next-generation anticancer agents, however, producing them remains a challenge and there is a need for mild, non-genetic, and site-specific conjugation method that can yield homogeneous dual-drug products. An orthogonal glycoengineering strategy that allows sequential site-specific conjugation of dual-drugs to native IgG antibody has been described. This method has been devised based on an observation that sialyltransferase (ST6Gal1) has a preference for the α1,3-Man-β1,2-GlcNAc-β1,4-Gal bottom arm of the glycan of IgG overtop arm. This unique property of ST6Gal1 has enabled the sequential introduction of reactive functional groups and conjugation of two payloads that can act via a differential mode of action. To demonstrate the benefits of ADC dual drug delivery, this method was applied to produce an anti-CD22 antibody modified with FDA approved antineoplastic anticancer agent such as paclitaxel and zosuquidar, a highly potent P-glycoprotein modulator currently under phase-III clinical trials for the treatment of acute myeloid leukemia. The anti-CD22 antibody modified by covalently linked dual-drugs in equivalent concentrations showed superior anti-cancer activities, selectivity and can bypass P-glycoprotein associated multidrug resistance in lymphoma cancer cells. We anticipate that the dual-drug ADC platform presented in this work is broadly suited for the delivery of many other novel drug combinations and generally applicable to any other therapeutic antibody.

Introduction

Antibody-drug conjugates (ADCs) have emerged as a promising class of therapeutics for the treatment of cancer. In recent years, they have made significant progress owing to their unique ability to selectively discriminate between healthy and diseased tissue, with an ability to

target cytotoxic drugs to cells overexpressing tumor-associated antigen[1]. This exciting class of targeted therapy has made into clinic with four US food and drug administration approved ADCs currently on the market namely brentuximab vedotin (ADCETRIS™)[2], ado-trastuzumab maytansine (KADCYLA™)[3], gemtuzumab ozogamicin (Mylotarg™)[4], and inotuzumab ozogamicin (Besponsa™)[5] for treatment of patients with relapsed Hodgkin lymphoma and anaplastic large-cell lymphoma, metastatic breast cancers, and relapsed or refractory B-cell precursor acute lymphoblastic leukemia (ALL) respectively. There are more than 200 ADCs[6] candidates currently undergoing clinical evaluation for the treatment of many other types of cancers. Most of these clinical candidates suffer from heterogeneous drug loading resulting in a narrow therapeutic window[7]. To achieve the full potential of ADCs, novel site-specific conjugation strategies that allow homogeneous drug loading, drug-linker constructs with high stability, novel drug release mechanisms, and attachment of dual payloads that work in synergistic fashion are highly desired for developing next generation of ADCs[7-8].

One of the major hurdles to treat cancer patients with ADC is the emergence of tumors with multi-drug resistant (MDR) phenotype. Many mechanisms of MDR have been described, out of which overexpression of MDR1 (also called as P-glycoprotein or ABCB1) or other ATP-dependent transporters that pump drugs out of the cancer cells have been well documented in many cancers leading to poor responses to chemotherapy[9] and some targeted therapies such as imatinib (Gleevec™)[10]. Unfortunately, majority of cytotoxic compounds used in the preparation of ADCs namely calicheamicin[11], doxorubicin, taxanes[9a, b]; monomethyl auristatin E (MMAE)[12], maytansinoids[13]; and analogues of dolastatin 10[14], are good substrates for MDR1 transporters resulting in poor ADC activity in MDR1 overexpressing cells. P-glycoprotein (P-gp)

actively efflux out a wide range of compounds sharing little structural similarities and keeping an intracellular level of many anticancer drugs below a cell-killing threshold[9b].

Strategies that circumvent P-gp associated multidrug resistance mainly involve co-administration of pump inhibitor and cytotoxic drug[9b, 15]. However, many P-gp inhibitors or modulators have failed in the clinical trials due to high systemic toxicity, off-target toxicity to MDR1 expressed in normal tissues, and most of the inhibitors were the substrate for P-gp resulting in short reversal effects[9a, b, 16]. Additionally, these inhibitors show pharmacokinetic interaction with several oncolytic tested in preclinical models making the interpretation of clinical results complicated[17]. In another approach, complementary drug combinations were designed to overcome differential drug sensitivities[18]. This method has been recently applied to ADC. For example, insensitivity to a particular ADC can be overcome through the delivery of a complementary warhead using the same antibody or in combination with unconjugated clinically approved anticancer drug[19] making this approach less practical, complicated and costly. Therefore, there is an urgent need to develop mild, non-genetic, and site-specific conjugation ADC technology for homogeneous incorporation of dual or multi drugs that have a complementary or synergistic mode of action.

In pursuit of this challenge, the first example of multi-drug conjugate has been reported unfortunately on antibody Fab fragment and required the genetic introduction of engineered cysteine residues to facilitate site-specific conjugation[20]. In another report, a number of approaches to assemble two separate agents to antibody requires site-specific amino-acid mutation, specialized reagents, or two distinct handles for conjugation[21]. Another site-specific conjugation method utilized pyridazine-dione re-bridging of native antibody disulfides followed by dual-click functionalization to construct homogeneous ADC but this method was

unfortunately applied to create a fluorophore-drug antibody conjugate and still relies upon CuAAC reaction for conjugation[22]. In both the previous examples Cu (I) assisted azide-alkyne cycloaddition (CuAAC) has been applied for conjugation of payload. However, recently It has been shown that Cu (I) used in CuAAC can mediate formation of reactive oxygen species (ROS)[23] leading to oxidative degradation of proteins and peptides by co-ordination with the thiol group of cysteine, methionine, and imidazole of histidine making this method less attractive.

To date, only a single example has shown a more elegant and practical approach for site-specific conjugation of dual-cytotoxic drug conjugate technology for native and non-engineered IgG. In this work[24], drug carrier bearing orthogonally protected cysteine residues that can be sequentially unmasked and conjugated with different drug linkers has been illustrated. Interestingly, this method produced homogeneous ADCs bearing 16 total drugs, split evenly between the two drug linkers that possess complementary physiochemical properties presents an intriguing route with enhanced cytotoxicity profile against MDR1 overexpressing cancer cells. Although conceptually elegant, conjugation of drug carrier to the antibody by reaction with cysteine thiols liberated from reduced interchain disulfides has limited impact on antibody structure but often gives a statistical mixture of products ranging from 2 to 8 with homogeneity up to 75%. In addition, deprotection of one of the cysteine protecting group such as acetamidomethyl (Acm) requires toxic metal salts such as aqueous $Hg(OAc)_2$ 5-6 equivalent per thiol and extra step has to be performed using Quadrasil MP resin to capture excess Hg^{+2} before obtaining fully functional dual-drug ADC.

In this work, we report site-specific conjugation method that can yield homogeneous dual-drug ADCs using chemoenzymatic remodeling of complex biantennary N-linked glycans of a

native antibody. In our previous work[25] we have shown that remodeling glycans of antibodies with azido-containing sialic acid using sialyltransferase (ST6Gal1) gave mainly a monosialylated structure even after 24 h of reaction condition. ST6Gal1 has a preference for the α1,3-Man-β1,2-GlcNAc-β1,4-Gal bottom arm of the glycan of IgG antibodies over top arm[25-26]. We envisaged that harnessing this unique property of ST6Gal1 could facilitate the sequential introduction of reactive functional groups such as azide or tetrazine that in turn can undergo sequential click reactions such as strain promoted azide-alkyne (SPAAC) and inverse electron demand Diels-Alder reaction. These conjugation chemistries are particularly attractive because azide is virtually absent in biological systems[27] and can be reacted by SPAAC. Moreover, methyl substituted tetrazinyl-phenyl-methanamine derivative has been chosen due to its high stability in fetal bovine serum (FBS) and exceptionally fast reaction kinetics with *trans*-cyclooctene (TCO)[28]. Interestingly, both SPAAC and inverse electron demand diels-alder conjugation pairs are bio orthogonal[29] with excellent selectivity making them suitable to introduce dual-drugs with quantitative yields.

Orthogonal glycoengineering of anti-CD22 antibody for dual drug conjugation

Homogeneous incorporation of dual drugs utilizing orthogonal glycoengineering has been demonstrated by two strategies. In the first strategy, as shown in Figure 3.1, the anti-CD22 antibody was treated first with galactosyltransferase (GalT) and UDP-Gal in the presence of calf intestine alkaline phosphatase (CIAP). This treatment generates G2 glycoform with complete galactosylation of the biantennary N-linked glycans. Next, C-5 azido sialic acid was incorporated using compound **1**, recombinant sialyltransferase (ST6GalI) and calf intestine alkaline phosphatase (CIAP). By optimizing the reaction parameters such as a concentration of **1**, ST6GalI and time complete monosialylation of on the bottom arm (of complex N-glycan) with

azide has been obtained which was revealed by detail glycan analysis and in agreement with our previous observation and literature report. The incorporated azide was then reacted with first bicyclononynol (BCN) modified by, for example, FDA approved antineoplastic anticancer agent such as paclitaxel (PCTX) (**8**) through strain promoted azide-alkyne (SPAAC). Further sequential exposure of anti-CD22 antibody with **1**, ST6GalI resulted in near quantitative bis-sialylation of the top arm on the complex N-glycan with another azide group.

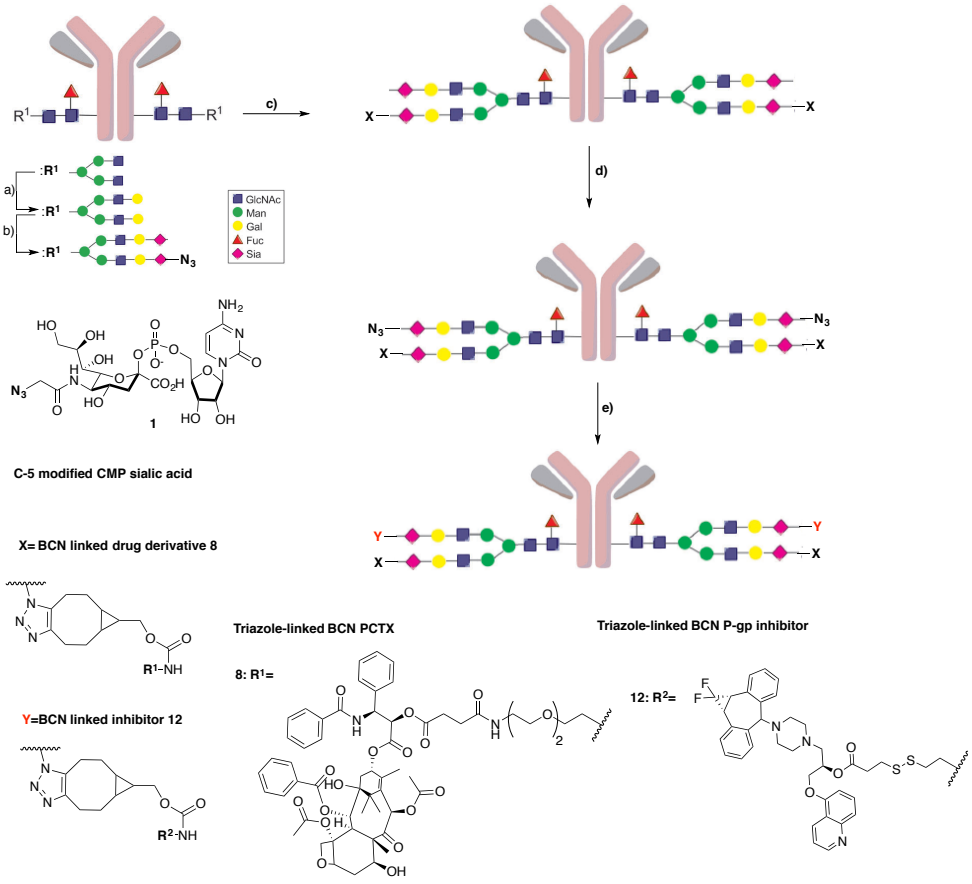

Figure 3.1 Orthogonal glycan engineering of anti-CD22 antibody using sequential C-5 azido sialic acid derivative; Reagents and conditions: a) UDP-Gal, galactosyltransferase, MOPS buffer, pH 7.2; b) CMP sialic acid derivative **1**, sialyltransferase (ST6Gal1), CIAP in cacodylate buffer pH 7.6; c) Compound **8** was added in cacodylate buffer, pH 7.6; d) CMP sialic acid derivative **1**,

sialyltransferase (ST6Gal1), CIAP in cacodylate buffer pH 7.6; e) Compound **12** was added in cacodylate buffer, pH 7.6.

The azide moiety was then further reacted with second strained alkyne modified (BCN) therapeutic agent such as zosuquidar (ZSQ); a highly potent P-glycoprotein modulator (**12**) through SPAAC yielded homogeneous dual-drug ADCs with equivalent (1:1) ratio of each payload. The quantification of each azide introduced on to biantennary N-glycan was done by reacting it with BCN modified Alexa fluor 488 (**15**) under similar conditions described previously.

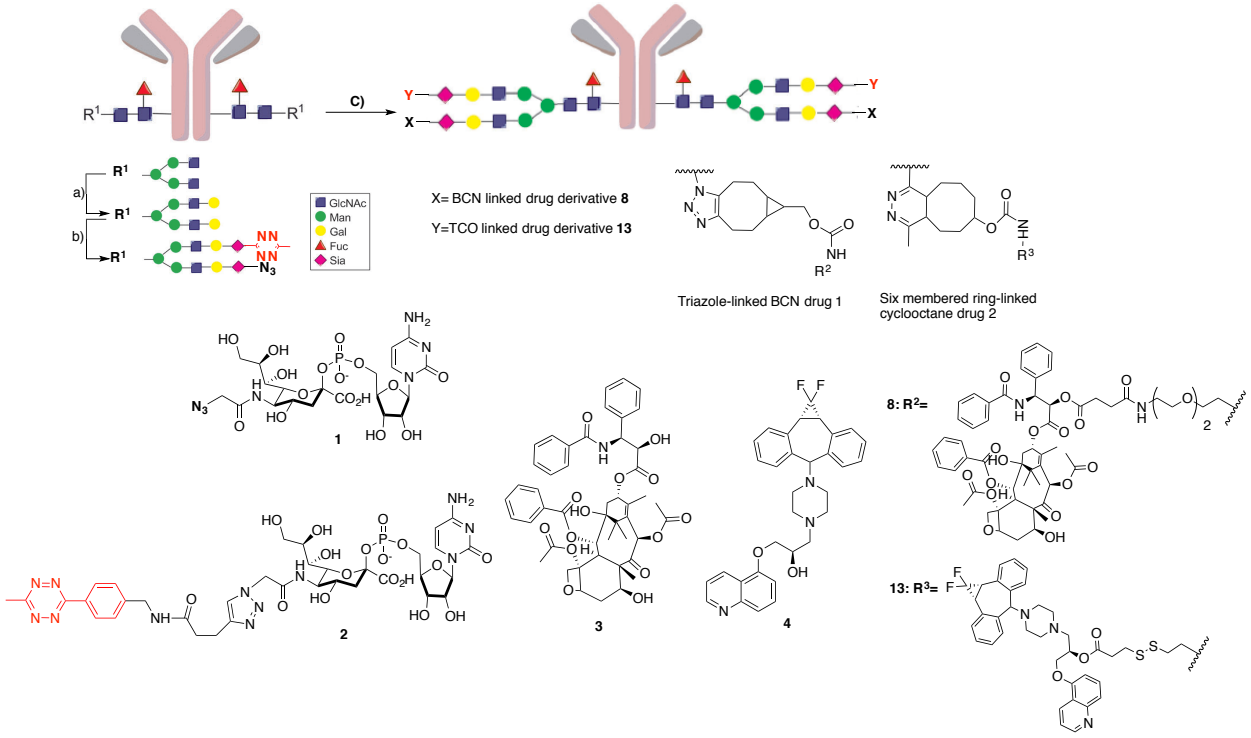

Figure 3.2 Orthogonal glycan engineering of anti-CD22 antibody using sequential C-5 azido and methyl substituted tetrazine derivatives; Reagents and conditions: a) UDP-Gal, galactosyltransferase, MOPS buffer, pH 7.2; b) CMP sialic acid derivative **1** and **2** sialyltransferases (ST6Gal1), CIAP in cacodylate buffer pH 7.6 added sequentially; c) compound **8** and **13** were added to antibody reaction mixture in cacodylate buffer, pH 7.6.

Interestingly, in the second strategy monosialylation of the bottom arm with of the C-5 azido sialic acid was a common modification step. This differentiation of arms allows sequential sialylation of top arms with C-5 modified methyl substituted tetrazinyl-phenyl-methanamine sialic acid using derivative **2** and ST6GalI over prolonged exposure at conditions mentioned in figure 3.2. The incorporation of bioorthogonal pair such as azide and methyl substituted tetrazine in equal ratio (1:1) was confirmed by detail glycan analysis obtained after peptide-N-glycosidase F (PNGase F) treated antibody and sialic acid analysis carried out using high-pH anionic exchange chromatography (HPAEC). The resulting dual labeled anti-CD22 antibody was then subjected to reaction with compound **8** and **13** through SPAAC and inverse electron demand Diels-Alder reaction forming stable triazole and tetrazine ligation products respectively. The various repeated experiments also demonstrate that the dual labeling procedure described here is highly efficient and selective for azido and tetrazine modified antibodies representing its superiority over previously reported methods.

Design and synthesis of cleavable yet clickable prodrugs of paclitaxel (PCTX) and zosuquidar (ZSQ)

Paclitaxel (PCTX) is the member of world health organization's most essential medicines. It has been FDA approved for the treatment of breast, ovarian, lung, bladder, prostate, melanoma, esophageal, as well as other types of solid tumors. It has also used for the treatment of Kaposi's sarcoma[30]. PCTX exerts its cytotoxic effect by binding to tubulin thereby preventing its depolymerization. This, in turn, leads to arresting the cell division at the G2/M phase and finally apoptotic cell death[31]. Although PCTX and its many reported derivatives have had a significant impact in the treatment of cancer, the efficacy of traditional PCTX formulations has been limited due to low aqueous solubility, eventually acquired chemoresistance, and many

undesired side effects[32]. For example, the efficacy of traditional formulations of PCTX made from cremophor EL, a solvent and excipient material necessary to solubilize PCTX have severe side effects such as hypersensitivity reaction, nephrotoxicity, myelosuppression, and neuropathy[33]. While, nanoformulations that make use of non-toxic surfactants like albumin (e.g. Abraxane), or amphiphilic block copolymers (e.g., Genexol-PM)[34] have proven to decrease the side effects and enabled higher PCTX dosing[35]. However, nanoformulations of PCTX were mainly fabricated based on encapsulation methods that yielded heterogeneous PCTX loading and relatively large sizes[36]. One of the major drawbacks of above passively targeted PCTX nanoformulations is the fast systemic release of PCTX and non-specific adsorption on to plasma proteins such as endogenous human serum albumin (HSA), thereby obliterating the controlled drug release[37].

In this regard, covalent attachment of PCTX to a water-soluble polymer or nanoparticles constructs has witnessed significant progress. Grafting onto or post-polymerization and grafting from drug approach has been a promising method to prepare well-defined conjugates[37-38] however lacks selectivity due to an absence of targeting ligand. The mode of action by which these polymer-PCTX conjugate or nanoformulations accumulate at the tumor site is by enhanced permeability and retention (EPR) effect or passive tumor targeting. However, it has been shown through many clinical studies that, therapeutic efficacy obtained through EPR effect is far from optimal and is not universal and varies across different human tumor types. EPR effect for tumors can also lead to accumulation of nanoparticles in liver and spleen, so it is highly unlikely that EPR alone can achieve full selectivity[39].

Zosuquidar (ZSQ), a 10,11-methanobenzosuberane derivative **4**, is extremely potent *in vitro* (K_D = 59 nM) and is among the most active modulators of P-gp-associated multidrug

resistance described to date[40]. It has also demonstrated good *in vivo* activity in preclinical animal studies. In addition, the compound does not appear to be a substrate for P-gp efflux, resulting in a relatively long duration of reversal activity in resistant cells. However, like PCTX, ZSQ possess limited solubility in aqueous solution, such that the formulation concentration is limited, resulting in a large number of vials to contain doses in the potentially efficacious range. To improve its solubility and efficacy various hydroxypropyl and sulfobutyl modified cyclodextrins (a polyanionic β-cyclodextrin derivative) were used in zosuquidar formulations. Although ZSQ is extremely potent, cyclodextrin formulations couldn't impart selectivity to ZSQ due to lack of bio-conjugation strategies to covalently install this molecule on to the suitable targeting agent without losing its potency[40-41].

To address above problems associated with the controlled drug delivery of PCTX and ZSQ and demonstrate the benefits of site-specific dual drug strategy as a proof of concept, FDA approved antineoplastic anticancer agent such as paclitaxel and zosuquidar, a highly potent P-glycoprotein modulator was chosen as dual payloads. We decided to design and synthesized cleavable yet clickable prodrugs of PCTX (**8**) and ZSQ (**12** and **13**) that in turn can be covalently linked to anti-CD22 antibody tethered with C-5 azide or tetrazine modified sialic acids shown in figure 3.1 and 3.2 through sequential SPAAC and inverse electron demand Diels-Alder reaction. To our surprise, site-specific dual-drug conjugation of compounds **8**, **12** or **8**, **13** to the complex biantennary N-linked glycans of anti-CD22 antibody in equal ratios has dramatically enhanced the aqueous solubility, selectivity, and efficacy of PCTX and ZSQ derivatives when tested against CD22 and P-gp overexpressing wild-type and multidrug-resistant (MDR) namalwa cells.

Synthesis of esterase cleavable and clickable prodrug of PCTX (8)

Our synthetic strategy has been depicted in Scheme 3.1. First, the most reactive C2' hydroxy group of was directly esterified by reaction with succinic anhydride to create PCTX derivative **5** with carboxylic acid[42]. Next, (1*R*, 8S, 9r)-Bicyclonon-4-yn-9-ylmethyl (4-nitrophenyl) carbonate (**6**)[43] was reacted with an excess of tris (ethylene glycol)-1,8-diamine in presence of triethylamine as a base to selectively modify the first amine in 3 h. A bifunctional linker **7** terminated with *endo*-bicyclononyne (BCN) on one end and free amine on other end was efficiently coupled with the carboxylic acid of PCTX derivative **5** under standard amide coupling conditions to furnish final compound **8** in excellent yields. Compound **8** were efficiently ligated to bottom arm C-5 azido sialic acid of complex biantennary N-linked glycans of anti-CD22 antibody through SPAAC in quantitative yields with a drug to antibody ratio ≈2.

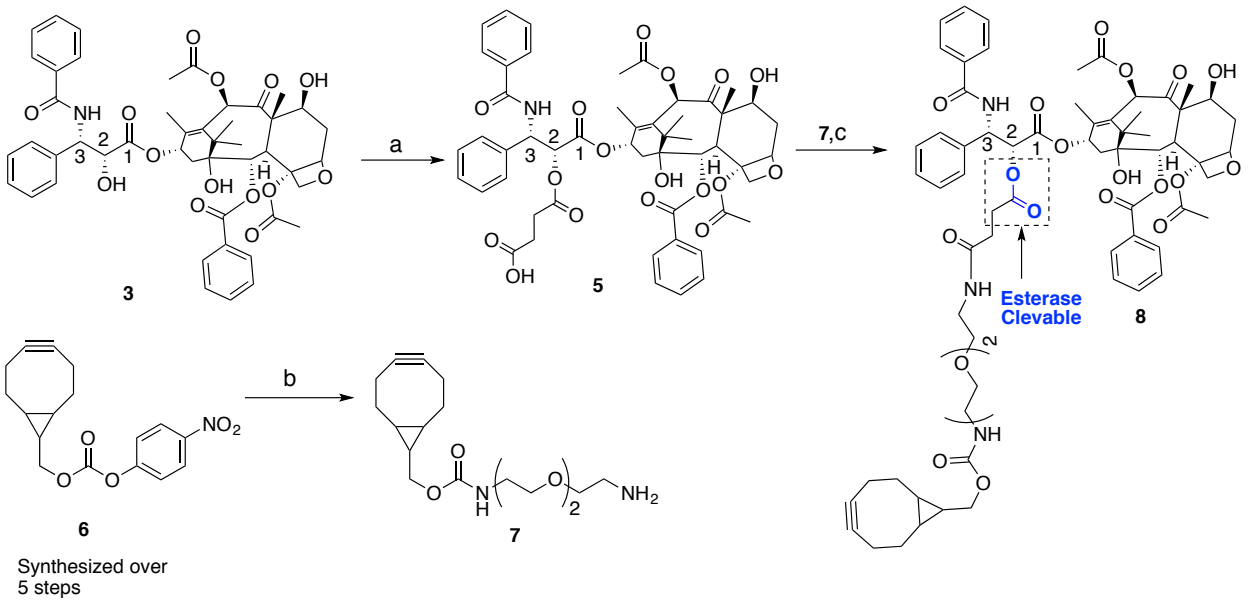

Scheme 3.1 Synthesis of esterase cleavable and clickable PCTX prodrug

Reagents and conditions: a) succinic anhydride, pyridine, 3 h, RT 92%; b) tris (ethylene glycol)-1,8-diamine, triethylamine, CH_2Cl_2, 3 h, RT 95%; c) **7**, HATU, DIPEA, DMF, 24 h, RT 90%.

Synthesis of glutathione (GSH) cleavable and clickable analogs of ZSQ (12 and 13)

Zosuquidar (ZSQ), a 10,11-methanobenzosuberane derivative (**4**) has a free hydroxyl group that can be esterified to introduce cleavable or non-cleavable linker for post-functionalization. However, according to structure activity relationship (Figure 3.3) studies and x-ray crystal structure of interaction between compound **4** with P-glycoprotein receptor (P-gp efflux pump) showed that the free hydroxyl is extremely important for H-bond interaction with A985 residue in the binding pocket of P-gp for its biological activity[44]. Therefore, we designed prodrug **12** or **13** of compound **4** that (Scheme 3.2) can undergo glutathione[45] mediated self-immolation to release active drug containing free hydroxyl group important for its biological activity.

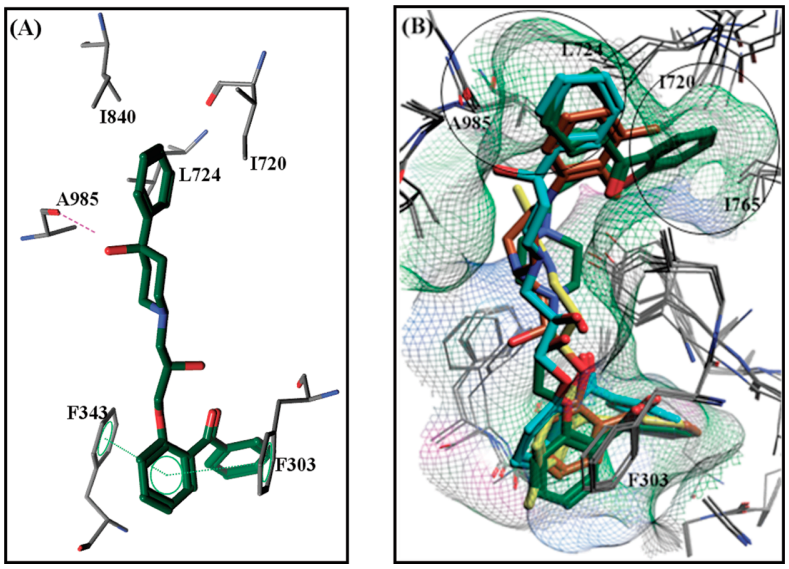

Figure 3.3 X-ray crystal structure representing interaction between zosuquidar and p-glycoprotein

To access desired compound **12** or **13**, the amine of glutathione sensitive portion of a target molecule such as 3-[(2-aminoethyl) dithio] propionic acid was first protected with trityl protecting group. Next, compound **10** was esterified with **4** using EDC as a carbodiimide

coupling agent and triethylamine as a base at room temperature giving beige solid in an excellent yield of 80%. The trityl-protecting group from compound **11** was then removed efficiently by reaction with 2% of TFA and TIPS as a scavenger in dichloromethane for 30 min at room temperature. The resulting amino-TFA salt compound **11** was used directly for next step without any further purification. In the final step, the amino-TFA salt of compound **11** was reacted with p-nitrophenyl carbonate activated clickable groups such as BCN or trans cyclooctene (TCO) in DMF at room temperature for 24 h resulting in target compound **12** and **13** in excellent yields of 90 and 85% yield after column purification. Compound **12** and **13** were ligated to top arm C-5 azido or tetrazine sialic acid of complex biantennary N-linked glycans of anti-CD22 antibody through SPAAC or inverse electron demand Diels-Alder reaction in quantitative yields with a drug to antibody ratio of ≈2.

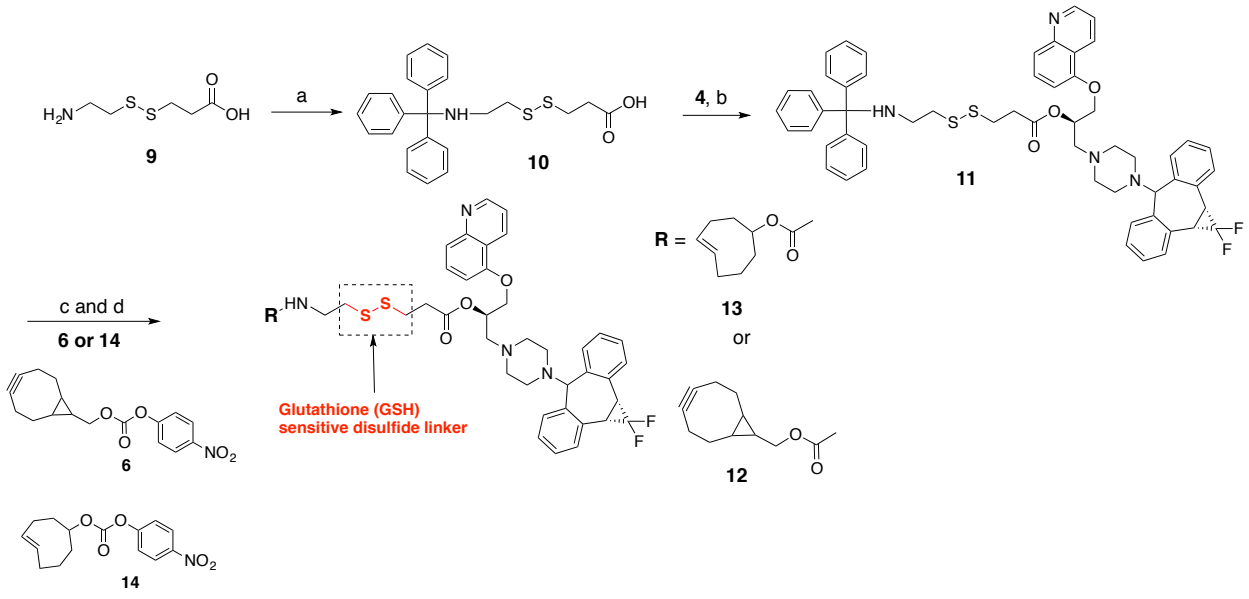

Scheme 3.2 Synthesis of glutathione (GSH) cleavable and clickable analogs of ZSQ

Reagents and conditions: a) trityl chloride, triethyamine in DMF at RT overnight, 85%; b) compound **4**, **10**, N-(3-Dimethylaminopropyl)-N′-ethylcarbodiimide hydrochloride (EDC), catalytic amount of dimethyl amino pyridine (DMAP), triethylamine in CH_2Cl_2 at RT overnight,

80%; c) 2% trifluoroacetic acid (TFA), 2% triisopropylsilane (TIPS) in CH_2Cl_2 at RT for 30 min, 95%; d) **6** or **14**, DIPEA in DMF at RT 24 h, 90% and 85% respectively.

***In vitro* cytotoxicity of PCTX conjugated ADC against wild-type lymphoma cells**

A sialoglycoprotein cell surface receptor such as CD22 is highly overexpressed in patients suffering from B-cell lymphoma. It is a well-characterized clinical target for designing ADCs due to its unique ability to undergoes constitutive endocytosis[5, 46]. To validate our orthogonal glycoengineering strategy, first, the cytotoxicity profile of PCTX derivative such as **8** or anti-CD22 conjugated **8** was determined against CD22 overexpressing namalwa wild-type cells using MTT assay. Namalwa cells were incubated with various concentration of compound **8** or anti-CD22 conjugated PCTX derivative **8** for 72 h.

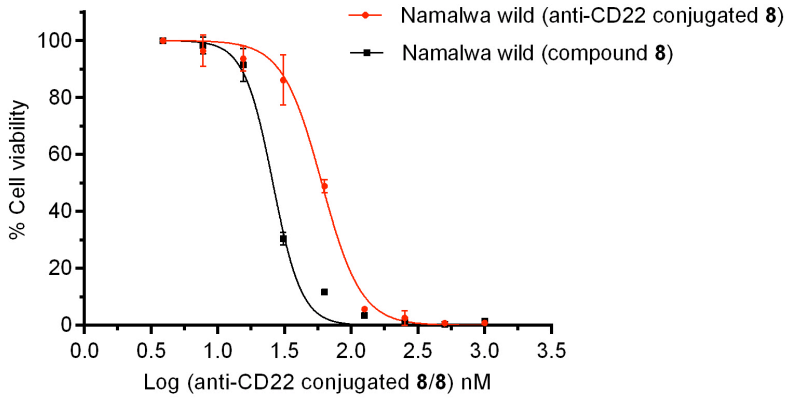

Figure 3.4 *In vitro* cytotoxicity profiles of compound **8** and anti-CD22 conjugated PCTX **8** against CD22 overexpressing namalwa wild-type cells. Data were fitted with prism nonlinear regression software.

As shown in Figure 3.4, compound **8** is approximately 2 times more potent than anti-CD22 conjugated PCTX since compound **8** is non-selective and highly cell permeable with EC_{50} values 27 and 56 nM respectively. It is important to note that, FDA approved nanoformulations such as Abraxane and Genexol-PM[38b] requires high % of PCTX encapsulation (21 to 35%) to achieve

EC_{50} values in 50 to 65 nM against the cancer cells. Surprisingly, above results demonstrated the superiority of our ADC approach where similar potency can be achieved with a drug to antibody ratio of 2. This demonstrates that covalent attachment of PCTX to anti-CD22 through the C2' hydroxy group (crucial for its biological activity) doesn't affect the activity of PCTX significantly.

***In vitro* cytotoxicity of dual-drug ADCs against multidrug-resistant namalwa cells**

It has been well established for many ADC payloads that conjugation often led to decreased potency compared to the parent free drug[47]. This is extremely critical when cancer patients stop responding to the treatment of various chemotherapeutic drugs due to an emergence of multidrug resistance associated with overexpression of MDR1 or P-glycoprotein (P-gp) transporter and are found to be a common mechanism of resistance in the majority of the cancers types. Especially many ADC drugs including PCTX were very good substrates of P-gp transporter resulting in poor ADC activity in MDR1 overexpressing cells[9].

To validate this phenomenon we first determined the cytotoxicity profiles of compound **8** and anti-CD22 conjugated **8** against multidrug-resistant (MDR+ve) namalwa cell line that has overexpression of P-gp and CD22 respectively. As expected from figure 3.5, compound **8** and its anti-CD22 conjugated form showed complete loss of activity with EC_{50} >1000 nM against multidrug resistant namalwa cell line. These results indicate that both compound **8** and its targeted anti-CD22 conjugate suffer from P-gp associated efflux mechanism and were good substrates for P-gp associated multidrug resistance and hence considered as a useful control for monitoring the activity of P-gp transporter.

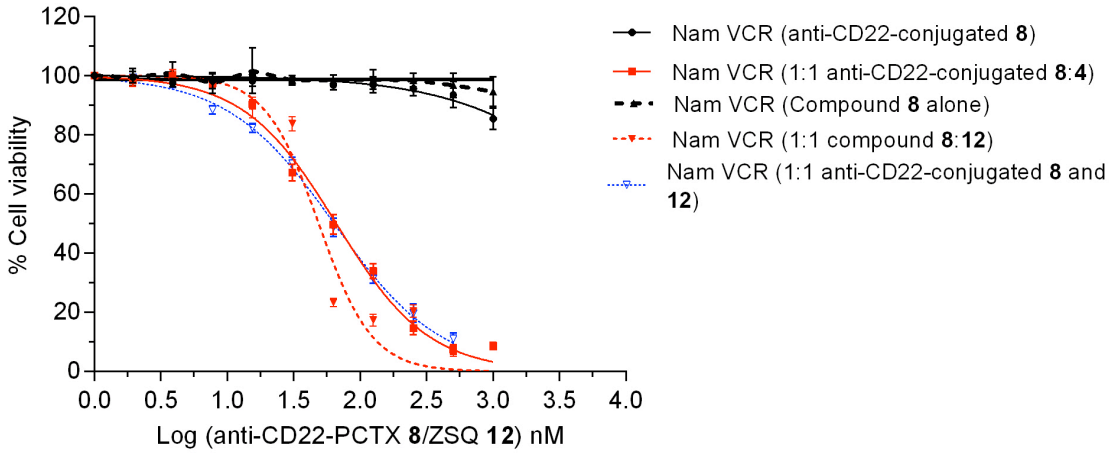

Figure 3.5 *In vitro* cytotoxicity of dual-drug ADCs; compound **8** alone or anti-CD22 conjugated **8** were used as a control with EC_{50}>1000 nM against MDR+ve namalwa cells. Dual-drugs such as compound **8**, **4** and **12** were added in equal concentrations (1:1) alone or in anti-CD22 conjugated form to study the multidrug resistance reversal effects. EC_{50} values for dual-drug ADCs were represented in nM of compound **8** and **12**. Data were fitted with prism nonlinear regression software.

To demonstrate a proof of principal and the benefits of dual-drug ADC platform first compound **8** was added in combination with **4** or **12** in 1:1 ratio to MDR+ve namalwa cells to mimic the concentrations of dual-drugs when they will be covalently linked in a sequential manner to biantennary N-glycans of anti-CD22 antibody. It is interesting to note that the addition of two payloads in free or prodrug form (figure 3.5) can not only completely retains the activity of PCTX derivatives in a dose-dependent manner but also effectively reverses the p-gp associated multidrug resistance. From these initial promising results prodrugs such as **8** and **12** were covalently linked to the anti-CD22 in 1:1 ratio through sequential glycoengineering and SPAAC chemistry.

No.	Compounds/anti-CD22 conjugates	EC_{50} in nM
1)	Compound **8** alone or anti-CD22 conjugated **8**	>1000
2)	1:1 ratio of anti-CD22 conjugated **8** and **4**	66
3)	1:1 ratio of compound **8** and **12**	48
4)	1:1 ratio of anti-CD22 conjugated **8** and **12**	63

Table 2 *In vitro* activity of various dual-drug combinations in free or prodrug or anti-CD22 conjugated form against MDR namalwa cells.

As shown in figure 3.5 and table 2 the covalently linked dual-drug ADC showed comparable synergistic activity as compared to its free drug or prodrug cocktail (Table 2) and can completely re-sensitize cancer cells to the dose-dependent cytotoxic effects of PCTX. Thus, the above unique dual-drug cocktail upon covalent attachment to the anti-CD22 antibody can undergo receptor-mediated endocytosis, followed by subsequent processing in endosomal/lysosomal vesicles, where esterases such as cathepsin B can transform an inactive prodrug **8** into parent drug molecule of PCTX[38b, 48]. At the same time, GSH sensitive ZSQ such as **12** after lysosomal processing can be released into the cytoplasm and can undergo glutathione-mediated self-immolation[45] releasing an active P-gp modulator. This in turns blocks the P-glycoprotein receptor allowing the released PCTX to reach its subcellular target such as microtubule and exert its cytotoxic effect. Dual-drug ADCs prepared using site-specific conjugation method are active *in vitro;* drug insensitivity to MDR can be overcome by attaching a complementary payload.

Conclusion

We have demonstrated that orthogonal glycoengineering strategy developed using ST6GalI enzyme is uniquely suited for constructing homogeneous dual-drug ADCs with DAR of 4. The stepwise modification method allows the sequential introduction of reactive functional groups such as azido/tetrazine modified sialic acids into complex biantennary N-glycans that in turn facilitate site-specific conjugation of dual fluorophores or payloads in equal ratio through SPAAC and inverse electron demand Diels-Alder reaction. These reactions are highly selective and bioorthogonal making above dual labeling technology broadly applicable to a variety of antibodies without the need of recombinant technologies and genetic engineering for site-specific conjugation. We envisaged that the above orthogonal glycoengineering platform could greatly facilitate rapid screening of antibody and new payload-linker libraries to identify novel dual-drug cocktails that take advantage of synergism between two payloads to enhance the activity of next-generation ADCs. We have shown proof of principal illustrating that dual-drug ADC composed of FDA approved antineoplastic anticancer agent such as paclitaxel and zosuquidar, a highly potent P-glycoprotein modulator currently under phase-III clinical trials showed superior anti-cancer activities, selectivity and can bypass P-glycoprotein associated multidrug resistance in lymphoma cancer cells. This work highlights the potential of the new class of targeted therapeutics where dual-drug ADC showed robust cell-killing response against cell types that are completely resistant to treatment of single drug ADCs.

Experimental section

General reagents and materials

Succinic anhydride pyridine, tris (ethylene glycol)-1,8-diamine, triethylamine, 1-[Bis(dimethylamino)methylene]-1H-1,2,3-triazolo[4,5-b]pyridinium 3-oxid hexafluorophosphate (HATU), *N,N*-diisopropylethylamine (DIPEA), trityl chloride, N-(3-Dimethylaminopropyl)-N′-ethylcarbodiimide hydrochloride (EDC), dimethylamino pyridine (DMAP), *N*-azidoacetyl-D-mannosamine, sodium pyruvate, sodium L-ascorbate, copper sulfate, TBTA ligand, trifluoroacetic acid (TFA), and triisopropylsilane (TIPS) were purchased from Sigma Aldrich. Paclitaxel and zosuquidar were purchased from LC laboratory and Apex Biotechnology Inc. Neu5Ac was purchased from Carbosynth LLC. Dichloromethane (DCM) was freshly distilled under a nitrogen atmosphere. Other organic solvents were purchased anhydrous and used without further purification. Unless otherwise noted, all reactions were carried out at room temperature (RT) in oven-dried glassware with magnetic stirring. Organic solutions were concentrated under reduced pressure with bath temperatures < 40^{o}C. Flash column chromatography was carried out on silica gel G60 (Silicycle, 60-200 μm, 60 Å). Thin-layer chromatography (TLC) was carried out on Silica gel 60 F254 (EMD Chemicals Inc.) with detection by UV absorption (254 nm) where applicable, and by spraying with 20% sulfuric acid in ethanol followed by charring at ~150^{o}C or by spraying with a solution of $(NH_4)_6Mo_7O_{24}.H_2O$ (25 g L-1) in 10% sulfuric acid in ethanol followed by charring at ~150^{o}C.

General methods for compound characterization

^{1}H and ^{13}C NMR spectra were recorded on a Varian Inova-300 (300/75 MHz), a Varian Inova-500 (500 MHz) and a Varian Inova-600 (600/150 MHz) spectrometer equipped with sun workstations. Multiplicities are quoted as singlet (s), doublet (d), doublet of doublets (dd), triplet

(t) or multiplet (m). NMR signals were assigned on the basis of 1H NMR, 13C NMR, gCOSY and gHSQC experiments. Chemical shifts are quoted on the δ-scale in parts per million (ppm). Residual solvent signals were used as an internal reference. Mass spectra were recorded on an Applied Biosystems 5800 MALDI-TOF or Shimadzu LCMS-IT-TOF mass spectrometer. The matrix used was 2,5-dihydroxy benzoic acid (DHB). Fluorescent spectroscopy was carried on a BMG Labtech POLAR star optima.

Biochemical reagents

CD22 antibody (HD239) was purchased from Santa Cruz. Biotechnology, Inc. Peptide N-glycosidase F was purchased from New England BioLabs. Cytidine-5'-(5-acetamido-9-azido-3,5,9-tri-deoxy-β-D-glycero-D-galacto-2-nonulopyranosylonic acid monophosphate) (CMP-Neu5Ac9N3) and recombinant rat α-(2,6)-sialyltransferase (ST6Gal I) were prepared by reported procedures. Sialic acid aldolase, CMP-sialic acid synthetase, and calf intestine alkaline phosphatase were purchased from Sigma Aldrich. Alexa Fluor 488 and BODIPY-TMR-C5 578/591 were purchased from life technologies.

Release of N-linked glycans[1]

An aliquot of an IgG antibody was dried by Speed Vac (Savant SC 110) and re-dissolved in an ammonium bicarbonate buffer (50 mM, pH 8.4) and heated at 100°C for 5 min to denature the glycoprotein. After cooling the mixture to RT, trypsin (trypsin/IgG = 1/30, w/w) was added and the solution was incubated at 37^{o}C for 22 h, after which it was heated to 100^{o}C for 5 min to deactivate trypsin. The solution was passed through a C18 reversed phase cartridge, washed with 5% aqueous acetic acid and eluted with a gradient of 2-propanol/5% acetic acid (20-100%) to give glycopeptides. Next, peptide N-glycosidase F (PNGase F, IgG/PNGase F = 1 mg/6 IUB milliunit) was added, and the resulting reaction mixture was incubated at 37^{o}C for 18 h to release

the N-linked glycans. The mixture was passed through a C18 reversed phase cartridge and the glycans were eluted with 5% aqueous acetic acid. The glycan-containing fractions were concentrated by lyophilization.

Glycan analysis by matrix-assisted laser-desorption ionization time-of-flight mass spectrometry (MALDI/TOF-MS) and ESI

The released N-glycans were permethylated with NaOH and methyl iodide following the procedure reported by Anamula and Tayler.[2] The permethylated glycans were analyzed by ESI or MALDI/TOF MS using 2,3-dihydroxybenzoic acid (DHBA, 20 mg mL^{-1} solution in 50% methanol in water) as the matrix. The spectra were acquired in the reflector positive ion mode.

Remodeling of the glycans anti-CD22 IgG antibodies[3]

The anti-CD22 antibody was dialyzed for 18 h against water and then lyophilized. The antibody was resuspended in MOPS buffer (50 mM, pH 7.2) containing $MnCl_2$ (20 mM). The galactosylation of the N-glycans was performed using UDP-galactose (10 mM), BSA (80 μg mL^{-1}), calf intestine alkaline phosphatase (85 U mL^{-1}) and bovine β-1,4-galactosyltransferase (100mU mL^{-1}) at a final concentration of 30 mg mL^{-1} IgG. The resulting reaction mixture was incubated at 37°C for 24 h. To ensure complete galactosylation, an additional aliquot of UDP galactose (4 mg) and galactosyltransferase (7 mU) were added and the reaction mixture was incubated at 37 °C for an additional 24 h. Galactosylated IgG was purified using a Protein A Sepharose Column (GE Healthcare) using a Tri-HCl buffer (50 mM, pH 7.05) for capture and washing, and a glycine buffer (100 mM, pH 3.0) for release. The antibody-containing solution S3 was exchanged to cacodylate buffer (50 mM pH 7.6) using an Amicon 10 kDa cutoff spin concentrator (Millipore). The monosialylation of the anti-CD22 antibody (final concentration of 14 mg mL^{-1}) was conducted in cacodylate buffer (50 mM, pH 7.6), CMP-Neu5Ac5N_3 (4 mM),

BSA (80 μg mL^{-1}), calf intestine alkaline phosphatase (85 U mL^{-1}) and GFP-ST6Gal I (1.5 mg mL^{-1}) at 37 °C for 24 h. The antibody was purified by Protein A Sepharose column chromatography and compound **8** was conjugated to the anti-CD22 antibody through SPAAC in cacodylate buffer, pH 7.6 in 24 h at RT. To achieve full sialylation, the reaction mixture was concentrated using an Amicon 10 kDa cutoff spin concentrator and the proteins were redissolved in 50 mM cacodylate (pH 7.6) and ST6GalI and CMP-Neu5Ac5N_3 were added. The exchange process was repeated twice to give a highly bis-sialylated anti-CD22 IgG as demonstrated by MALDI-TOF MS analysis of the released N-glycan. The second payload such as compound **12** was then added in cacodylate buffer, at pH 7.6 to bis-sialylated antibody and conjugated to top arm azido-sialic acid through SPAAC chemistry. The excess drug in both the conjugation steps was removed by Amicon 10 kDa cutoff spin filtration.

Quantitation of the Neu5Ac and Neu5Ac5N_3 content of the anti-CD22 antibodies

The Sialic acid content of the antibody preparations was determined by high-pH anion-exchange chromatography (HPAEC) using an ICS-3000 Ion Chromatography System (Dionex, Sunnyvale, CA, USA) using 100 mM NaOH and 8%-20% gradient of 1 M sodium acetate in 100 mM NaOH in 20 min. The system consists of a SP gradient pump with an AS auto-sampler, ICS-3000 thermal compartment, and an ICS-3000 electrochemical detector equipped with an amperometry cell. The cell consists of a gold electrode, a combination reference electrode of glass and Ag/AgCl (3 M KCl) and titanium counter electrode consisting of the cell body. Separation was carried out on a CarboPac PA 20 column set consisting of an amino trap column (30 mm Å~ 3 mm I.D.) and an analytic column (150 mm Å~ 3 mm I.D.) The column and the electrochemical detection cell were placed inside the ICS-3000 thermal compartment for temperature control. The chromatographic system control, data acquisition, and analysis were

carried out using Chromeleon Software (Dionex). Sample preparation: 0.2-0.8 mg of anti-CD22 or remodeled anti-CD22 antibody and the standards Neu5Ac and $Neu5Ac5N_3$ were treated with 2 M acetic acid in water (400 μL) at 80^{o}C for 3 h. The samples and standards were dried by spin-vacuo centrifugation and redissolved in water. The content of Neu5Ac and $Neu5Ac5N_3$ in the samples was determined based on the calibration curves of the corresponding standards.

One-pot two-enzyme system approach for synthesis of compound (1)[4]

Sialic acid aldolase (0.2U/μL, 5μL), and CMP-sialic acid synthetase (0.2U/μL, 5μL) were added to a mixture of *N*-azidoacetyl-D-mannosamine (5 mg, 0.019 mmol) in tris-HCl buffer (100mM, pH 8.9, 20mM $MgCl_2$, 1.9 mL), containing sodium pyruvate (10.5 mg, 0.095 mmol) and CTP (10 mg, 0.019 mmol). The tube was incubated at 37 ^oC, and progress of the reaction was monitored by TLC (EtOH : aq. NH_4HCO_3 (1 M) 7:3, v:v), which after 5 hour indicated completion of the reaction. EtOH (3 mL) was added, and the precipitate was removed by centrifugation and the supernatant was concentrated under reduced pressure. The residue was redissolved in distilled water (500 μL) followed by lyophilization to provide a crude material that was applied to a Biogel fine P-2 column (50* 1 cm, eluted with 0.1 M NH_4HCO_3 at 4 ^oC in dark.). TLC detected the product, and appropriate fractions were combined and lyophilized to provide **1** as an amorphous white solid (10.1 mg, 81%).

^1H NMR (500 MHz, D_2O) δ 7.86 (d, *J* = 7.6 Hz, 1H, H-6, cyt), 6.02 (d, *J* = 7.5 Hz, 1H, H-5, cyt), 5.88 (d, *J* = 4.5 Hz, 1H, H-1, rib), 4.27 – 4.19 (m, 2H, H-2 + H-3, rib), 4.12 (dd, *J* = 9.1, 7.6 Hz, 4H), 4.08 – 3.97 (m, 3H, H-4 + N_3CH_2CO), 3.92 (t, *J* = 10.3 Hz, 1H), 3.83 (ddd, *J* = 9.4, 6.5, 2.6 Hz, 1H), 3.78 (dd, *J* = 11.8, 2.5 Hz, 1H), 3.52 (dd, *J* = 11.9, 6.6 Hz, 1H), 3.34 (dd, *J* = 9.6, 1.2 Hz, 1H), 2.40 (dd, *J* = 13.2, 4.8 Hz, 1H, H-3eq), 1.55 (ddd, *J* = 13.3, 11.3, 5.8 Hz, 1H, H-3ax). HRMS (ESI): m/z calcd for $C_{20}H_{30}N_7O_{16}P$ $[M-H]^-$: 654.1414; found: 654.2023.

Synthesis of Tetrazine-CMP-Neu5triazole (2)

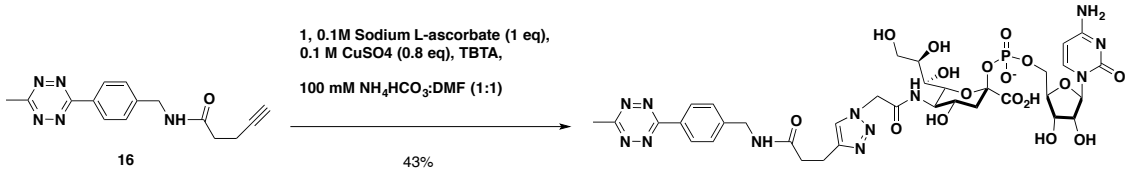

A solution of (4.7 mg, 0.017 mmol) in DMF (1.5 mL) was added to the solution of CMP-Neu5N_3 (**1**, 10 mg, 0.015 mmol) in Tris-HCl buffer (100 mM, pH 7.5, 1.5 mL). To this mixture was added $CuSO_4$ (100 mM, 123 µL), sodium L-ascorbate (100 mM, 153 µL) and TBTA (1.6 mg, 0.0031 mmol). After stirring for 1 hour at ambient temperature, the reaction mixture was lyophilized to provide a residue that was applied to a C18 column, which was eluted with a gradient of methanol in 0.1 M NH_4HCO_3 buffer (3% →20%). Fractions containing product were concentrated under reduced pressure, and the residue was redissolved in 1 mL water and lyophilized to provide **2** (6.1 mg, 43%) as a purple solid. ^{1}H NMR (600 MHz, d_2o) δ 8.43 (d, *J* = 7.9 Hz, 2H, PhH), 8.16 (dd, *J* = 18.3, 7.4 Hz, 1H, H-6, cyt), 7.89 (d, *J* = 8.1 Hz, 1H, CH=C, triazole), 7.48 (dd, *J* = 8.2, 6.2 Hz, 2H, PhH), 6.30 (m, 1H, H-5, cyt), 6.11 – 6.02 (m, 1H, H-1, rib), 5.33 (t, *J* = 4.7 Hz, 2H, triazole-CH_2-C=O), 4.53 (s, 2H, NH-CH_2-Ph), 4.42 (dt, *J* = 12.0, 3.0 Hz, 2H, H-2,3 rib), 4.38 – 4.26 (m, 4H, H-4, 5 rib, H-6), 4.26 – 4.15 (m, 1H, H-4), 4.08 (t, *J* = 10.3 Hz, 1H, H-5), 4.05 – 3.98 (m, 1H, H-8), 3.95 (dd, *J* = 11.6, 2.2 Hz, 1H, H-9a), 3.73 – 3.65 (m, 1H, H-9b), 3.54 (d, *J* = 9.1 Hz, 1H, H-7), 3.16 (m, 5H, O=CCH_2CH_2-triazole, CH_3), 2.82 (t, *J* = 6.4 Hz, 2H, O=CC$H_2$$CH_2$-triazole), 2.58 (d, *J* = 12.5 Hz, 1H, H-3eq), 1.74 (s, 1H, H-3ax). ^{13}C NMR (151 MHz, d_2o) δ 142.7, 128.6, 128.0, 126.8, 89.3, 83.1, 74.2, 71.5, 69.6, 69.2, 68.8, 66.6, 64.7, 62.9, 62.9, 52.1, 52.0, 42.6, 41.0, 41.0, 35.7, 21.1, 20.0. HRMS (ESI): m/z calcd for $C_{35}H_{44}N_{12}O_{17}P$ $[M-H]^-$: 935.2690; found m/z: 935.2063.

Synthetic procedures for compound 8

4-(((1*S*,2*R*)-1-benzamido-3-(((4*S*,4a*S*,6*R*,9*S*,11*S*,12*S*,12a*R*,12b*S*)-6,12b-diacetoxy-12-(benzoyloxy)-4,11-dihydroxy-4a,8,13,13-tetramethyl-5-oxo-2a,3,4,4a,5,6,9,10,11,12,12a,12b-dodecahydro-1*H*-7,11-methanocyclodeca[3,4]benzo[1,2-*b*]oxet-9-yl)oxy)-3-oxo-1-phenylpropan-2-yl)oxy)-4-oxobutanoic acid (5)

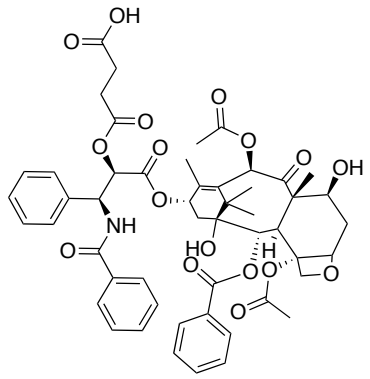

A reaction mixture of **3** (0.05 g, 0.06 mmol) and succinic anhydride (0.076 g, 0.76 mmol) in 1.2 mL pyridine was stirred at room temperature for 3 h. After 3 h, pyridine was evaporated to dryness in vacuo. The residue was then treated with 2 ml of water, stirred for 20 min, and filtered. The obtained precipitate was then dissolved in acetone and water was added slowly, and the fine crystals of product were collected. This yielded 0.048 g (86%) of **5**.

^{1}H NMR (DMSO-d6, 500 MHz): δ 12.25 (br s, 1H), 9.19 (d, 1H), 7.94-8.00 (d, 2H), 7.81-7.85 (d, 2H), 7.70-7.73 (m, 1H), 7.63-7.66 (m, 2H), 7.49-7.56 (m, 1H), 7.45-7.50 (m, 2H), 7.40-7.44 (m, 4H), 7.11-7.21 (m, 1H), 6.27 (s, 1H), 5.76-5.83 (t, 1H), 5.73 (s, 1H), 5.50-5.54 (t, 1H), 5.40 (d, 1H), 5.34 (d, 1H), 4.88-4.90 (d, 2H), 4.61 (s, 1H), 4.08-4.11(m, 1H), 3.97-4.02 (m, 2H), 3.56 (d, 1H), 2.57-2.63 (t, 2H), 2.27-2.37 (m, 1H), 2.22 (s, 3H), 2.09 (s, 3H), 1.76-1.83 (m, 1H), 1.74 (s, 3H), 1.58-1.65 (t, 1H), 1.48 (s, 3H), 1.21 (s, 1H), 0.95-1.00 (d, 6H).

^{13}C NMR 134, 131.9, 130, 129.2, 129.20, 129.09, 128.85, 128.09,127.93, 84.15, 75.76, 75.11, 75, 75.14, 71.41,71,55.34, 54.43,46.51, 40.28, 37.11, 37, 34.86, 34.86, 29.28, 29, 26.74, 23.11, 22.05, 21.16, 14.39, 10.63, 10.33. MALDI HRMS for $C_{51}H_{55}NO_{17}$ m/z [M+Na^{+}] 976.35; found 976.346.

Bicyclo[6.1.0]non-4-yn-9-ylmethyl (4-nitrophenyl) carbonate (6)

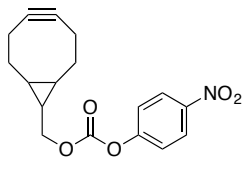

To a solution of ((1*R*, 8S, 9r)-Bicyclo [6.1.0] non-4-yn-9-ylmethanol (100 mg, 0.66 mmol) in CH_2Cl_2 (10 mL) was added pyridine (134.70 µL, 1.66 mmol) and 4-nitrophenyl chloroformate (200 mg, 1 mmol). After stirring for 3 h at room temperature the reaction mixture was quenched with saturated ammonium chloride solution (10 mL) and extracted with CH_2Cl_2 (3×10 mL). The organic layer was dried using $MgSO_4$ and concentrated *in vacuo*. The residue was further purified by column chromatography on silica gel (EtOAc: Hexane, 1:5) to afford desired product **6** (162 mg, 77%) as a white solid.

^{1}H NMR ($CDCl_3$, 500 MHz): δ 8.28 (d, 2H), 7.40 (d, 2H), 4.31(d, 2H), 2.15-2.5 (m, 6H), 1.35-1.45 (m, 2H), 0.64-0.75 (m, 3H). ^{13}C NMR (150 MHz, $CDCl_3$): δ 155.6, 152.5, 145.3, 125.3, 121.7, 98.7, 68.0, 29.0, 21.3, 20.5, 17.2.

((1*R*, 8S, 9r)-Bicyclo [6.1.0] non-4-yn-9-ylmethyl (2-(2-(2-aminoethoxy) ethoxy) ethyl) carbamate (7)

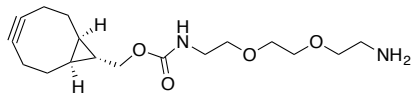

Et_3N (339 µL, 1.945 mmol) was added to stirred solution of **6** (150 mg, 0.389 mmol) and tris (ethylene glycol)-1,8-diamine (569 µL, 3.89 mmol) in CH_2Cl_2 (10 mL). The reaction mixture was stirred for 3 h, after which the solvent was removed under reduced pressure. The residue was purified by flash chromatography over latrobeads ($MeOH/CH_2Cl_2$, 5 to 25%, v/v) to give compound **7** as a light-yellow liquid (116 mg, 92%).

^{1}H NMR ($CDCl_3$, 500 MHz): δ 5.48 (br s, NH), 4.15 (d, 2H), 3.5-3.75 (m, 8H), 3.4 (br s, 2H), 2.9 (br s, 2H), 2.5 (br s, $2NH_2$), 2.16-2.36 (m, 6H), 1.5-1.65 (m, 2H), 1.2-1.44 (m and s, 3H),

0.79-1.00 (m, 2H) ^{13}C NMR (150 MHz, $CDCl_3$): δ 98.8, 73.4, 70.3, 70.2, 70.1, 62.7, 41.7, 40.8, 29.1, 21.4, 20.1, 17.8. MALDI HRMS for $C_{17}H_{28}N_2O_4$ m/z calcd $(M + H)^+$ 325.2124, found: 325.2122.

(4*S*,4a*S*,6*R*,9*S*,11*S*,12*S*,12a*R*,12b*S*)-9-(((19*R*)-19-((*S*)-benzamido(phenyl)methyl)-1-(bicyclo[6.1.0]non-4-yn-9-yl)-3,14,17-trioxo-2,7,10,18-tetraoxa-4,13-diazaicosan-20-oyl)oxy)-12-(benzoyloxy)-4,11-dihydroxy-4a,8,13,13-tetramethyl-5-oxo-3,4,4a,5,6,9,10,11,12,12a-decahydro-1*H*-7,11-methanocyclodeca[3,4]benzo[1,2-*b*]oxete-6,12b(2a*H*)-diyl diacetate (8)

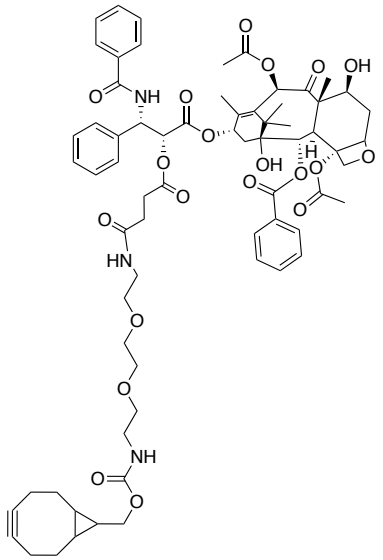

A mixture of **5** (5 mg, 0.0052 mmol) and **7** (2.1 mg, 0.0062 mmol) was dissolved in anhydrous DMF (1 mL). *N, N*-Diisopropylethylamine (2.73 µL, 0.0157 mmol) and 1-[Bis(dimethylamino) Methylene]-1H-1, 2,3-triazolo [4,5-b] pyridinium 3-oxid hexafluorophosphate (HATU, 3mg, and 0.00786 mmol) was added sequentially and reaction mixture was stirred for 2 h at room temperature. TLC showed complete reaction after stirring reaction for 2 h at room temperature. Solvents were evaporated under reduced pressure, and the crude product was purified by silica gel chromatography using EtOAc: Hexane (5 to 15%, v/v) as a mobile phase giving pure **8** as a white solid (6.5 mg, 98%).

^{1}H NMR ($CDCl_3$, 500 MHz): δ 8.15 (d, 1H), 7.83 (d, 1H), 7.63 (t, 1H), 7.52 (dt, 2H), 7.48 – 7.37 (m, 3H), 7.32 (s, 1H), 6.30 (s, 1H), 6.25 – 6.13 (m, 1H), 5.69 (d, 1H), 5.46 (d, 0H), 5.31 (s, 0H), 5.03 – 4.92 (m, 0H), 4.32 (d, 1H), 4.21 (d, 1H), 4.13 (q, 1H), 3.96 (d, 1H), 3.81 (d, 1H), 3.60 (d, 4H), 3.48 (s, 1H), 3.37 (s, 2H), 2.77 (t, 1H), 2.54 (d, 2H), 2.44 (s, 1H), 2.39 (d, 1H), 2.35 – 2.28

(m, 1H), 2.24 (s, 2H), 2.15 (d, 1H), 2.06 (s, 1H), 1.93 (s, 2H), 1.69 (s, 2H), 1.64 (s, 4H), 1.50 (dd, 3H), 1.33 – 1.20 (m, 5H), 1.14 (s, 2H), 0.93 – 0.85 (m, 1H), 0.73 (s, 1H).

^{13}C NMR (150 MHz, $CDCl_3$): δ 130.22, 127.36, 133.70, 128.72, 131.85, 126.78, 129.00, 128.43, 75.61, 71.74, 53.19, 75.08, 74.37, 84.43, 72.10, 76.42, 76.42, 69.23, 45.60, 70.23, 69.77, 39.36, 40.73, 43.72, 29.44, 35.13, 30.76, 22.68, 33.27, 35.47, 21.39, 21.39, 35.48, 14.82, 35.57, 9.62, 23.39, 9.62, 18.63, 17.32, 33.28, 22.68, 31.61, 29.66, 26.80, 22.13, 14.12, 22.87, 23.69. MALDI HRMS for $C_{68}H_{81}N_3O_{20}$ m/z calcd $(M + Na)^+$ 1282.54, found: 1282.534.

Synthetic procedure for compounds 12 and 13

3-((2-(tritylamino)ethyl)disulfaneyl)propanoic acid (10)

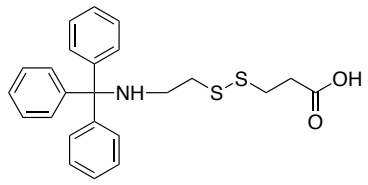

Trityl group protected amino-ethyldithiopropanoic acid linker was prepared by adding trityl chloride (46 mg, 0.165 mmol) to the stirred solution of **9** (10 mg, 0.055 mmol) and triethylamine (16.7 mg, 23 μL, 0.165mmol) in 1 mL dimethylformamide for 24 h at RT. After stirring the reaction mixture overnight, solvent was evaporated under reduced pressure, and the crude product was purified by silica gel chromatography using MeOH: DCM (2 to 5%, v/v) as a gradient column system to give compound **10** as yellow solid (19 mg, 82%).

^{1}H NMR (500 MHz, $CDCl_3$): δ 7.53 – 7.46 (m, 6H), 7.35 – 7.27 (m, 6H), 7.24 – 7.18 (m, 3H), 4.62 (s, 1H), 2.86 (t, 2H), 2.80 – 2.70 (m, 4H), 2.51 (t, 2H). MALDI HRMS for $C_{24}H_{25}NO_2S_2$ m/z calcd $(M + H)^+$ 424.14, found: 424.136.

(2*R*)-1-(4-((1a*R*,10b*S*)-1,1-difluoro-1,1a,6,10b-tetrahydrodibenzo[*a*,*e*]cyclopropa[*c*][7]annulen-6-yl)piperazin-1-yl)-3-(quinolin-5-yloxy)propan-2-yl 3-((2-(tritylamino)ethyl) disulfaneyl) propanoate (11)

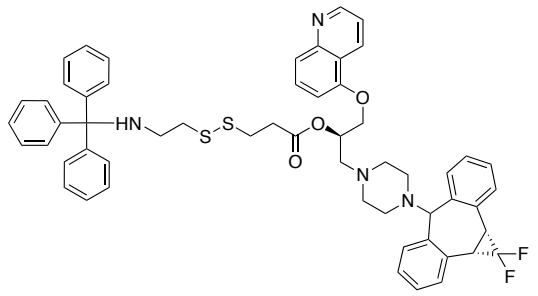

A reaction mixture of **10** (12 mg, 0.0284 mmol), N-(3-Dimethylaminopropyl)-N′ethylcarbodiimide hydrochloride (7.2 mg, 0.0376 mmol), catalytic amount of dimethyl amino pyridine (DMAP), and triethylamine (4.8 mg, 7 µL, 0.047 mmol) was dissolved in 2 ml CH_2Cl_2 and cooled to 0^oC. Compound **4** (5 mg, 0.0094 mmol) was added at 0^oC and reaction mixture was stirred for 24 h at room temperature. After overnight stirring, reaction mixture was diluted with 8 ml CH_2Cl_2 and extracted with brine and saturated sodium bicarbonate (5 ml each) and dried over magnesium sulfate. Solvents were evaporated under reduced pressure and crude product was purified over silica gel chromatography using MeOH: DCM (0 to 3%, v/v) as gradient system to obtained pure compound **11** as beige solid (7 mg, 81%).

^1H NMR (500 MHz, $CDCl_3$): δ 8.90 (dd, 1H), 8.56 – 8.50 (m, 1H), 7.72 (d, 1H), 7.61 (t, 1H), 7.48 (d, 8H), 7.32 – 7.25 (m, 10H), 7.22–7.12 (m, 6H), 6.87 (d, 1H), 5.52 (dd, 1H), 5.32 (s, 1H), 4.35 (dd, 1H), 4.26 (dd, 2H), 4.15 (q, 1H), 3.92 (s, 1H), 3.20 (d, 2H), 2.92 – 2.67 (m, 8H), 2.64 – 2.23 (m, 10H), 2.09 (d, 1H).

^{13}C NMR (150 MHz, $CDCl_3$) δ 150.80, 130.75, 122.08, 129.23, 128.57, 128.57, 120.39, 127.87, 127.88, 132.70, 132.71, 127.94, 126.34, 129.26, 127.56, 105.18, 70.03, 53.43, 68.43, 68.43, 77.96, 28.96, 40.76, 40.38, 33.18, 33.90, 34.24, 58.07, 58.07, 53.69, 54.19, 41.74, 52.25. MALDI HRMS for $C_{56}H_{54}F_2N_4O_3S_2$ m/z calcd $(M + H)^+$ 933.36, found: 933.354.

(2*R*)-1-(4-((1a*R*,10b*S*)-1,1-difluoro-1,1a,6,10b tetrahydrodibenzo[*a*,*e*]cyclopropa[*c*][7]annulen-6-yl)piperazin-1-yl)-3-(quinolin-5 yloxy)propan-2-yl-3-((2-(((bicyclo[6.1.0]non-4-yn-9-ylmethoxy)carbonyl)amino)ethyl)disulfaneyl)propanoate (12)

Compound **11** (5 mg, 0.0053 mmol) was dissolved in 1 ml dichloromethane. 2% TFA and TIPS v/v were added to reaction mixture and stirred for 30 min at room temperature. After 30 min, solvent was evaporated under reduced pressure and resulting amino-TFA salt was used for the next step without purification. Next, amino-TFA salt was added to the reaction mixture containing **6** (2.53 mg, 0.008 mmol), N,N-diisopropylethylamine (2.1 mg, 3 μL, 0.016 mmol) in DMF and stirred for 16 h at room temperature. After stirring for 16 h, solvents were evaporated under reduced pressure and crude product was purified over silica gel column using mobile phase of MeOH: DCM (0 to 2% v/v) yielding compound **13** (4 mg, 89%) in excellent yields.

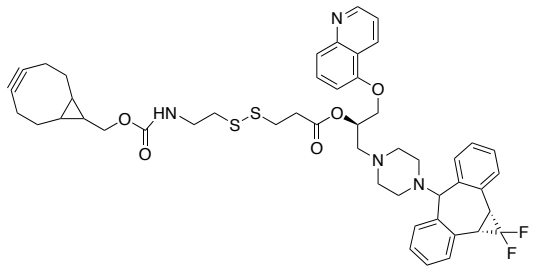

^{1}H NMR (600 MHz, $CDCl_3$): δ 8.90 (dd, 1H), 8.56 – 8.45 (m, 1H), 7.71 (d, 1H), 7.59 (t, 1H), 7.38 (dd, 1H), 7.25 – 7.22 (m, 1H), 7.22 – 7.17 (m, 3H), 7.12 (tdd, 5H), 6.86 (d, 1H), 5.55 (s, 2H), 5.10 (s, 1H), 4.38 – 4.22 (m, 2H), 3.95 (t, 3H), 3.49 – 3.37 (m, 2H), 3.34 (s, 2H), 3.16 (d, 2H), 2.90 (t, 2H), 2.82 – 2.69 (m, 4H), 2.46 – 2.00 (m, 9H), 0.90 – 0.77 (m, 4H), 0.76 – 0.61 (m, 3H). ^{13}C NMR (151 MHz, $CDCl_3$) δ 130.92, 122.03, 129.42, 120.42, 77.11, 132.78, 128.12, 129.65, 127.68, 105.32, 76.87, 68.39, 68.40, 69.25, 70.03, 77.78, 39.58, 39.63, 56.01, 28.94, 33.10, 33.07, 38.31, 34.25, 38.14, 33.37, 33.33, 21.42, 21.41, 21.41, 33.37, 29.35, 31.71, 22.91, 23.69. MALDI HRMS for $C_{48}H_{52}F_2N_4O_5S_2$ m/z calcd $(M + Na)^+$ 889.33, found: 889.32.

(2*R*)-1-(4-((1a*R*,10b*S*)-1,1-difluoro-1,1a,6,10b-tetrahydrodibenzo[*a*,*e*]cyclopropa[*c*][7]annulen-6-yl)piperazin-1-yl)-3-(quinolin-5-yloxy)propan-2-yl3-((2-(((((*E*)-cyclooct-4-en-1-yl)oxy) carbonyl)amino)ethyl)disulfaneyl)propanoate(13)

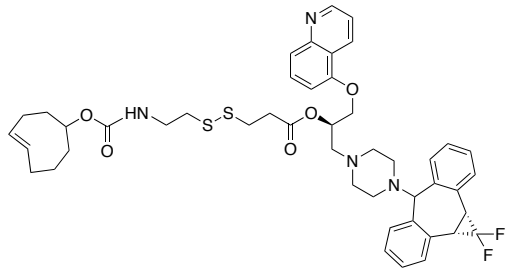

Compound **13** was synthesized using same procedure that was used for synthesizing compound **12**. After deprotection of trityl of compound **11** (5 mg, 0.0053 mmol) in 1 ml dichloromethane, 2% TFA and TIPS v/v over 30 min at RT. Amino-TFA salt was added to the reaction mixture containing **14** (2.32 mg, 0.008 mmol), N,N-diisopropylethylamine (2.1 mg, 3 μL, 0.016 mmol) in DMF and stirred for 16 h at room temperature. After stirring for 16 h, solvents were evaporated under reduced pressure and crude product was purified over silica gel column using mobile phase of MeOH: DCM (0 to 2% v/v) yielding compound **13** (3.8 mg, 86%) in excellent yields.

MALDI HRMS for $C_{46}H_{52}F_2N_4O_5S_2$ m/z calcd $(M + H)^+$ 843.33, found: 843.326.

Biological examination of compounds 3,4, 8, 12 or 13 and anti-CD22 conjugated derivatives

Cell lines and Culture

Multidrug-resistant lymphoma cells lines stably expressing p-gp and CD22 were provided by Dr. Maria-Ana Ghetie, The Cancer Immunobiology Center, UT Southwestern Medical Center at Dallas, 6000 Harry Hines Boulevard, NB9.116, Dallas, TX 75390-8576, USA.

Generation of new MDR cells

Three cell lines (Namalwa, Raji, and DHL-4) were exposed to vincristine (VCR) at a starting concentration of 3 nM. VCR was increased every 10 days by 3 nM increments until cells became resistant to 12-21 nM VCR. The cells were named by the parental cell names and the final concentration of VCR to which they were resistant for example Namalwa 21nM VCR, Raji 18nM VCR, DHL-4 12nM VCR and Namalwa wild-type as a control cell line.

Cell culture conditions

Namalwa 21nM VCR, DHL-4 12nM VCR, Raji 18nM VCR and Namalwa wild type cells were cultured in ATCC-formulated RPMI- 1640 medium with L-glutamine (2 mM), sodium bicarbonate (1.5 g L-1), glucose (4.5 g L^{-1}), HEPES (10 mM) and sodium pyruvate (1.0 mM). The media was supplemented with penicillin (100 U mL^{-1}) and streptomycin (100 μg mL^{-1}, Mediatech) and fetal bovine serum (FBS, 10%, BenchMark). In case of Raji 18 nM VCR 1% Pen/Amp/Strep and 1100 μL Normocin (50 μg/ml) will be added. Cells were maintained in a humid 5% CO_2 atmosphere at 37^{o}C and subcultured every 2-3 days.

Cytotoxicity assay

Cytotoxicity of compounds **3, 4, 8, 12, 13** or anti-CD22 antibody modified with **8** and **12** or **13** was determined using the MTT assay. On the day of exposure, exponentially growing cells were plated at 25000 cells/well in 160 μL in 96-well tissue culture plates (Nunc). Cells then were

incubated with medium (control), compound **3** or **8** or anti-CD22 modified **8** (20 μL, 10X in cell culture medium) for 30 min at 37° C. Next, compound **4**, or **12** or **13** or anti-CD22 modified **12** (20 μL, 10X in cell culture medium) were added and cells were incubated for 68 h. At 68 h, MTT reagent (5 mg mL^{-1} in PBS, 20 μL/well) was added to each well. Incubate the plate for 4 hours at 37° C. View the cells periodically for the Appearance of punctate, intracellular precipitate using an inverted microscope. When purple precipitate is clearly visible under the microscope, the plate was centrifuged at 1400 rpm for 10 min at 4°C and supernatant were removed carefully (with a syringe). At 72 h the water-insoluble formazan salt was dissolved in DMSO (100 μL/well). The absorbance was measured at 545 nm using a microplate reader (BMG Labtech). Data points were collected in triplicate and expressed as normalized values for untreated control cells (100%). Data were fitted using Prism software (GraphPad Software, Inc).

A

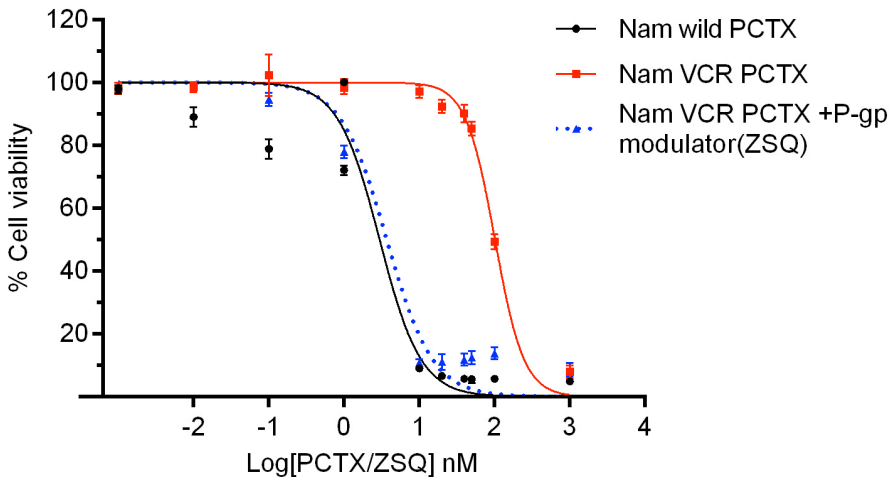

B

No.	Compound used alone or in 1:1 ratio	Cell lines	EC_{50} value in nM
1)	PCTX	Namalwa MDR (+) ve	101.3
2)	PCTX	Namalwa wild	5
3)	PCTX and ZSQ (1:1)	Namalwa MDR (+) ve	5.5
4)	ZSQ	Namalwa MDR and wild	No activity

Figure 3.6 *In vitro* cytotoxicity profiles (A) of PCTX and ZSQ when used alone or in 1:1 combination against Namalwa wild and MDR +ve (VCR) cell lines; (B) EC_{50} value comparison between PCTX and ZSQ when used alone or in 1:1 ratio.

References for supplementary information

[1] H. H. Freeze, C. Kranz. *Curr. Protoc. Immunol.* **2010**, *89*, 12.41.-12.14.25.

[2] K.R. Anumula, P.B. Taylor *Anal. Biochem.,* **1992**, *203*, 101-108.

[3] S. T. Jung. *Biotechnol. Bioprocess Eng.* **2013**, *18*, 625-636.

[4] H. Yu, H. A. Chokhawala, S. Huang, X. Chen, *Nat. Protoc.* **2006**, *1*, 2485–2492.

[5] I. Pop, L. Pop, E.S. Vitetta, M.A. Ghetie. *Oncology Reports.* **2008,** *19 (4),* 889-895.

References

[1] a) J. R. Adair, P. W. Howard, J. A. Hartley, D. G. Williams and K. A. Chester, *Expert Opinion on Biological Therapy* **2012**, *12*, 1191-1206; b) R. V. J. Chari, M. L. Miller and W. C. Widdison, *Angewandte Chemie International Edition* **2014**, *53*, 3796-3827; c) U. Iyer and V. J. Kadambi, *Journal of Pharmacological and Toxicological Methods* **2011**, *64*, 207-212.

[2] a) P. D. Senter and E. L. Sievers, *Nat Biotech* **2012**, *30*, 631-637; b) A. Younes , N. L. Bartlett , J. P. Leonard , D. A. Kennedy , C. M. Lynch , E. L. Sievers and A. Forero-Torres *New England Journal of Medicine* **2010**, *363*, 1812-1821.

[3] S. Verma, D. Miles, L. Gianni, I. E. Krop, M. Welslau, J. Baselga, M. Pegram, D.-Y. Oh, V. Diéras, E. Guardino, L. Fang, M. W. Lu, S. Olsen and K. Blackwell, *New England Journal of Medicine* **2012**, *367*, 1783-1791.

[4] M. L. Linenberger, T. Hong, D. Flowers, E. L. Sievers, T. A. Gooley, J. M. Bennett, M. S. Berger, L. H. Leopold, F. R. Appelbaum and I. D. Bernstein, *Blood* **2001**, *98*, 988-994.

[5] J. F. DiJoseph, D. C. Armellino, E. R. Boghaert, K. Khandke, M. M. Dougher, L. Sridharan, A. Kunz, P. R. Hamann, B. Gorovits, C. Udata, J. K. Moran, A. G. Popplewell, S. Stephens, P. Frost and N. K. Damle, *Blood* **2004**, *103*, 1807-1814.

[6] J. M. Lambert and C. Q. Morris, *Advances in Therapy* **2017**, *34*, 1015-1035.

[7] V. Chudasama, A. Maruani and S. Caddick, *Nat Chem* **2016**, *8*, 114-119.

[8] a) P. Agarwal and C. R. Bertozzi, *Bioconjugate Chemistry* **2015**, *26*, 176-192; b) B. E. C. G. de Goeij and J. M. Lambert, *Current Opinion in Immunology* **2016**, *40*, 14-23; c) R. P. Lyon, J. R. Setter, T. D. Bovee, S. O. Doronina, J. H. Hunter, M. E. Anderson, C. L. Balasubramanian, S.

M. Duniho, C. I. Leiske, F. Li and P. D. Senter, *Nat Biotech* **2014**, *32*, 1059-1062; d) P. Polakis, *Pharmacological Reviews* **2016**, *68*, 3-19.

[9] a) T. Kohji, S. Toshiyuki and O. Katsuhiko, *Current Pharmaceutical Design* **2006**, *12*, 273-286; b) G. Szakacs, J. K. Paterson, J. A. Ludwig, C. Booth-Genthe and M. M. Gottesman, *Nat Rev Drug Discov* **2006**, *5*, 219-234; c) T. R. Wilson, D. B. Longley and P. G. Johnston, *Annals of Oncology* **2006**, *17*, x315-x324.

[10] Y. Assef, F. Rubio, G. Coló, S. del Mónaco, M. A. Costas and B. A. Kotsias, *Leukemia Research 33*, 710-716.

[11] a) R. B. Walter, T. A. Gooley, V. H. J. van der Velden, M. R. Loken, J. J. M. van Dongen, D. A. Flowers, I. D. Bernstein and F. R. Appelbaum, *Blood* **2007**, *109*, 4168-4170; b) R. B. Walter, B. W. Raden, T. C. Hong, D. A. Flowers, I. D. Bernstein and M. L. Linenberger, *Blood* **2003**, *102*, 1466-1473.

[12] a) R. Chen, J. Hou, E. Newman, Y. Kim, C. Donohue, X. Liu, S. H. Thomas, S. J. Forman and S. E. Kane, *Molecular Cancer Therapeutics* **2015**, *14*, 1376-1384; b) C. O'Brien, G. Cavet, A. Pandita, X. Hu, L. Haydu, S. Mohan, K. Toy, C. S. Rivers, Z. Modrusan, L. C. Amler and M. R. Lackner, *Cancer Research* **2008**, *68*, 5380-5389.

[13] R. Tang, S. Cohen, J.-Y. Perrot, A.-M. Faussat, C. Zuany-Amorim, Z. Marjanovic, H. Morjani, F. Fava, E. Corre, O. Legrand and J.-P. Marie, *BMC Cancer* **2009**, *9*, 199.

[14] D. L. Toppmeyer, C. A. Slapak, J. Croop and D. W. Kufe, *Biochemical Pharmacology* **1994**, *48*, 609-612.

[15] L. Imamovic and M. O. A. Sommer, *Science Translational Medicine* **2013**, *5*, 204ra132-204ra132.

[16] H. K. Erickson, P. U. Park, W. C. Widdison, Y. V. Kovtun, L. M. Garrett, K. Hoffman, R. J. Lutz, V. S. Goldmacher and W. A. Blättler, *Cancer Research* **2006**, *66*, 4426-4433.

[17] L. Gustav, *Current Drug Targets* **2000**, *1*, 85-99.

[18] a) N. McGranahan and C. Swanton, *Cancer Cell 27*, 15-26; b) C. E. Meacham and S. J. Morrison, *Nature* **2013**, *501*, 328-337.

[19] a) M. A. Fanale, S. M. Horwitz, A. Forero-Torres, N. L. Bartlett, R. H. Advani, B. Pro, R. W. Chen, A. Davies, T. Illidge, D. Huebner, D. A. Kennedy and A. R. Shustov, *Journal of Clinical Oncology* **2014**, *32*, 3137-3143; b) A. Younes, J. M. Connors, S. I. Park, M. Fanale, M. M. O'Meara, N. N. Hunder, D. Huebner and S. M. Ansell, *The Lancet Oncology 14*, 1348-1356.

[20] S. Puthenveetil, S. Musto, F. Loganzo, L. N. Tumey, C. J. O'Donnell and E. Graziani, *Bioconjugate Chemistry* **2016**, *27*, 1030-1039.

[21] A. Maruani, D. A. Richards and V. Chudasama, *Organic & Biomolecular Chemistry* **2016**, *14*, 6165-6178.

[22] A. Maruani, M. E. B. Smith, E. Miranda, K. A. Chester, V. Chudasama and S. Caddick, **2015**, *6*, 6645.

[23] S. Li, H. Cai, J. He, H. Chen, S. Lam, T. Cai, Z. Zhu, S. J. Bark and C. Cai, *Bioconjugate Chemistry* **2016**, *27*, 2315-2322.

[24] M. R. Levengood, X. Zhang, J. H. Hunter, K. K. Emmerton, J. B. Miyamoto, T. S. Lewis and P. D. Senter, *Angewandte Chemie International Edition* **2017**, *56*, 733-737.

[25] X. Li, T. Fang and G.-J. Boons, *Angewandte Chemie International Edition* **2014**, *53*, 7179-7182.

[26] A. W. Barb, L. Meng, Z. Gao, R. W. Johnson, K. W. Moremen and J. H. Prestegard, *Biochemistry* **2012**, *51*, 4618-4626.

[27] M. F. Debets, C. W. J. van der Doelen, F. P. J. T. Rutjes and F. L. van Delft, *ChemBioChem* **2010**, *11*, 1168-1184.

[28] M. R. Karver, R. Weissleder and S. A. Hilderbrand, *Bioconjugate Chemistry* **2011**, *22*, 2263-2270.

[29] D. M. Patterson, L. A. Nazarova and J. A. Prescher, *ACS Chemical Biology* **2014**, *9*, 592-605.

[30] J. Dubois, *Expert Opinion on Therapeutic Patents* **2006**, *16*, 1481-1496.

[31] A. F. Wahl, K. L. Donaldson, C. Faircnild, F. Y. F. Lee, S. A. Foster, G. W. Demers and D. A. Galloway, *Nat Med* **1996**, *2*, 72-79.

[32] R. Panchagnula, *International Journal of Pharmaceutics* **1998**, *172*, 1-15.

[33] a) A. K. Singla, A. Garg and D. Aggarwal, *International Journal of Pharmaceutics* **2002**, *235*, 179-192; b) C. Ta-Chung, C. Zyting, T. Ling-Ming, C. Tzeon-Jye, H. Ruey-Kuen, W. Wei-Shu, Y. Chueh-Chuan, Y. Muh-Hwa, H. Liang-Tsai, L. Jin-Hwang and C. Po-Min, *Investigational New Drugs* **2005**, *23*, 171-177.

[34] a) M. Elsabahy and K. L. Wooley, *Chemical Society Reviews* **2012**, *41*, 2545-2561; b) S. Kasmi, B. Louage, L. Nuhn, A. Van Driessche, J. Van Deun, I. Karalic, M. Risseeuw, S. Van Calenbergh, R. Hoogenboom, R. De Rycke, O. De Wever, W. E. Hennink and B. G. De Geest, *Biomacromolecules* **2016**, *17*, 119-127.

[35] a) N. Desai, V. Trieu, Z. Yao, L. Louie, S. Ci, A. Yang, C. Tao, T. De, B. Beals, D. Dykes, P. Noker, R. Yao, E. Labao, M. Hawkins and P. Soon-Shiong, *Clinical Cancer Research* **2006**, *12*, 1317-1324; b) T.-Y. Kim, D.-W. Kim, J.-Y. Chung, S. G. Shin, S.-C. Kim, D. S. Heo, N. K. Kim and Y.-J. Bang, *Clinical Cancer Research* **2004**, *10*, 3708-3716.

[36] A. P. Griset, J. Walpole, R. Liu, A. Gaffey, Y. L. Colson and M. W. Grinstaff, *Journal of the American Chemical Society* **2009**, *131*, 2469-2471.

[37] H. Chen, S. Kim, L. Li, S. Wang, K. Park and J.-X. Cheng, *Proceedings of the National Academy of Sciences* **2008**, *105*, 6596-6601.

[38] a) F. Greco and M. J. Vicent, *Advanced Drug Delivery Reviews* **2009**, *61*, 1203-1213; b) B. Louage, L. Nuhn, M. D. P. Risseeuw, N. Vanparijs, R. De Coen, I. Karalic, S. Van Calenbergh and B. G. De Geest, *Angewandte Chemie International Edition* **2016**, *55*, 11791-11796; c) E. M. Pelegri-O'Day, E.-W. Lin and H. D. Maynard, *Journal of the American Chemical Society* **2014**, *136*, 14323-14332; d) N. Vanparijs, S. Maji, B. Louage, L. Voorhaar, D. Laplace, Q. Zhang, Y. Shi, W. E. Hennink, R. Hoogenboom and B. G. De Geest, *Polymer Chemistry* **2015**, *6*, 5602-5614.

[39] a) R. Korsmeyer, *Regenerative Biomaterials* **2016**, *3*, 143-147; b) Y. Zhong, F. Meng, C. Deng and Z. Zhong, *Biomacromolecules* **2014**, *15*, 1955-1969.

[40] J. Schwegman, M. Edgar, B. Sikic, D. Hoth, D. Socks, S. Glenn, J. Marcelletti, M. Walsh and P. Multani in *Chemotherapeutic formulations of zosuquidar trihydrochloride and modified cyclodextrins*, *Vol.* Google Patents, **2007**.

[41] A. H. Dantzig, R. L. Shepard, J. Cao, K. L. Law, W. J. Ehlhardt, T. M. Baughman, T. F. Bumol and J. J. Starling, *Cancer Research* **1996**, *56*, 4171-4179.

[42] H. M. Deutsch, J. A. Glinski, M. Hernandez, R. D. Haugwitz, V. L. Narayanan, M. Suffness and L. H. Zalkow, *Journal of Medicinal Chemistry* **1989**, *32*, 788-792.

[43] J. Dommerholt, S. Schmidt, R. Temming, L. J. A. Hendriks, F. P. J. T. Rutjes, J. C. M. van Hest, D. J. Lefeber, P. Friedl and F. L. van Delft, *Angewandte Chemie International Edition* **2010**, *49*, 9422-9425.

[44] I. Jabeen, K. Pleban, U. Rinner, P. Chiba and G. F. Ecker, *Journal of Medicinal Chemistry* **2012**, *55*, 3261-3273.

[45] V. M. Vrudhula, J. F. MacMaster, Z. Li, D. E. Kerr and P. D. Senter, *Bioorganic & Medicinal Chemistry Letters* **2002**, *12*, 3591-3594.

[46] A. Molina, *Annual Review of Medicine* **2008**, *59*, 237-250.

[47] a) B. C. Laguzza, C. L. Nichols, S. L. Briggs, G. J. Cullinan, D. A. Johnson, J. J. Starling, A. L. Baker, T. F. Bumol and J. R. F. Corvalan, *Journal of Medicinal Chemistry* **1989**, *32*, 548-555; b) P. Trail, D. Willner, S. Lasch, A. Henderson, S. Hofstead, A. Casazza, R. Firestone, I. Hellstrom and K. Hellstrom, *Science* **1993**, *261*, 212-215.

[48] A. Eldar-Boock, K. Miller, J. Sanchis, R. Lupu, M. J. Vicent and R. Satchi-Fainaro, *Biomaterials* **2011**, *32*, 3862-3874.

CHAPTER 4

SEMISYNTHESIS OF HIGHLY POTENT C-3'/C-3'-N-ACYL MODIFIED PACLITAXEL ANALOGS FOR ANTIBODY-DRUG CONJUGATES

Hudlikar, Manish. Li, Xiuru. and Boons, Geert-Jan.

To be submitted to *Chemical Communications*

Abstract

In this work, a reliable and practical route to a series of highly potent paclitaxel (PCTX) analogs modified at C3' and C3'-N-acyl position have been developed. A novel PCTX scaffold was synthesized through efficient coupling of racemic β-lactam modified (*E*)-6-((*tert*-butoxycarbonyl)amino) hex-2-enoic acid and 2-methylprop-1-enyl with properly protected baccatin. It has been found that PCTX scaffold containing 2-methylprop-1-enyl group at C3' and (*E*)-6-((*tert*-butoxycarbonyl)amino) hex-2-enoic acid group at C3'-N-acyl position showed enhanced cytotoxicity against namalwa wild and multidrug-resistant (MDR) lymphoma cells. Interestingly, the resulting scaffold is not a substrate for P-glycoprotein (MDR1) associated multidrug resistance. In addition, the resulting scaffold was amenable to facile modification with various clickable groups or introduction of stable yet cleavable linkers through simple deprotection of di-tert-butyl dicarbonate (Boc) group at C3'-N-acyl position without compromising the potency of the parent molecule making them ideal payloads for the development of next-generation antibody-drug conjugates.

Introduction

Taxol^{R} (PCTX) and its semisynthetic analog[1], Taxotere^{R} (docetaxel)[2], have emerged as the most exciting drugs for the treatment of cancer. Both paclitaxel and docetaxel exhibit significant antitumor activity against various cancers through their unique antimitotic mechanism of action[3]. It has been FDA approved for the treatment of breast, ovarian, lung, bladder, prostate, melanoma, esophageal, as well as other types of solid tumor cancers[4]. However, despite their potent antitumor activity, the amount of a drug required to achieve a clinically effective level of cell killing often causes severe damage to actively propagating healthy cells such as cells of the gastrointestinal tract and bone marrow, resulting in a variety of undesirable

side effects such as hypersensitivity reaction, nephrotoxicity, myelosuppression, and neuropathy[5]. Many potent derivatives of paclitaxel suffer from the lack of tumor specificity and were susceptible to multidrug resistance (MDR) showing a substantial loss in activities[6]. It is clear from the current understanding of the requirements for effective ADCs that the cytotoxicity level of paclitaxel or docetaxel is not sufficient especially against MDR resistant cancers[6]. Therefore, it is very important to develop new chemotherapeutic agents with improved tumor specificity, fewer side effects, improved pharmacological properties, and higher potency.

On the basis of structure-activity relationship (SAR) study of taxoids, Ojima and co-workers have developed a series of highly potent second-generation taxoids. Most of these taxoids exhibited 2-3 orders of magnitude higher potency than that of paclitaxel and docetaxel against drug-resistant cell lines expressing MDR phenotypes[7]. One of these second-generation taxoids, SB-T-110131 (IDN5109; BAY59-8862), exhibited excellent pharmacological profile in preclinical studies and is currently undergoing phase II human clinical trials sponsored by Bayer Corporation[8]. Therefore, in principle, it is possible to develop novel chemotherapeutic agents with high potency and exceptional tumor specificity by covalently attaching above second-generation taxoids to a monoclonal antibody. Based on these assumptions, Ojima and co-workers have synthesized more potent analogs of paclitaxel by replacing C3' phenyl and C3'-N-benzoyl groups with t-butoxycarbonyl and 2-methylpropenyl[8-9]. Targeted delivery of second-generation taxoid to cancer cells using monoclonal antibody (mAb) requires an appropriate linker system that needs to be stable for an extended period of time in circulation *in vivo*, while it should be readily cleaved inside cancer cells.

To meet this criterion[8], methyldisulfanyl (MDS) propanoyl group that contains a disulfide linker unit was installed on to C-2, C-7, and C-10 position of taxoid. It is expected that the mAb

component of the conjugate binds to the specific antigens on tumor surfaces and the whole conjugate is internalized via endocytosis. The disulfide bond is then cleaved by an intracellular thiol such as glutathione to release the drug in its active form. Unfortunately, C-2 and C-10 modified analogs showed a substantial loss in the activity as compared to parent molecule when delivered through randomly conjugated mAb. Previous SAR studies have also depicted that C-7 position is well tolerated for modification however, C-7 modified analogs also exhibited compromised activity against multidrug-resistant (MDR) breast (MCF-7) cancer cells, epidermoid carcinoma (A431), and non-small-cell lung carcinoma (A549).

To address the problems associated with 2nd generation taxoids due to substantial loss in the activity, there is an urgent need to investigate the right position in the molecule that will not only increase the potency of current taxoids but also allows flexibility of installing various stable yet cleavable linkers without compromising the substantial activity was a challenging task. Based on x-ray crystal structure of PCTX bound microtubule[10], through a careful literature survey and previous SAR[11] studies, we found that the modification at C-3'-N-acyl group[12] was well tolerated but has given very little attention for introducing new modifications that allow post-synthetic modifications. It is important to emphasize from x-ray crystal structure of PCTX bound microtubule that by keeping C-3'-N-acyl group intact in PCTX molecule, it should maintain its biological activity.

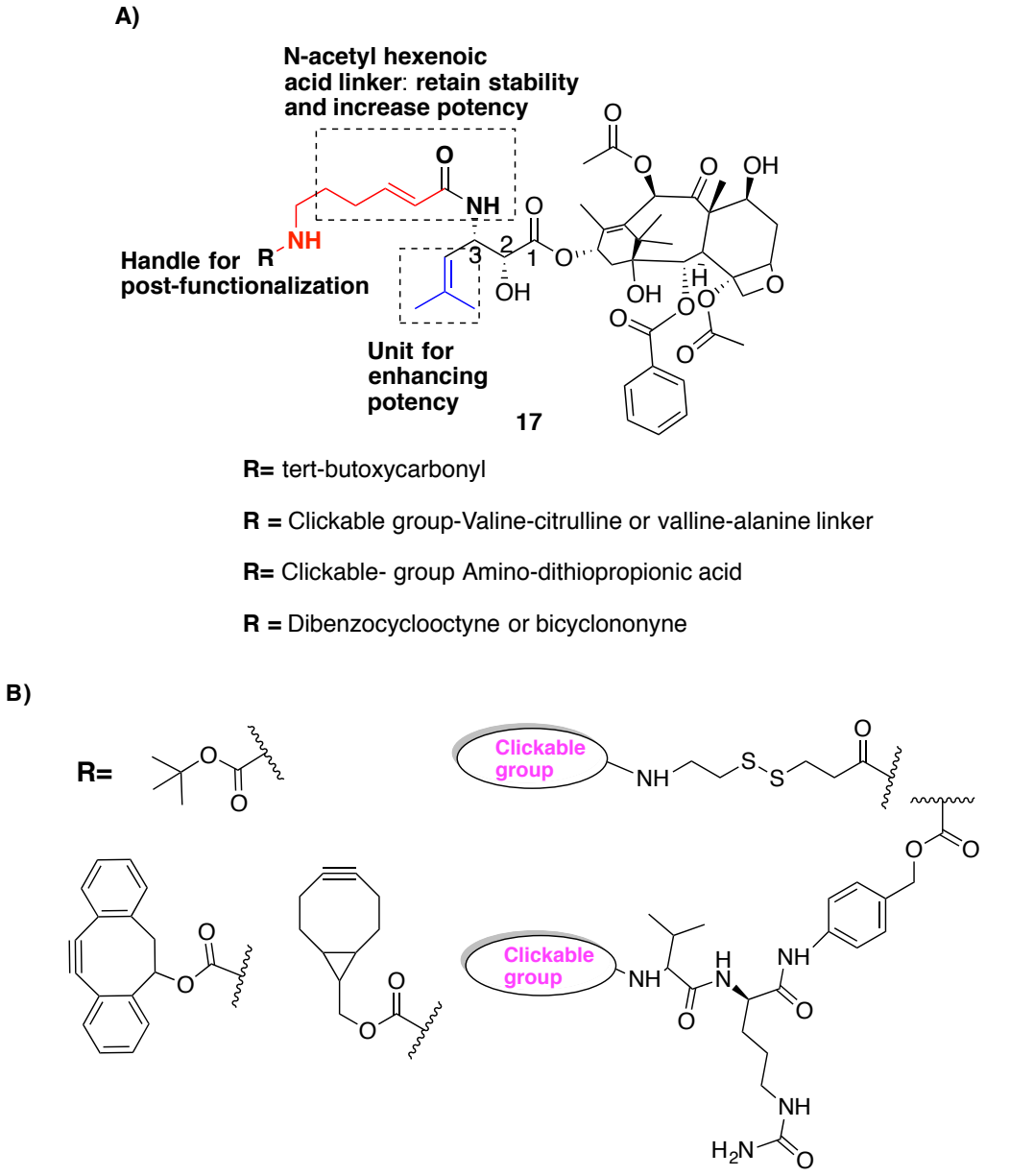

Figure 4.1 Design of highly potent PCTX scaffold **17** as a payload for ADCs.

In this work, a novel PCTX scaffold (Figure **1**) was synthesized through efficient coupling of racemic β-lactam modified (*E*)-6-((*tert*-butoxycarbonyl)amino) hex-2-enoic acid and 2-methylprop-1-enyl with properly protected baccatin. It has been found that PCTX scaffold containing 2-methylprop-1-enyl group at C3' and (*E*)-6-((*tert*-butoxycarbonyl)amino) hex-2-enoic acid group at C3'-N-acyl position was well tolerated and showed enhanced cytotoxicity

against namalwa wild and multidrug-resistant (MDR) lymphoma cells. Moreover, the resulting scaffold was amenable to facile modification with various clickable groups or introduction of stable yet cleavable linkers through simple deprotection of di-tert-butyl dicarbonate (Boc) group at C3'-N-acyl position without compromising the potency of the parent molecule demonstrating the superiority of our analogs over currently available PCTX analogs.

Synthesis of 7-TES-10-Acetyl baccatin (3)

Semisynthesis of highly potent C-3'/C-3'-N-Acyl modified PCTX scaffold **17** can be

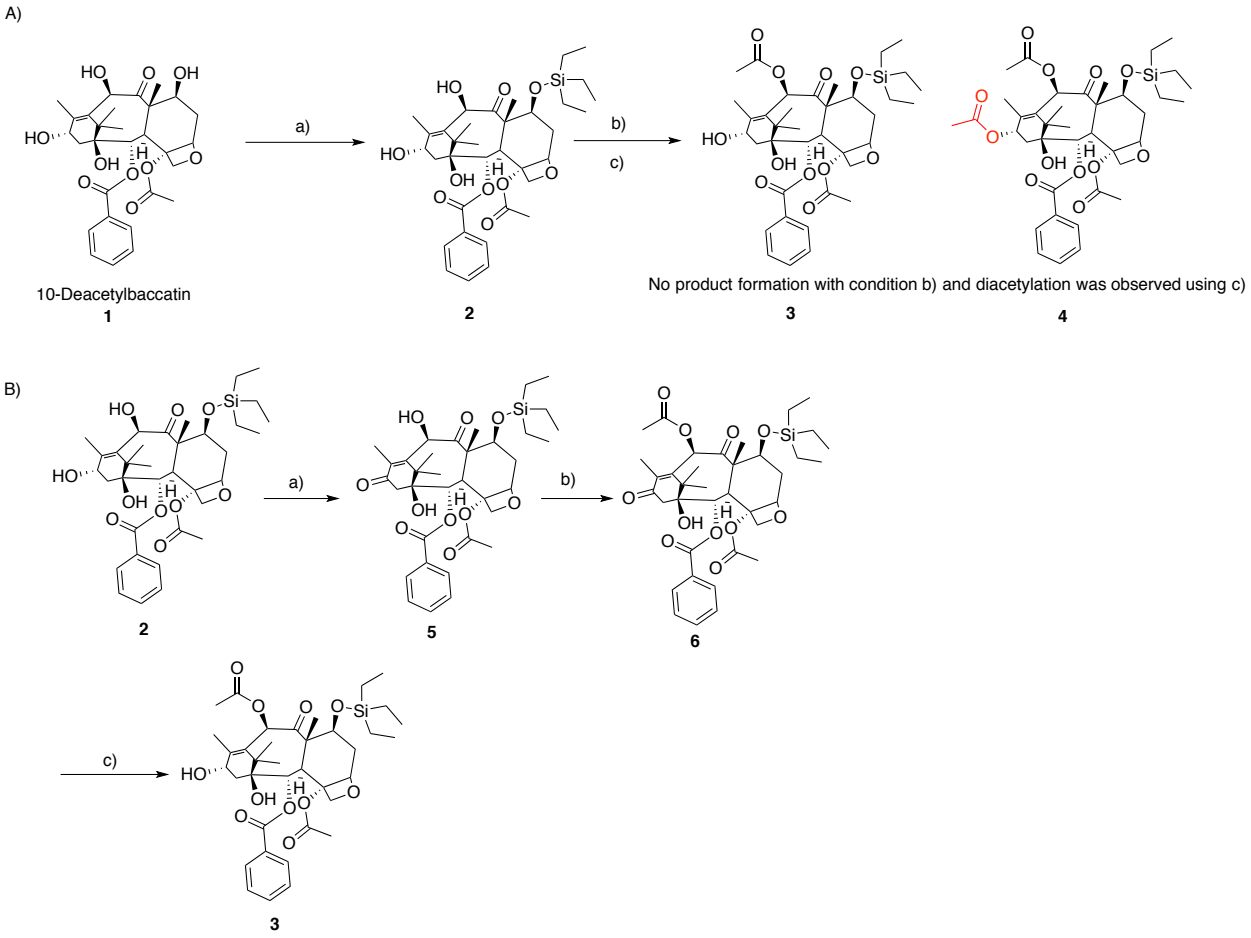

Scheme 4.1 Synthesis of 10-acetyl-7-triethylsilyl-baccatin **3**; A) reagents and conditions: a) chlorotriethylsilane, pyridine/DMF (1:1), 12 h, RT; b) Acetyl Chloride, Pyridine, 0^{o}C to RT for 48 h and c) Acetic anhydride, DMAP, CH_2Cl_2, 25^{o}C 1-3 h. B) reagents and conditions: a) N-

methyl morpholine N-oxide (NMO), tetrapropylamine perruthenate, CH_2Cl_2, 25^oC, 2 h; b) Acetic anhydride, DMAP, CH_2Cl_2, 25^oC 1-3 h; and c) 15-100 $NaBH_4$, MeOH or MeOH/THF 0^oC to RT for 6 h.

accomplished through efficient coupling of racemic β-lactam (**12** and **16**) with acetyl and triethylsilyl (TES) protected baccatin **3** (Scheme 4.1, 4.3 and 4.4)[7b-e, 9]. The clear differentiation of the similarly reactive C-7 and C-10 hydroxyl group in 10-deacetyl baccatin (**1**) with specific bulky protecting groups could be successfully achieved only under specially developed reaction conditions described below. In both the cases (scheme 4.1), first triethylsilylation under carefully optimized conditions (20 eq. of chlorotriethylsilane, 1:1 pyridine/DMF at RT for 12 h) gave 7-TES-10 deacetyl baccatin **2** reproducibly in 84-86% yield[7b]. Using reported procedure, acetylation of C-10 hydroxyl using 5 eq. of acetyl chloride, 25 ml pyridine/mmol, and 0^oC for 48 h was attempted but this procedure didn't yield desired product **3** even after several attempts[13]. Also, acetylation using acetic anhydride and DMAP compromised the selectivity yielding di-acetylated product **4**. Finally, compound **3** can be efficiently synthesized a method developed by Nicolaou and co-workers[14]. By following this procedure, compound **2** first underwent chemoselective oxidation at C-4 with TPAP-NMO leading to diketone **5** in excellent yield. Next, acetylation of C-10 hydroxyl under standard acetic anhydride and DMAP conditions cleanly gave compound **6**. Subsequent reduction of diketone at C-4 carbonyl group proceeded both chemo and stereoselectively with $NaBH_4$ in methanol or methanol-THF system to afford good to excellent yields of the corresponding baccatin **3**.

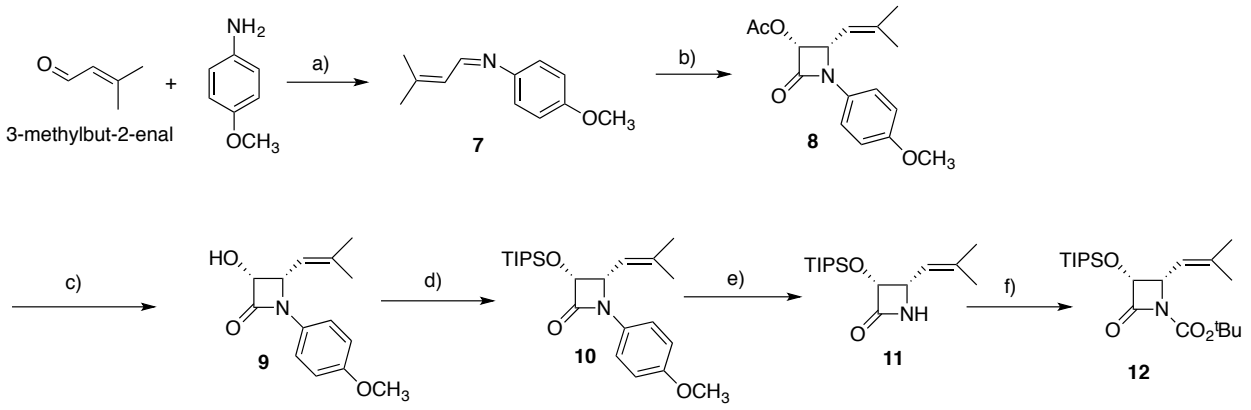

Scheme 4.2 Synthesis of (±)-1-(tert-Butoxycarbonyl)-3-triisopropylsilyloxy-4-(2-methylprop-1-enyl)azetidin-2-one (**12**); Reagents and conditions: a) Sodium sulfate, CH_2Cl_2, 30 min at RT; b) acetoxyacetyl chloride, triethylamine, CH_2Cl_2, -78^oC to RT for 12 h; c) potassium carbonate, MeOH/H_2O (2/1), 30 min to 3 h at RT; d) DMAP, CH_2Cl_2, triethylamine, triisopropylsilyl chloride at RT for 18 h; e) Ceric ammonium nitrate, MeCN/H_2O, -10^oC, 3-4 h; f) di-tert butyl dicarbonate, triethylamine, DMAP for 20 h at RT.

Synthesis of NH and NBoc-β-lactam (11 and 12)

(±)-1-(tert-Butoxycarbonyl)-3-triisopropylsilyloxy-4-(2-methylprop-1-enyl)azetidin-2-one (**12**) (Scheme 4.2) has been synthesized efficiently using β-lactam synthon method[9]. First, Racemic 1-(4-methoxyphenyl)-2-(2-methylprop-1-en-1-yl)-4-oxoazetidin-3-yl-acetate (± **8**) was obtained in 76% yield through the [2+2] cycloaddition of N-p-methoxyphenyl (PMP)-3-methyl-2-butaldimine with acetoxyketene generated in situ from acetoxyacetyl chloride and triethylamine in dichloromethane at −78°C. Treating (± **8**) with potassium carbonate in methanol/water (2/1), resulted in deprotection of the acetyl group of β-lactam (± **8)** and was subsequently protected with a TIPS group (TIPS = triisopropylsilyl) to afford 3-TIPSO-β-lactam (± **10**) in 90% yield. The PMP group of β-lactam (± **10**) was oxidatively cleaved by CAN (CAN = cerium(IV) ammonium nitrate) to afford the NH-β-lactam (± **11**) in 92% yield, which was then

further reacted with tert-butoxycarbonyl (Boc) in the presence of DMAP and triethylamine to afford racemic (±)-1-(tert-Butoxycarbonyl)-3-triisopropylsilyloxy-4-(2-methylprop-1-enyl)azetidin-2-one (± **12**) in 95% yield.

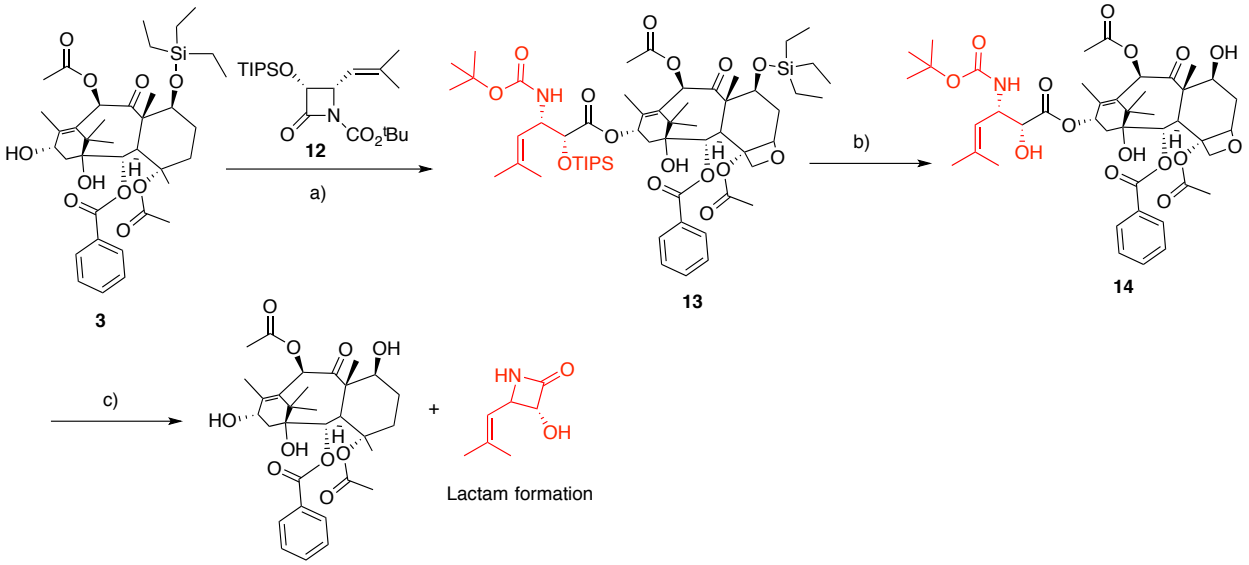

Scheme 4.3 Assembly of taxoids **14** via coupling of β-lactam (±) **12** and **3**; Formation of β-lactam through di-tert-butyl dicarbonate deprotection; Reagents and conditions: a) **3**, **12**, and 1M LiHMDS in THF, -35°C to 0°C for 2 h; b) acetonitrile: pyridine (1:1), HF/Pyridine, 0°C to RT for 12-18 h; and c) 5% trifluoroacetic acid in 1 ml CH_2Cl_2 for 1 h.

Assembly of toxoid 14 via coupling of β-lactam and baccatin

Ring-opening couplings of racemic β-lactams (± **12**) and ± **16**) with baccatins **3** were carried out following the reported protocol developed before (Scheme 4.3 and 4.4)[9]. To a mixture of baccatin **3** (1.0 equiv.) and β-lactam (±), **12** or β-lactam (±) **16**, (3.0 equiv.) in THF was added LiHMDS (1.5 equiv.) at −20°C. The reaction mixture was warmed to 0°C in 30-60 min and stirred for additional 1 h at that temperature and quenched with aqueous ammonium chloride solution. Since the determination of the diastereomeric purity of the coupling product at this stage was found to be difficult, the crude product mixture was passed through a short silica gel

column to remove the unreacted β-lactams. The coupling product thus obtained was treated with HF/pyridine in acetonitrile/pyridine (1/1) at room temperature to achieve complete deprotection of TES and TIPS to afford target compound **14** and **17** in excellent yields.

In an attempt to access target compound **17** from **14**, we thought that the deprotection of tert-butoxycarbonyl (Scheme 4.3) of **14**, in turn, could be reacted with *tert*-butyl (*E*)-(6-chloro-6-oxohex-4-en-1-yl)carbamate (**15**) under standard amide coupling conditions. However, after several attempts of Boc deprotection using 5% TFA in dichloromethane reproducibly gave self-immolation β-lactam and 10-acetyl baccatin as products. This self-immolation of taxoid **14** can occur by the following mechanism.

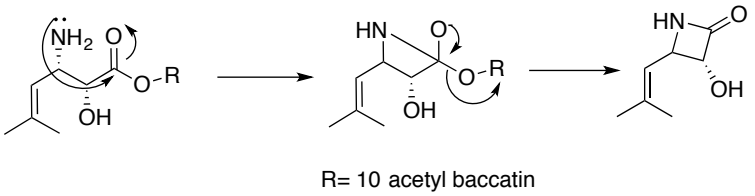

R= 10 acetyl baccatin

Figure 4.2 Mechanism of self-immolation of taxoid **14** after tert-butoxycarbonyl (Boc) deprotection

After deprotection of Boc, the nucleophilic attack of the amine on the adjacent carbonyl leads to a cyclized intermediate which, in turn, facilitates the second attack by carbonyl oxygen that results in the self-immolation to release of 10-acetyl baccatin and cyclized β-lactam product.

Assembly of C3'/C3'-N-acyl modified taxoid 17 via coupling of β-lactam and baccatin

To circumvent the problem of β-lactamization, we decided to synthesize compound **16** (Scheme 4.4) with preinstalled 2-methylprop-1-enyl and (*E*)-6-((*tert*-butoxycarbonyl)amino) hex-2-enoic acid modification. (*E*)-6-((*tert*-butoxycarbonyl)amino) hex-2-enoic acid was converted into acid chloride generated using oxalyl chloride and a catalytic amount of dimethylformamide. After the completion of the reaction, the acid chloride was used as such

without any purification and coupled to NH-β-lactam (± **11**) in the presence of a super base (Pka ≈ 50)[7b], n-butyl lithium at -78°C to yield β-lactam carbamate (± **16**) in 80% yield. Ring-opening couplings of racemic β-lactams (± **16**) with baccatins **3** is the key step to assemble target taxoid scaffold **17**.

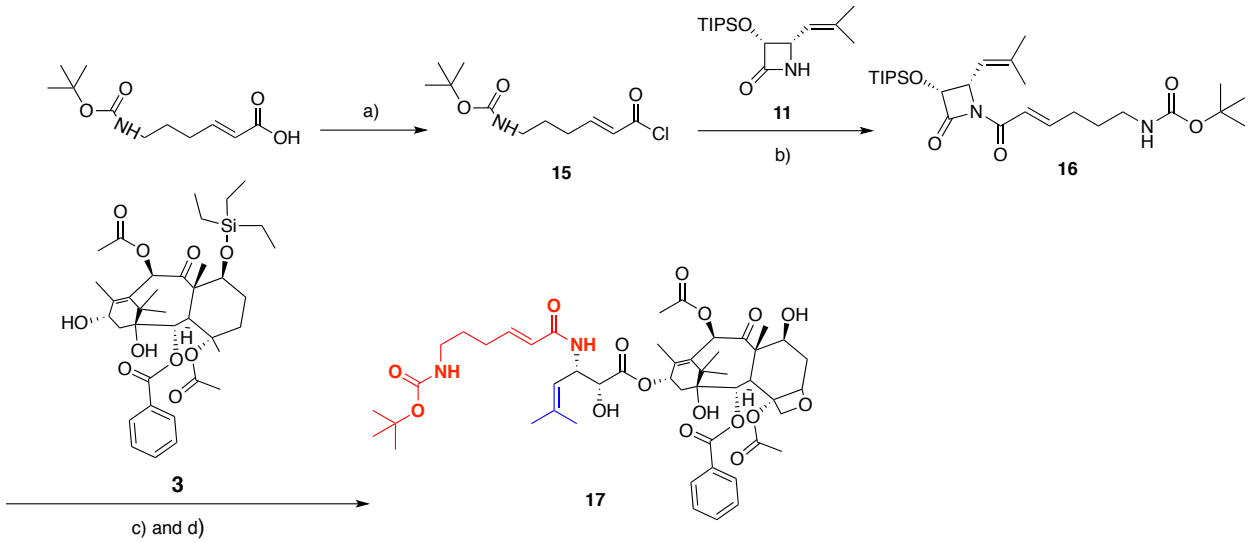

Scheme 4.4 Assembly of C3'/C3'-N-acyl modified taxoid **17** via coupling of β-lactam (±) **16** and **3**; Reagents and conditions: a) a) 1M oxalyl chloride in DCM, catalytic DMF, dry CH_2Cl_2 for 3-4 h at RT; b) **11**,**15**, 1.5 M n-butyl lithium, dry THF, -78°C, 2 h; c) **16**, **3**, and 1M LiHMDS in THF, -20°C to 0°C over 60 min stirred for 2 h at 0°C; and d) acetonitrile: pyridine (1:1), HF/Pyridine, 0°C to RT for 12-18 h.

We initially thought that the installation of (*E*)-6-((*tert*-butoxycarbonyl)amino) hex-2-enoic acid on NH-β-lactam (± **11**) could have an influence on the outcome of the ring opening coupling reaction with **3**. Since this new modification appears to be bulky and has not been shown before to couple with **3**. However, the coupling reaction between β-lactam (±) **16** and **3** proceeded cleanly to afforded final target **17** utilizing lithiated organosilicon reagent (LiHMDS) followed by deprotection of TES and TIPS in HF/pyridine in acetonitrile/pyridine (1/1) at room temperature to afford target compound **17** in excellent yields.

Mechanistic studies on the ring opening coupling reactions have demonstrated that in each transition state, the lithium-oxygen bond of the lithium alkoxide of baccatin is aligned with the carbonyl of the β-lactam, which is required for the nucleophilic ring opening of the β-lactam[9].

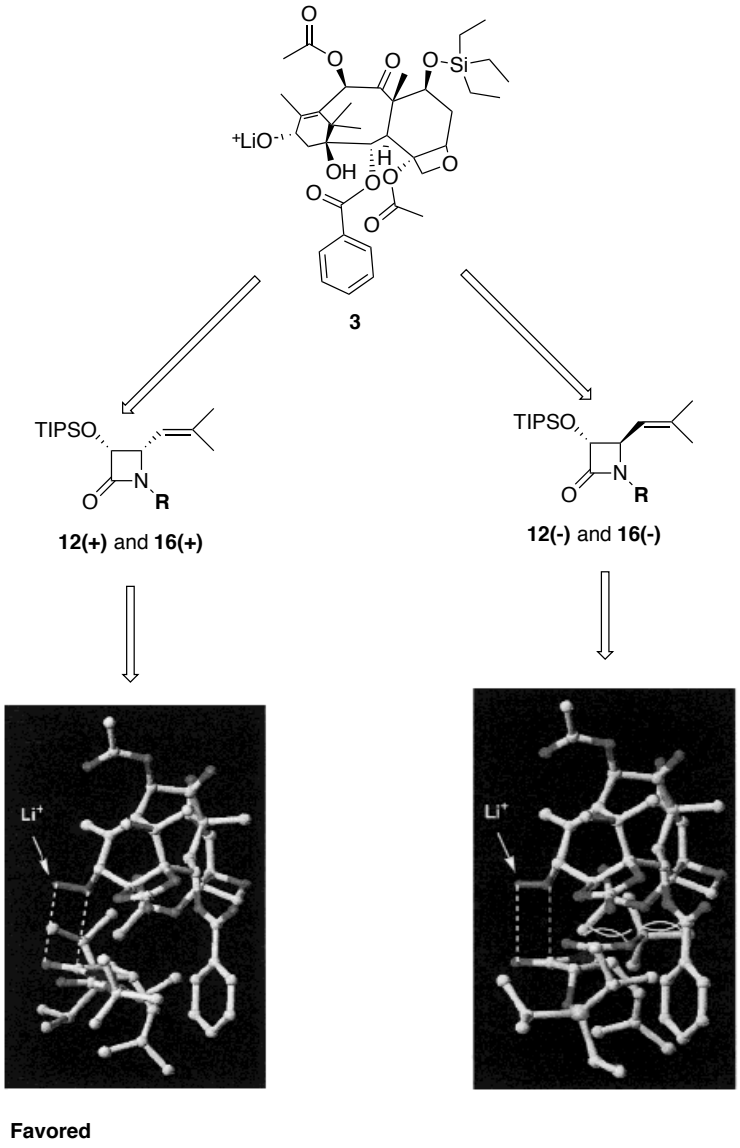

Figure 4.3 Possible transition states for the coupling of β-lactam (a) (+12), (+16), b) (-12), and (-16) with baccatin **3**.The transition states show for (a) are the most favorable ones; and **R**=**12**= Boc and **16**=(*E*)-6-((*tert*-butoxycarbonyl)amino)hex-2-enoic) carbamate.

In the transition state (a), TIPSO-β-lactam (+) **12** and **16**, the precursor of the C-13 side chain with correct stereochemistry, is situated underneath the baccatin with the orientation in such a manner that the C-3 and C-4 substituents are pointing away from the baccatin core and the bulky t-Boc group is located outside the baccatin framework (Figure 4.3a). This transition state creates no significant steric crowding, and thus this reaction should proceed smoothly. In contrast to this, the transition state for the reaction of enantiomeric β-lactam (-) **12** and **16**, there is a substantial steric interaction between the t-Boc group of the β-lactam and the acetyl moiety of the baccatin (Figure 4.3b). Another obvious steric crowding is the interaction between the 1,14-carbonate moieties of the baccatin with one of the isopropyl groups of the 3-TIPSO group of the β-lactam (Figure 4.3b).

It is thus strongly suggested that the bulky group substitution (e.g. in case of **12** and **16**) at NH-β-lactam doesn't interfere with the outcome of ring opening coupling protocol giving efficient access to target scaffold **17**.

Biological evaluation of C3' and C3'-N-Acyl modified analogs against wild-type and multidrug-resistant (MDR) lymphoma cells

Many chemotherapeutic drugs and payloads used currently in ADCs constructs were very good substrates for P-glycoprotein or ABCB1 or other ATP-dependent transporters allowing them to pump drugs out of the cancer cells leading to poor responses to chemo and targeted therapies. Thus, developing new payloads that can overcome multidrug resistance in cancer treatment are highly desired in the field of cancer chemotherapy and antibody-drug conjugates[15]. We hypothesized that the C3'/C3'-N-acetyl modified PCTX analogs (**14** and **17**) could circumvent the P-glycoprotein associated multidrug-resistance. To test our hypothesis namalwa wild and namalwa MDR (+ve) type cell lines were incubated with compound **14** at

various concentrations (1000 to 0.001 nM) for 72 h and 37°C. After 72 h, % cell viability was determined by MTT assay. Data were fitted with Prism nonlinear regression software.

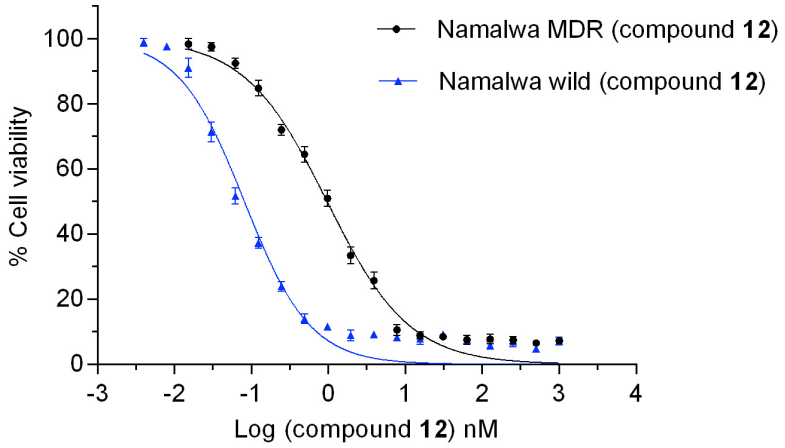

Figure 4.4 Cytotoxicity profiles of compound **14** against MDR1 and CD22 overexpressing namalwa MDR1 and wild-type cell lines.

From the cytotoxicity profiles (Figure 4.4), it is clear that the compound **12** were found to be very potent showing EC_{50} values 0.081 nM and 1.47 nM in wild and MDR1 overexpressing namalwa cells respectively. Thus, it is expected from above results that the PCTX scaffolds **17** should be more potent due to the presence of additional modification of (*E*)-6-((*tert*-butoxycarbonyl)amino) hex-2-enoic acid at C3'-N-acyl position as compared to **12** and hence could circumvent p-glycoprotein associated multidrug resistance. Efforts to test the biological activity of compound **17** are currently under investigation in our laboratory.

Conclusion

Through a critical literature survey, detailed SAR studies and x-ray crystal structure of PCTX bound microtubule makes it possible to design and synthesized highly potent PCTX scaffolds modified at C3' and C3'-N-Acyl position through highly robust coupling protocol of β-lactams with baccatin. Introduction of the bulky group at NH-β lactam doesn't affect the final coupling step important for modification at C-3'-N-acyl group which was well tolerated. This synthetic methodology makes it possible to install dual modifications such as 2-methylprop-1-enyl and (*E*)-6-((*tert*-butoxycarbonyl) amino) hex-2-enoic acid that has greatly enhanced the cytotoxicity of PCTX scaffold with EC_{50} in subnanomolar to picomolar range against wild and MDR lymphoma cells demonstrating the clear advantage of the dual modifications. From cytotoxicity studies, it was confirmed that the new scaffold is not susceptible to P-glycoprotein associated MDR phenotype.

The resulting PCTX scaffold was amenable to facile modification with various clickable groups such as dibenzocyclooctyne (DIBO)[16], bicyclononyne (BCN)[17] or introduction of stable yet cleavable linkers such as val-cit or val-ala (cathepsin B cleavable)[18] or disulfide linkers (glutathione sensitive)[19] through simple deprotection of di-tert-butyl dicarbonate (Boc) group at C3'-N-acyl position without compromising the potency of the parent molecule and provide an additional handle for site-specific conjugation to antibody of choice demonstrating the superiority of our approach. In future, we anticipate utilizing novel scaffold for the development of next-generation antibody-drug conjugates against multidrug resistant cancers.

Experimental section

General reagents and materials

10-deacetylbaccatin was purchased from Medchem Express LLC. Sodium sulfate, acetoxyacetyl chloride, triisopropylsilyl chloride, ceric ammonium nitrate, chlorotriethylsilane, N-methyl morpholine N-oxide (NMO), tetrapropylamine per-ruthenate (TPAP), acetyl chloride were purchased from Oakwood chemicals Inc. Acetic anhydride, dimethylamino pyridine (DMAP), sodium borohydride, potassium carbonate, triethylamine, 1M LiHMDS, HF/pyridine, 1M oxalyl chloride in dichloromethane, 1.5 M n-butyl lithium in hexane, and trifluoroacetic acid were purchased from Sigma Aldrich. Dichloromethane (DCM) was freshly distilled under a nitrogen atmosphere. Other organic solvents were purchased anhydrous and used without further purification. Unless otherwise noted, all reactions were carried out at room temperature (RT) in oven-dried glassware with magnetic stirring. Organic solutions were concentrated under reduced pressure with bath temperatures < 40^{o}C. Flash column chromatography was carried out on silica gel G60 (Silicycle, 60-200 μm, 60 Å). Thin-layer chromatography (TLC) was carried out on Silica gel 60 F254 (EMD Chemicals Inc.) with detection by UV absorption (254 nm) where applicable, and by spraying with 20% sulfuric acid in ethanol followed by charring at ~150^{o}C or by spraying with a solution of $(NH_4)_6Mo_7O_{24}.H_2O$ (25 g L^{-1}) in 10% sulfuric acid in ethanol followed by charring at ~150^{o}C.

General methods for compound characterization

^{1}H and ^{13}C NMR spectra were recorded on a Varian Inova-300 (300/75 MHz), a Varian Inova-500 (500 MHz) and a Varian Inova-600 (600/150 MHz) spectrometer equipped with sun workstations. Multiplicities are quoted as singlet (s), doublet (d), doublet of doublets (dd), triplet

(t) or multiplet (m). NMR signals were assigned on the basis of 1H NMR, 13C NMR, gCOSY and gHSQC experiments. Chemical shifts are quoted on the δ-scale in parts per million (ppm). Residual solvent signals were used as an internal reference. Mass spectra were recorded on an Applied Biosystems 5800 MALDI-TOF or Shimadzu LCMS-IT-TOF mass spectrometer. The matrix used was 2,5-dihydroxy benzoic acid (DHB).

Synthetic procedures for compound 3

(4*S*,4a*S*,6*R*,9*S*,11*S*,12*S*,12a*R*,12b*S*)-12b-acetoxy-6,9,11-trihydroxy-4a,8,13,13-tetramethyl-5-oxo-4-((triethylsilyl)oxy)-2a,3,4,4a,5,6,9,10,11,12,12a,12b-dodecahydro-1*H*-7,11-methanocyclodeca[3,4]benzo[1,2-*b*]oxet-12-yl benzoate (2)

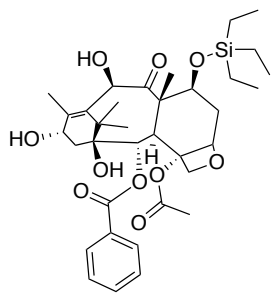

To a stirred solution of 10-deacetylbaccatin **1** (150 mg, 0.275 mmol) in pyridine: DMF 11ml each (1:1) was added chlorotriethylsilane (830 mg, 0.925 ml, 5.512 mmol) drop wise using syringe at room temperature. After stirring the reaction mixture for 12 h, the reaction was quenched by adding ethyl acetate (40 mL) and pyridine was removed by successive washing with aqueous saturated $CuSO_4$ until no color change was observed. The organic layer was washed with water, dried over $MgSO_4$ and concentrated. Silica gel chromatography (hexane/ethyl acetate: 1/1) afforded compound (**2**) (154 mg, 85% yield) as a white solid. ^{1}H NMR ($CDCl_3$): δ 0.50 (m, 6H), 0.97 (m, 9H), 1.21 (s, 3H), 1.58 (s, 3H), 1.58 (s, 3 H), 1.73 (s, 3H), 1.85 (dt, 1H), 1.99 (s, 3H), 2.32 (s, 3H), 2.10 (s, 2H), 2.47 (ddd, 1H), 3.94

(d, J =7.2 Hz, 1H), 4.14 (d, J=8.4 Hz, 1H), 4.32 (d, J =8.1 Hz, 1H), 4.41 (d, J = 6.3 Hz, 1H), 4.84 (t, 1H), 4.94 (d, J=8.4 Hz, 1H), 5.14 (s, 1H), 5.19 (s, 1H), 5.58 (d, J = 7.2 Hz, 1H), 7.40 (t, 2

H),7.54 (t, 1H), 8.10 (d, 2H); ^{13}C NMR ($CDCl_3$): δ 5.1, 6.7, 9.9, 15.1, 19.5, 22.6, 26.8, 37.2, 38.6, 42.7, 47.0, 57.9, 67.9, 72.9, 74.7, 74.8, 76.5, 78.8, 80.7, 84.2, 128.6, 129.4, 130.0, 133.6, 135.1, 141.9, 167.0, 170.7, 210.3; MALDI HRMS for $C_{35}H_{50}O_{10}Si$ m/z [M+Na^+] 681.32; found 681.325.

(4*S*,4a*S*,6*R*,9*S*,11*S*,12*S*,12a*R*,12b*S*)-12-(benzoyloxy)-11-hydroxy-4a,8,13,13-tetramethyl-5-oxo-4-((triethylsilyl)oxy)-3,4,4a,5,6,9,10,11,12,12a-decahydro-1*H*-7,11-methanocyclodeca[3,4]benzo[1,2-*b*]oxete-6,9,12b(2a*H*)-triyl triacetate (4)

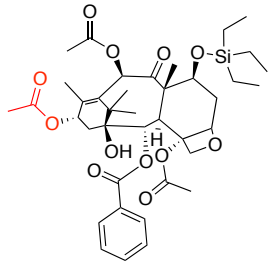

A solution of alcohol **2** (5 mg, 0.0075 mmol) and 4-dimethylaminopyridine (DMAP, 4.6 mg, 0.0375 mmol) in 1 ml CH_2CI_2 at 25°C was treated with Ac_2O (71 µL, 0.75 mmol) and stirred for 1 h. The reaction mixture was diluted with CH_2CI_2 (2 mL), treated with aqueous $NaHCO_3$ (3 mL), and stirred vigorously for 30 min. The organic layer was separated and the aqueous layer was extracted with CH_2CI_2 (2x3 mL). The combined organic layer was washed with brine (3 mL), dried over $MgSO_4$, concentrated, and purified by flash chromatography (10 to 35% EtOAc in hexanes) to give **4** (4.45 mg, 80%) white solid. ^{1}H NMR ($CDCl_3$): δ 0.50 (m, 6H), 0.97 (m, 9H), 1.21 (s, 3H), 1.58 (s, 3H), 1.58 (s, 3 H), 1.73 (s, 3H), 1.85 (dt, 1H), 1.99 (s, 3H), 2.32 (s, 3H), 2.25 (dd, 6H), 2.10 (s, 2H), 2.47 (ddd, 1H), 3.94 (d, J =7.2 Hz, 1H), 4.14 (d, J=8.4 Hz, 1H), 4.32 (d, J =8.1 Hz, 1H), 4.41 (d, J = 6.3 Hz, 1H), 4.94 (d, J=8.4 Hz, 1H), 5.14 (s, 1H), 5.58 (d, J = 7.2 Hz, 1H), 6.18 (t, 1H), 6.48(s, 1H), 7.40 (t, 2 H), 7.54 (t, 1H), 8.10 (d, 2H); MALDI HRMS for $C_{39}H_{54}O_{12}Si$ m/z [M+Na^+] 765.34; found 765.328.

(4*S*,4a*S*,6*R*,11*S*,12*S*,12a*R*,12b*S*)-12b-acetoxy-6,11-dihydroxy-4a,8,13,13-tetramethyl-5,9-dioxo-4-((triethylsilyl)oxy)-2a,3,4,4a,5,6,9,10,11,12,12a,12b-dodecahydro-1*H*-7,11-methanocyclodeca[3,4]benzo[1,2-*b*]oxet-12-yl benzoate (5)

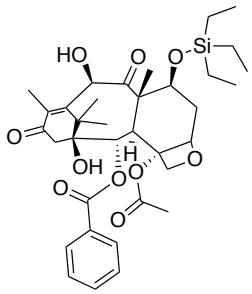

To a solution of 7-TES deacetylbaccatin **2** (150 mg, 0.2278 mmol) and 4-methylmorpholine N-oxide (NMO, 24 mg, 0.205 mmol) in CH_2Cl_2 (2 mL) were added 4A^o molecular sieves (10 mg), and the suspension was stirred at 25^{o}C for 10 min. A catalytic amount of tetrapropylammonium per-ruthenate (TPAP, 4 mg, 0.0109 mmol) was added by portions, and the reaction mixture was stirred at 25^{o}C for 30 min. Small amounts of 4-methylmorpholine N-oxide and TPAP were added alternatively at 0.5 h intervals until TLC showed complete consumption of starting material to the extent of approximate 95%. The reaction mixture was filtered through silica gel, eluted with CH_2Cl_2 (100 mL), and concentrated to give enone **5** (142 mg, 95%) as a white solid.

^{1}H NMR (500 MHz, $CDCl_3$): δ 8.05 (dd, J = 8.0, 1.0 Hz, 2H), 7.61 (t, J = 7.5 Hz, lH), 7.45 (t, J = 7.5 Hz, 2H), 5.63 (d, J = 7.5 Hz, lH), 5.30 (d, J = 2.0 Hz, lH), 4.90 (d, J = 8.0 Hz, lH), 4.36 (dd, J= 10.5, 7.0 Hz, lH), 4.31 (d, J = 8.5 Hz, lH), 4.30 (d, J= 2.0 Hz, lH), 4.11 (d, J = 8.5 Hz, 1H), 3.93 (d, J =7.5 Hz, lH), 2.92 (d, J = 19.5 Hz, lH), 2.62 (d, J = 19.5 Hz, lH), 2.50-2.42 (m, lH), 2.17 (s, 3H), 2.08 (s, 3H), 1.90-1.82 (m, lH), 1.77 (s, lH), 1.70 (s, 3H), 1.21 (s, 3H), 1.14 (s, 3H), 0.90 (t, J = 8.0 Hz, 9H), 0.60-0.42 (m, 6H).

^{13}C NMR (125 MHz, $CDC1_3$): δ 208.2, 198.1, 170.2, 166.8, 156.6, 139.1, 134.0, 130.0, 128.8, 128.8, 84.0, 80.4, 78.5, 76.2, 75.7, 72.9, 72.8, 58.8, 45.9, 43.4, 42.5, 37.2, 33.0, 21.7, 17.5, 13.6, 9.6, 6.7, and 5.1. MALDI HRMS for $C_{35}H_{48}O_{10}Si$ m/z [M+Na^+] 679.30; found 679.283.

(4*S*,4a*S*,6*R*,11*S*,12*S*,12a*R*,12b*S*)-12-(benzoyloxy)-11-hydroxy-4a,8,13,13-tetramethyl-5,9-dioxo-4-((triethylsilyl)oxy)-3,4,4a,5,6,9,10,11,12,12a-decahydro-1*H*-7,11-methanocyclodeca[3,4]benzo[1,2-*b*]oxete-6,12b(2a*H*)-diyl diacetate (6)

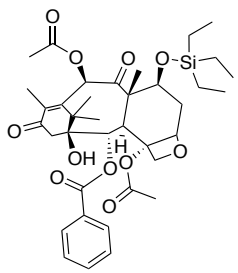

A solution of enone **5** (140 mg, 0.213 mmol) and 4-dimethylarninopyridine (DMAP, 130 mg, 1.06 mmol) in CH_2Cl_2 (10 mL) at 25°C was treated with Ac_2O (0.806 mL, 8.52 mmol) and stirred for 2.5 h. The reaction mixture was diluted with CH_2CI_2 (25 mL), treated with aqueous $NaHCO_3$ (20 mL), and stirred vigorously for 25 min. The organic layer was separated and the aqueous layer was extracted with CH_2Cl_2 (2 x 25 mL). The combined organic layer was washed with brine (15 mL), dried over $MgSO_4$, concentrated, and purified by flash chromatography (10 to 20% EtOAc in hexane) to give **6** (121 mg, 81%) as an amorphous solid.

^{1}H NMR (500 MHz, $CDCl_3$): δ 8.05 (dd, J = 8.0, 1.0 Hz, 2H), 7.61 (t, J = 7.5 Hz, lH), 7.45 (t, J = 7.5 Hz, 2H), 6.48 (s, 1H), 5.63 (d, J = 7.5 Hz, lH), 4.98 (d, J = 8.0 Hz, lH), 4.36 (dd, J= 10.5, 7.0 Hz, lH), 4.31 (d, J = 8.5 Hz, lH), 4.30 (d, J= 2.0 Hz, lH), 4.11 (d, J = 8.5 Hz, 1H), 3.93 (d, J =7.5 Hz, lH), 2.92 (d, J = 19.5 Hz, lH), 2.62 (d, J = 19.5 Hz, lH), 2.50-2.42 (m, lH), 2.23 (s, 3H), 2.18 (s, 3H), 2.17 (s, 3H), 1.90-1.82 (m, lH), 1.77 (s, lH), 1.70 (s, 3H), 1.21 (s, 3H), 1.14 (s, 3H), 0.90 (t, J = 8.0 Hz, 9H), 0.60-0.42 (m, 6H); MALDI HRMS for $C_{37}H_{50}O_{11}Si$ m/z [M+Na^+] 721.31; found 721.298.

(4*S*,4a*S*,6*R*,9*S*,11*S*,12*S*,12a*R*,12b*S*)-12-(benzoyloxy)-9,11-dihydroxy-4a,8,13,13-tetramethyl-5-oxo-4-((triethylsilyl)oxy)-3,4,4a,5,6,9,10,11,12,12a-decahydro-1*H*-7,11-methanocyclodeca[3,4]benzo[1,2-*b*]oxete-6,12b(2a*H*)-diyl diacetate (3)

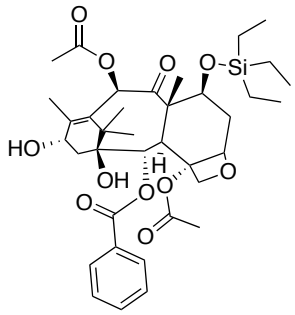

A solution of enone **6** (120 mg, 0.1718 mmol) in MeOH-THF (5:1, 8 mL) at 0°C was treated with $NaBH_4$ (324 mg, 8.60 mmol, added by portions) and stirred for 8 h. The reaction mixture was diluted with CH_2Cl_2 (20 mL), treated with aqueous NH_4Cl (10 mL), and stirred for 10 min. The organic layer was separated, and the aqueous layer was extracted with CH_2Cl_2 (2 x 20 mL). The combined organic layer was washed with brine (10 mL), dried over $MgSO_4$, concentrated, and purified by flash chromatography (silica, 30% EtOAc in hexanes) to give **3** (107.6 mg, 89%) as amorphous solids.

^{1}H NMR (500 MHz, $CDCl_3$) δ 8.16 – 8.10 (m, 2H), 7.67 – 7.58 (m, 1H), 7.49 (t, 3H), 6.47 (s, 1H), 5.65 (d, 1H), 5.02 – 4.95 (m, 1H), 4.85 (t, 1H), 4.50 (dd, 1H), 4.32 (d, 1H), 4.21 – 4.12 (m, 1H), 3.90 (d, 1H), 2.54 (ddd, 1H), 2.30 (s, 4H), 2.23 – 2.17 (m, 6H), 1.93 – 1.84 (m, 1H), 1.69 (s, 3H), 1.26 (s, 2H), 1.21 (s, 3H), 1.08 – 0.79 (m, 15 H), 0.59 (m, 6H).

^{13}C NMR (126 MHz, $CDCl_3$) δ 129.76, 133.26, 128.24, 74.73, 84.22, 67.53, 72.36, 76.90, 76.54, 47.26, 37.24, 22.69, 38.25, 14.94, 20.95, 37.26, 9.95, 29.68, 20.08, 26.84, 6.77, and 5.1.

MALDI HRMS for $C_{37}H_{52}O_{11}Si$ m/z [M-H] 699.33; found 699.318.

Synthetic procedure for compounds 10 and 11

(2*S*,3*R*)-1-(4-methoxyphenyl)-2-(2-methylprop-1-en-1-yl)-4-oxoazetidin-3-yl acetate (8)

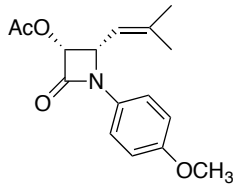

To a mixture of p-anisidine (1.52 g, 12.34 mmol) and anhydrous sodium sulfate in dichloromethane (30 mL) was added 3-methylbut-2-enal (1.31 mL, 13.58 mmol) and the mixture was stirred at room temperature for 30 min. The organic phase in this flask was transferred to another flask and concentrated in vacuo. The residue was dissolved in dichloromethane (60 mL) and triethylamine (2.58 mL, 18.51 mmol) was added at −78°C. To the mixture was added acetoxyacetyl chloride

(1.59 mL, 14.81 mmol) and the reaction mixture was warmed to room temperature overnight for 12 h. To the reaction mixture was added saturated ammonium chloride solution (20 mL) and the mixture was extracted with dichloromethane (40 mL×3). The combined organic layers were washed with hydrochloric acid (3%), water, brine, dried over magnesium sulfate, and concentrated in vacuo. Column chromatography of this residue on silica gel using hexane/ethyl acetate (4/1, 2/1, then 1/1) as the eluent to afford **8** as a white solid (2.71 g, 76% yield); ^{1}H NMR ($CDCl_3$): δ 1.70 (s, 3 H), 1.72 (s, 3 H), 2.01 (s, 3 H), 3.67 (s, 3 H), 4.83 (dd, J = 9.9, 4.8 Hz, 1 H), 5.02 (d, J = 9.3 Hz, 1 H), 5.67 (d, J = 4.8 Hz, 1 H), 6.74 (d, J = 8.9 Hz, 2 H), 7.20 (d, J = 8.9 Hz, 2 H); ^{13}C NMR ($CDCl_3$): δ 18.3, 20.2, 27.0, 76.1, 114.3, 117.5, 118.4, 130.7, 141.8, 156.4, 161.3, 169.3.

(3*R*,4*S*)-3-hydroxy-1-(4-methoxyphenyl)-4-(2-methylprop-1-en-1-yl)azetidin-2-one (9)

To a solution of β-lactam **8** (450 mg, 1.555 mmol) in 30 mL, aqueous methanol ($MeOH/H_2O$ = 2/1, v/v) was added potassium carbonate (376 mg, 2.722 mmol) and the mixture was stirred for 30 min at room temperature. The reaction was quenched with aqueous saturated ammonium chloride solution (15 mL), and the aqueous layer was extracted with ethyl acetate (40 ml×3).

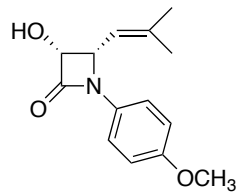

The combined extracts were then washed with brine, dried over anhydrous magnesium sulfate, and concentrated in vacuo to afford a white solid.

^{1}H NMR ($CDCl_3$): δ 1.85 (s, 6 H), 3.75 (s, 3 H), 4.63 (d, J = 7.5 Hz, 1 H), 4.86 (dd, J = 9.2, 5.2 Hz, 1 H), 5.04 (dd, J = 7.0, 5.2 Hz, 1 H), 5.33 (d, J = 9.2 Hz, 1 H), 6.79 (d, J = 9.0 Hz, 2 H), 7.27 (d, J = 9.0 Hz, 2 H); ^{13}C NMR (62.5 MHz, $CDCl_3$): δ 18.6, 26.2, 55.4, 57.3, 76.3, 114.3, 118.1, 118.6, 130.8, 141.2, 156.3, 166.6.

(3*R*,4*S*)-4-(2-methylprop-1-en-1-yl)-3-((triisopropylsilyl)oxy)azetidin-2-one (10)

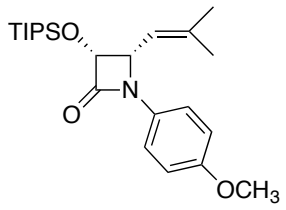

To a solution of the solid **9** thus obtained and 4-dimethyl-aminopyridine (DMAP) (47.5 mg, 0.389 mmol) in 15 mL dichloromethane was added triethylamine (0.501 mL, 3.60 mmol) and triisopropylsilyl chloride (0.4 mL, 1.890 mmol) at room temperature, and then the mixture was stirred for 18 h at room temperature. The reaction was quenched with aqueous saturated ammonium chloride solution (10 mL), and the reaction mixture was extracted with dichloromethane (30 ml×3). The combined extracts were dried over anhydrous magnesium sulfate and concentrated in vacuo. Column chromatography of the residue on silica gel using ethyl acetate/hexane (10 to 25%) as the eluent afforded **10** as a white solid (565 mg, 90% yield for two steps): ^{1}H NMR ($CDCl_3$): δ 1.06 (m, 21 H), 1.77 (s, 3 H), 1.82 (s, 3 H), 3.73 (s, 3 H) (OMe), 4.76 (dd, J = 4.9, 10.2 Hz, 1 H) (H4), 5.01 (d, J = 4.9 Hz, 1 H) (H3), 5.30 (d, J = 10.1 Hz, 1 H), 6.80 (d, J = 8.8 Hz, 2 H), 7.33 (d, J = 9.0 Hz, 2 H).

(3*R*,4*S*)-4-(2-methylprop-1-en-1-yl)-3-((triisopropylsilyl)oxy)azetidin-2-one (11)

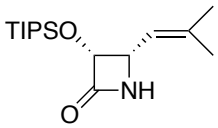

To a solution of b-lactam **11** (1.01 g, 2.50 mmol) in 100 mL of acetonitrile and 20 mL of water was added dropwise a solution of ceric ammonium nitrate (CAN) (4.80 g, 8.76 mmol) in water (80 mL) at −10°C. The reaction mixture was stirred at −10°C for 3.5 h. The reaction was then quenched with aqueous saturated sodium sulfite solution (30 mL). The aqueous layer was extracted with ethyl acetate (80 mL×3), and the combined organic layers were washed with sodium sulfite solution, brine, dried over anhydrous magnesium sulfate, and concentrated in vacuo. The crude product was purified on a silica gel column using hexane/ethyl acetate (4/1) as the eluent to afford compound **11** as a white solid (675 mg, 90.7% yield); ^{1}H NMR ($CDCl_3$): δ 1.06 (m, 21 H), 1.67 (s, 3 H), 1.74 (s, 3 H),

4.43 (dd, J = 10.6, 4.7 Hz, 1 H), 4.97 (d, J = 4.7 Hz, 1 H), 5.30 (d, J = 9.5 Hz, 1 H), 6.31 (bs, 1 H).

***tert*-butyl(2*S*,3*R*)-2-(2-methylprop-1-en-1-yl)-4-oxo-3-((triisopropylsilyl)oxy)azetidine-1-carboxylate (12)**

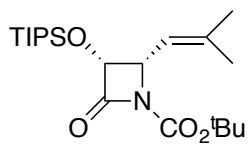

To a solution of N-H-β-lactam **11** thus obtained (1.90 g, 6.384 mmol), di-tert-butyl dicarbonate (1.67 g, 7.661 mmol) and DMAP (195 mg, 1.596 mmol) in 50 mL dichloromethane was added dropwise triethylamine (2.67 mL, 19.152 mmol) at room temperature. The mixture was stirred for 20 h at room temperature and the reaction was quenched with aqueous saturated ammonium chloride solution (50 mL). The mixture was then extracted with ethyl acetate (60 mL×3). The combined extracts were dried over anhydrous magnesium sulfate and concentrated in vacuo. The crude product was purified on a silica gel column using hexane/ethyl acetate (10/1) as the eluent to afford **12** as a white powder (2.52 g, 99% yield): ^{1}H NMR ($CDCl_3$): δ 1.03 (m, 21 H), 1.46 (s, 9 H), 1.74 (s, 3 H), 1.76 (s, 3 H), 4.73 (dd, J = 9.8, 5.6 Hz, 1 H), 4.94 (d, J = 5.6 Hz, 1 H), 5.25 (d, J = 9.8 Hz, 1 H); ^{13}C NMR ($CDCl_3$): δ 11.8, 17.5, 18.2, 26.0, 28.0, 56.8, 77.2, 82.8, 128.4, 139.6, 148.1, 166.3.

Synthetic procedure for compounds 14

(4*S*,4a*S*,6*R*,9*S*,11*S*,12*S*,12a*R*,12b*S*)-12-(benzoyloxy)-9-(((2*R*,3*S*)-3-((*tert*-butoxycarbonyl)amino)-2-hydroxy-5-methylhex-4-enoyl)oxy)-4,11-dihydroxy-4a,8,13,13-tetramethyl-5-oxo-3,4,4a,5,6,9,10,11,12,12a-decahydro-1*H*-7,11-methanocyclodeca[3,4]benzo[1,2-*b*]oxete-6,12b(2a*H*)-diyl diacetate (14)

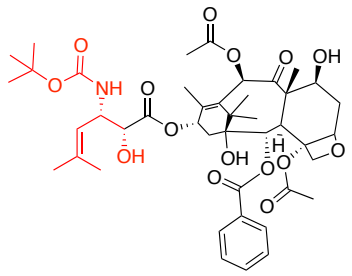

To a solution of β-lactam (±) **12** (28.6 mg, 0.072 mmol) and baccatin **3** (34 mg, 0.048 mmol) in 2 mL dry THF was added a 1.0 M LiHMDS in THF (0.06 mL, 0.06 mmol) dropwise at −20°C, and the solution was allowed to warm to 0°C over a period of 30–60 min, and stirred at 0°C for 30–60 min. After TLC analysis revealed the complete conversion of β-lactam, the reaction was quenched with aqueous saturated ammonium chloride solution (5 mL), and the aqueous layer was extracted with dichloromethane (15 ml×3). The combined extracts were then dried over anhydrous magnesium sulfate and concentrated in vacuo. The residue was purified on a silica gel column using hexane/ethyl acetate (6/1 followed by 3/1) to afford the coupling product as a white solid **13**. To a solution of the coupling thus obtained in 2 mL of pyridine/acetonitrile (1/1) was added dropwise HF/pyridine (70/30, 0.1–0.3 mL) at 0°C, and the mixture was stirred at room temperature for 12–18 h. The reaction was quenched with aqueous saturated sodium carbonate solution (5.0 mL). The mixture was then extracted with ethyl acetate (50 mL), washed with aqueous saturated copper sulfate solution (5 ml×3) and water (5 mL), dried over anhydrous magnesium sulfate, and concentrated in vacuo. The crude product mixture was then purified on a silica gel column using hexane/ethyl acetate (1/1 followed by 1/2) as the eluent to afford taxoid

14 as a white solid (31 mg, 78% over two steps).

^{1}H NMR (500 MHz, $CDCl_3$): δ 8.18 – 8.04 (m, 2H), 7.69 – 7.58 (m, 1H), 7.55 – 7.45 (m, 2H), 6.31 (s, 1H), 6.23 – 6.13 (m, 1H), 5.69 (d, 1H), 5.40–5.26 (m, 1H), 4.98 (dd, 1H), 4.82 – 4.71 (m, 2H), 4.44 (dd, 1H), 4.32 (d, 1H), 4.25 – 4.18 (m, 2H), 3.83 (d, 1H), 3.37 (d, 1H), 2.57 (ddd, 1H), 2.37 (s, 6H), 2.25 (s, 3H), 1.94 –1.89 (m, 4H), 1.78 (dd, 3H), 1.69 (s, 3H), 1.37 (s, 9H), 1.27 (d, 3H), 1.16 (s, 3H). ^{13}C NMR (126 MHz, $CDCl_3$): δ 129.64, 132.98, 127.95, 75.64, 71.83, 74.55, 120.11, 84.41, 51.11, 71.82, 75.55, 73.76, 75.95, 44.94, 35.56, 35.59, 22.40, 20.52, 14.97, 14.97, 35.56, 25.73, 18.57, 9.54, 9.54, 28.28, 28.23, 26.14, 29.68, 21.85. MALDI HRMS for $C_{43}H_{57}NO_{15}$ m/z [M+Na^+] 850.37; found 850.365.

***tert*-butyl ((*E*)-6-((2*S*,3*R*)-2-(2-methylprop-1-en-1-yl)-4-oxo-3-((triisopropylsilyl)oxy)azetidin-1-yl)-6-oxohex-4-en-1-yl)carbamate (16)**

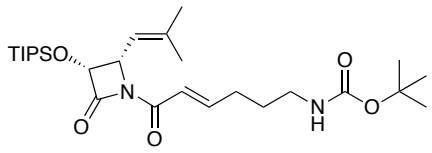

A solution of (*E*)-6-((*tert*-butoxycarbonyl) amino) hexenoic acid (10 mg, 0.0436 mmol) in 1 ml anhydrous CH_2Cl_2 was cooled to 0^{o}C. Oxalyl chloride (11.06 mg, 8μL, 0.0872 mmol) and catalytic amount of DMF was added dropwise and reaction was warmed to room temperature and stirred for 3 h. After 3 h, the resulting (*E*)-6-((*tert*-butoxycarbonyl) amino) hexenoic acid chloride **15** was used for next step without any purification. A solution of N-H β-lactam (±) **11** (9 mg, 0.030 mmol) and 2.5 M n-butyl lithium (2.90 mg, 19 μL, 0.0454 mmol) in 0.2 ml THF was cooled to -78^{o}C after 10 min stirring compound **15** (11 mg, 0.0454 mmol) was added dropwise in dry THF and stirred for 1 h. After 1 h, reaction was quenched with saturated 1 mL of saturated aqueous sodium bicarbonate and extracted with three 5 mL portions of ethyl acetate. The combined ethyl acetate extracts were dried over sodium sulfate and the crude oil was chromatographed on silica gel column eluting

with ethyl acetate/hexane (1 to 10%) to afford compound **16** as colorless oil (18.5 mg, 80%).

^{1}H NMR (500 MHz, $CDCl_3$): δ 6.54 (d, 1H), 5.65 (dd, 1H), 5.08 (d, 2H), 4.85 (d, 1H), 1.84 (s, 3H), 1.29 (d, 9H), 1.22 – 1.12 (m, 3H), 1.09 (d, 21H), 0.94 – 0.82 (m, 3H).

^{13}C NMR (126 MHz, $CDCl_3$): δ 135.92, 124.94, 118.56, 74.90, 18.39, 22.65, 31.59, 29.67, 12.02, 17.77, 12.02, 27.87, 7.83, 8.28, 17.83, 14.11.

Biological examination of compounds 14, 17 and anti-CD22 conjugated derivatives

Cell lines and Culture

Multidrug-resistant lymphoma cells lines stably expressing p-gp and CD22 were provided by Dr. Maria-Ana Ghetie, The Cancer Immunobiology Center, UT Southwestern Medical Center at Dallas, 6000 Harry Hines Boulevard, NB9.116, Dallas, TX 75390-8576, USA.

Generation of new MDR cells

Three cell lines (Namalwa, Raji, and DHL-4) were exposed to vincristine (VCR) at a starting concentration of 3 nM. VCR was increased every 10 days by 3 nM increments until cells became resistant to 12-21 nM VCR. The cells were named by the parental cell names and the final concentration of VCR to which they were resistant for example Namalwa 21nM VCR, Raji 18nM VCR, DHL-4 12nM VCR and Namalwa wild type as a control cell line.

Cell culture conditions

Namalwa 21nM VCR, DHL-4 12nM VCR, Raji 18nM VCR and Namalwa wild-type cells were cultured in ATCC-formulated RPMI- 1640 medium with L-glutamine (2 mM), sodium bicarbonate (1.5 g L-1), glucose (4.5 g L^{-1}), HEPES (10 mM) and sodium pyruvate (1.0 mM). The media was supplemented with penicillin (100 U mL^{-1}) and streptomycin (100 μg mL^{-1}, Mediatech) and fetal bovine serum (FBS, 10%, BenchMark). In case of Raji 18 nM VCR 1% Pen/Amp/Strep and 1100 μL Normocin (50 μg/ml) will be added. Cells were maintained in a humid 5% CO_2 atmosphere at 37 ^oC and subcultured every 2-3 days.

Cytotoxicity assay

Cytotoxicity of compounds **14, 17** or anti-CD22 antibody modified with **14** or **17** was determined using the MTT assay. On the day of exposure, exponentially growing cells were plated at 25000 cells/well in 160 μL in 96-well tissue culture plates (Nunc). Cells then were

incubated with medium (control), compound **14**, **17**, and anti-CD22 modified **14** or **17** (20 μL, 10X in cell culture medium) were added and cells were incubated for 68 h. At 68 h, MTT reagent (5 mg mL^{-1} in PBS, 20 μL/well) was added to each well. Incubate the plate for 4 hours at 37° C. View the cells periodically for the Appearance of punctate, intracellular precipitate using an inverted microscope. When purple precipitate is clearly visible under the microscope, plate was centrifuged at 1400 rpm for 10 min at 4°C and supernatant were removed carefully (with a syringe). At 72 h the water-insoluble formazan salt was dissolved in DMSO (100 μL/well). The absorbance was measured at 545 nm using a microplate reader (BMG Labtech). Data points were collected in triplicate and expressed as normalized values for untreated control cells (100%). Data were fitted using Prism software (GraphPad Software, Inc).

References

[1] M. C. Wani, H. L. Taylor, M. E. Wall, P. Coggon and A. T. McPhail, *Journal of the American Chemical Society* **1971**, *93*, 2325-2327.

[2] D. Guenard, F. Gueritte-Voegelein and P. Potier, *Accounts of Chemical Research* **1993**, *26*, 160-167.

[3] A. F. Wahl, K. L. Donaldson, C. Faircnild, F. Y. F. Lee, S. A. Foster, G. W. Demers and D. A. Galloway, *Nat Med* **1996**, *2*, 72-79.

[4] J. Dubois, *Expert Opinion on Therapeutic Patents* **2006**, *16*, 1481-1496.

[5] a) R. V. J. Chari, *Advanced Drug Delivery Reviews* **1998**, *31*, 89-104; b) R. Panchagnula, *International Journal of Pharmaceutics* **1998**, *172*, 1-15; c) A. K. Singla, A. Garg and D. Aggarwal, *International Journal of Pharmaceutics* **2002**, *235*, 179-192; d) C. Ta-Chung, C. Zyting, T. Ling-Ming, C. Tzeon-Jye, H. Ruey-Kuen, W. Wei-Shu, Y. Chueh-Chuan, Y. Muh-Hwa, H. Liang-Tsai, L. Jin-Hwang and C. Po-Min, *Investigational New Drugs* **2005**, *23*, 171-177.

[6] a) T. Kohji, S. Toshiyuki and O. Katsuhiko, *Current Pharmaceutical Design* **2006**, *12*, 273-286; b) G. Szakacs, J. K. Paterson, J. A. Ludwig, C. Booth-Genthe and M. M. Gottesman, *Nat Rev Drug Discov* **2006**, *5*, 219-234.

[7] a) I. Ojima and M. Das, *Journal of Natural Products* **2009**, *72*, 554-565; b) I. Ojima, S. D. Kuduk, P. Pera, J. M. Veith and R. J. Bernacki, *Journal of Medicinal Chemistry* **1997**, *40*, 279-285; c) I. Ojima, J. C. Slater, S. D. Kuduk, C. S. Takeuchi, R. H. Gimi, C.-M. Sun, Y. H. Park, P. Pera, J. M. Veith and R. J. Bernacki, *Journal of Medicinal Chemistry* **1997**, *40*, 267-278; d) I. Ojima, J. C. Slater, E. Michaud, S. D. Kuduk, P.-Y. Bounaud, P. Vrignaud, M.-C. Bissery, J. M. Veith, P. Pera and R. J. Bernacki, *Journal of Medicinal Chemistry* **1996**, *39*, 3889-3896; e) I.

Ojima, T. Wang, M. L. Miller, S. Lin, C. P. Borella, X. Geng, P. Pera and R. J. Bernacki, *Bioorganic & Medicinal Chemistry Letters* **1999**, *9*, 3423-3428.

[8] I. Ojima, X. Geng, X. Wu, C. Qu, C. P. Borella, H. Xie, S. D. Wilhelm, B. A. Leece, L. M. Bartle, V. S. Goldmacher and R. V. J. Chari, *Journal of Medicinal Chemistry* **2002**, *45*, 5620-5623.

[9] S. Lin, X. Geng, C. Qu, R. Tynebor, D. J. Gallagher, E. Pollina, J. Rutter and I. Ojima, *Chirality* **2000**, *12*, 431-441.

[10] D. Mastropaolo, A. Camerman, Y. Luo, G. D. Brayer and N. Camerman, *Proceedings of the National Academy of Sciences* **1995**, *92*, 6920-6924.

[11] D. G. I. Kingston, *Trends in Biotechnology* **1994**, *12*, 222-227.

[12] E. J. Roh, D. Kim, C. O. Lee, S. U. Choi and C. E. Song, *Bioorganic & Medicinal Chemistry* **2002**, *10*, 3145-3151.

[13] J. N. Denis, A. E. Greene, D. Guenard, F. Gueritte-Voegelein, L. Mangatal and P. Potier, *Journal of the American Chemical Society* **1988**, *110*, 5917-5919.

[14] K. C. Nicolaou, J. Renaud, P. G. Nantermet, E. A. Couladouros, R. K. Guy and W. Wrasidlo, *Journal of the American Chemical Society* **1995**, *117*, 2409-2420.

[15] H. K. Erickson, P. U. Park, W. C. Widdison, Y. V. Kovtun, L. M. Garrett, K. Hoffman, R. J. Lutz, V. S. Goldmacher and W. A. Blättler, *Cancer Research* **2006**, *66*, 4426-4433.

[16] X. Ning, J. Guo, M. A. Wolfert and G.-J. Boons, *Angewandte Chemie International Edition* **2008**, *47*, 2253-2255.

[17] J. Dommerholt, S. Schmidt, R. Temming, L. J. A. Hendriks, F. P. J. T. Rutjes, J. C. M. van Hest, D. J. Lefeber, P. Friedl and F. L. van Delft, *Angewandte Chemie International Edition* **2010**, *49*, 9422-9425.

[18] J. R. McCombs and S. C. Owen, *The AAPS Journal* **2015**, *17*, 339-351.

[19] V. M. Vrudhula, J. F. MacMaster, Z. Li, D. E. Kerr and P. D. Senter, *Bioorganic & Medicinal Chemistry Letters* **2002**, *12*, 3591-3594.

CHAPTER 5

CONCLUSION

"Engineer better medicine" is one of the fourteen grand challenges articulated by the US National Academy of Engineering. There are many ways to engineer better medicines. However, deliver the therapeutic molecule more precisely to the desired target is one of the most promising approaches. If drug carriers (nanoparticles, antibody etc.) could be engineered to deliver therapeutic molecules selectively to the desired target, it should be possible to greatly improve safety and efficacy of therapy. The field of targeted nanoparticles has been extraordinarily active in the academic realm, with thousands of articles published over the last few years demonstrating very promising results in in vitro studies and even in animal models. Yet, the biopharmaceutical industry has been relatively slow to make major investments in targeted drug delivery programs. Commercialization of targeted drug delivery devices has been challenging due to complexity in their design, lack of detail understanding at the molecular level, ability to manufacture drug carriers reproducibly in large scale, and producing homogeneous drug products due to a lack of orthogonal conjugation chemistries that combines covalent drug attachment with targeted delivery on a single platform.

We first describe a bio-orthogonal multifunctional nanoparticle tethered with hydrazine, amine, or dibenzocyclooctynol moieties for sequential conjugation of the anticancer drug, imaging modality, and a glycan-based ligand for the cell surface receptor CD22 of B-cells with excellent % conjugation efficiencies over conventional non-selective chemistries. The resulting

targeted nanoparticle showed remarkable ≈60 fold enhancement in cytotoxicity against CD22 (+) lymphoma cells compared to nontargeted nanoparticles.

Treatment of multidrug-resistant cancers with anticancer drugs often results in poor clinical outcomes. To this end, we describe site-specific conjugation method for sequential attachment of dual-drugs using SPAAC. This was based on the observation that ST6Gal1 has a preference for the α1,3-Man-β1,2-GlcNAc-β1,4-Gal bottom arm of the glycan of IgG over top arm. ST6Gal1 has enabled the sequential introduction of reactive functional groups and attachment of two payloads that can act via a differential mode of action such as FDA approved anticancer agent such as paclitaxel and zosuquidar, a highly potent P-glycoprotein modulator (Phase III clinical trial). The resulting dual-drugs ADC showed superior anti-cancer activities, selectivity and can bypass P-glycoprotein associated multidrug resistance in lymphoma cancer cells.

In another attempt, a novel paclitaxel scaffold with dual modification such as 2-methylpropenyl at C3' and (*E*)-6-((*tert*-butoxycarbonyl)amino) hexenoic acid modification at C3'-N-acyl position has been described. The dual modification furnished highly potent analogs of paclitaxel and showed potent cytotoxicity against multidrug-resistance cancer cells. The new scaffold enabled flexibility of introducing various clickable groups or stable yet cleavable linkers for site-specific conjugation to target antibody.

Despite there being a link between numbers of parameters that one needs to consider when constructing a targeted drug delivery devices (for example, location of cytotoxic agent, drug-to-carrier ratio and homogeneity) and the efficacy and pharmacokinetic profile, (For example, required dosage, bio-distribution, clearance rate, toxicity and accumulation at tumor), the detailed understanding of the interdependencies of these links and combinations of parameters

will need a significant amount of work before they are fully understood.